Towards A Semi-Autonomous Brain-Computer Interface

Christopher Wirth

Department of Automatic Control and Systems Engineering
University of Sheffield

A thesis submitted for the degree of
Doctor of Philosophy

2021

Acknowledgements

Firstly, I must extend my deep and sincere gratitude to my supervisor, Dr. Mahnaz Arvaneh. She has been an oustanding guide in every way. I could not possibly have wished for a better mentor.

The Automatic Control and Systems Engineering department at the University of Sheffield has provided an encouraging and thought-provoking environment for my research. I must especially thank my second supervisor Prof. Lyudmila Mihaylova, and my fellow lab members.

I am grateful to the Engineering and Physical Sciences Research Council (EPSRC) for the the Doctoral Training Partnership scholarship that funded this research.

I am forever thankful for my incredible family, not least for countless hours of childcare, but also for their constant support and inspiration.

I thank my son Lucas, whose laughter tells me what it is all for.

Finally, I would like to dedicate this work to my wonderful wife Helen. If not for her love, support, and belief, I could not have begun this journey, let alone completed it.

Abstract

Brain-computer interfaces (BCI) provide severely disabled people with the means to control assistive devices. However, there is a high mental workload for many BCI users. In many systems, users must actively control each of the machine's low-level actions. Recent studies postulate an alternative approach, using spontaneously-generated brain signals, while users merely observe machine actions.

It is possible to differentiate the brain's responses to correct and incorrect machine actions, using single-trial electroencephalography (EEG). Furthermore, having classified actions as correct or erroneous, robots can use machine learning to find quasi-optimal routes to a target. A few studies have differentiated the brain's responses to errors of different direction or severity. However, errors cannot always be categorised in these ways.

This thesis firstly shows that it is possible to differentiate, using single-trial EEG, subtly different errors that could not be distinguished by existing metrics: stepping off a target, or moving further from the target when starting from an off-target location. An additional data set is used to further validate the feasibility of distinguishing different error types. This thesis then shows for the first time that it is possible to distinguish EEG responses to different correct navigational actions, gaining specific information indicating when a target has been reached. Finally, a system is presented which responds to the detailed classification of these navigational actions in real-time. Four-way classification of EEG responses to robot movements is implemented, with additional binary classification of target selections. A dynamic probabilistic model of likely target loci is built via Bayesian learning, based on these classifications. This novel strategy facilitates more efficient virtual robot navigation and target identification than current state-of-the-art approaches.

In bringing these advances together, this thesis presents the foundation of a new framework for detailed implicit brain-machine communication. This facilitates semi-autonomous robot control, reducing the mental burden for BCI users.

Contents

List of Figures

List of Tables

Chapter 1

Introduction to the Research Project

1.1 Background

Brain-Computer Interfaces (BCI) provide a mechanism through which brain signals can be observed, usually through electroencephalography (EEG), and interpreted [10, 166, 167]. These signals can then be used for communication [16], or to control a device. Early applications for BCI generally focused on providing a means of control or communication to people who are completely paralyzed, for whom standard methods are not available. However, more recently, the scope of applications has expanded to include healthy users [18, 21].

A common approach for existing BCI is to attempt to control a device, such as a cursor, prosthesis, or wheelchair, via the classification of EEG signals produced when a person imagines movement of specific parts of the body, also known as motor imagery [56, 106, 174]. Similarly, some systems present stimuli to a user and use techniques such as steady-state visual evoked potentials (SSVEP) [116] or P300 signals [119] to select options for device control.

However, the aforementioned approaches place a heavy mental workload on the user, because the user is required to control all of the device's actions. For example, to pick up a bottle with a prosthesis, using a motor-imagery-based BCI, users would have to control every detail of the action, such as, *imagine right hand movement to move the prosthesis to the right, imagine right hand movement again to move the prosthesis further to the right, imagine foot movement to move the prosthesis forward...* and so on, gradually moving the prosthesis into position, before performing a particular grasp - which in itself may require further fine control - and moving the arm to a new position using the same laborious method.

Rather than using a step-by-step method such as this, it could be favourable to create novel systems wherein the human simply has to select a high-level action, such as *"pick up the bottle"*, or *"move my wheelchair to the window"*, and the computer selects and performs the appropriate action(s). In recent years, a small number of studies have proposed approaches to this challenge. For example, studies have presented methods by which users can select high-level actions using P300 signals [55, 133] or motor imagery [98]. Another potential approach to this challenge is to make use of brain signals that are produced spontaneously as we observe actions, and to couple the information from these signals with machine learning. Error-related potentials (ErrP) are an example of spontaneously-generated signals. ErrP are produced in our brains when we notice an error. These signals can be detected in EEG, making it possible to identify when a human considers an action to be an error, and when they consider an action to be correct [48, 121, 142]. This information can be utilised in machine learning, in order to teach the machine to choose the correct actions, and avoid erroneous ones, thus allowing the machine to develop optimal, or quasi-optimal, control strategies [63]. By allowing the machine to learn how to control a device in a manner that the user deems to be "correct", the burden of this low-level control can be removed from the human user.

A very small number of recent studies have shown that it is possible not only to distinguish between errors and correct actions, but to distinguish between different errors if, for example, they have different directions or severities [64], or to distinguish between errors committed by a human and those committed by the machine [151].

This is still a young field and there are still many avenues to be explored. It could be extremely useful to progress beyond merely combining *error vs correct* information with machine learning, by incorporating various kinds of information from spontaneously-generated brain signals. The more information that can be made available to a learning system such as this, the more power it would have to efficiently learn optimal strategies.

1.2 Motivation

Great advances have been made in BCI over recent years. However, one issue that affects many systems is the need for the user to perform step-by-step, low-level control. This can lead to mental fatigue, and also results in a low information transfer rate, due to the number of commands that must be made in order to achieve an overall task. However, humans already automatically produce various brain signals in response to things that they observe. By using the signals generated when a human merely observes a machine in action, and employing machine learning, we can allow the machine to learn the optimal actions and control strategies. Therefore, my motivation for this project was to advance BCI

such that interaction can be performed without any explicit signals having to be generated - instead utilising a variety of spontaneously produced brain signals for implicit brain-machine communication. By combining this implicit communication with machine learning, the burden of step-by-step, low-level control could be transferred from the human to the machine.

1.3 Aims and Objectives

The aim of this project is to investigate the feasibility of creating a more autonomous BCI, where much of the workload is removed from the human, with the burden being moved to the machine. To do this, I propose to create a new framework for implicit human-robot interaction, using various spontaneously generated brain signals.

To achieve this overall aim, the following objectives are addressed in this thesis:

1. Investigate whether it is possible to process and decode human EEG signals produced in response to different errors, even if the errors conditions are similar to one another in terms of severity, direction etc. In the first instance, this is performed "offline" using previously collected EEG data. To achieve this objective, neurophysiological differences between the different errors are investigated. Thereafter, appropriate signal processing and machine learning algorithms, capable of accurately classifying the different errors, are developed. This is carried out in two stages:

   (a) Classification of various response errors, committed by humans. As an exemplar case-study, data are used from time-critical reaction tasks, where users were presented with stimuli and asked to respond under time pressure, thus inducing the users to commit some errors. Errors induced by different types of stimuli are considered as different error conditions.

   (b) Classification of various navigational errors made by a machine. As an exemplar case-study, users observe a computer cursor as it navigates towards, and then reaches, a target. The errors that can occur during the navigation are:

   - The cursor, not yet at the target location, moves further away from the target.
   - The cursor, having already reached the target location, steps off the target.

2. Investigate whether it is possible to process and decode human EEG signals related to various non-erroneous actions, using data from a navigational task. Specifically, users observe a computer cursor as it navigates toward, and then reaches, a target. EEG data are collected from users during observation. These data are used to train

a classifier that can distinguish, on a single-trial basis, whether a correct action is merely *towards* a target, or one that actually *reached* the target. Thus, the output of the classifier can control a robot for reaching and selecting a relevant target among several locations. As with objective 1, the classifier is initially trained and tested offline, after EEG data collection has been completed.

3. Develop a novel system in which the classification strategies described in objectives 1 and 2, (decoding EEG signals related to different errors and correct actions) are applied in real time. As a human user observes a real or virtual navigating robot aiming to reach and select a target, the human's EEG signals are classified in a timely manner. The system should then react accordingly, e.g. if an error was detected, the system should immediately correct it if possible. The performance of the proposed system is compared with conventional BCI systems where only errors can be detected using EEG signals.

4. Apply intelligent control to the system described in objective 3, in the form of reinforcement learning. This should enable the robot to use all of the available information - not only whether actions are correct or erroneous, and which specific category of correct or erroneous action was performed, but also what the next possible action would be, based on the previously performed actions. Thus, using previous actions, the robot efficiently "learns" optimal, or quasi-optimal, control strategies such that the likelihood of committing errors is minimised.

These objectives come together as indicated in **Figure 1.1**. All of these objectives require appropriate artifact rejection, signal processing, feature generation, and classification to be carried out in order to decode EEG signals into the appropriate categories. There are also significant challenges inherent in the tasks set out here. Some common challenges of working single-trial EEG classification are described in section 2.2. Furthermore, while there are established features that distinguish the EEG responses to errors from those of correct actions, the signals in response to different types of errors are more similar to each other. As such, subclassifying different types of errors, or indeed different types of correct actions, presents a greater challenge than distinguishing errors from correct actions. This is exacerbated by the poor signal-to-noise ratio of EEG, making it harder to differentiate reliably between the relatively similar signals. In addition to this, the nature of the tasks from which my data are derived resulted in more correct actions occurring than errors, and imbalanced numbers between the different types of errors and correct actions [29, 59]. As such, an additional challenge is to train classifiers using small, and imbalanced, training data sets.

By achieving these objectives, we can theorise that the resulting framework would shift much of the burden in human-machine interactions from the user to the machine. By utilising various spontaneously-generated brain signals for implicit communication between human and machine, this could lead the way toward a more convenient, user-friendly BCI experience.

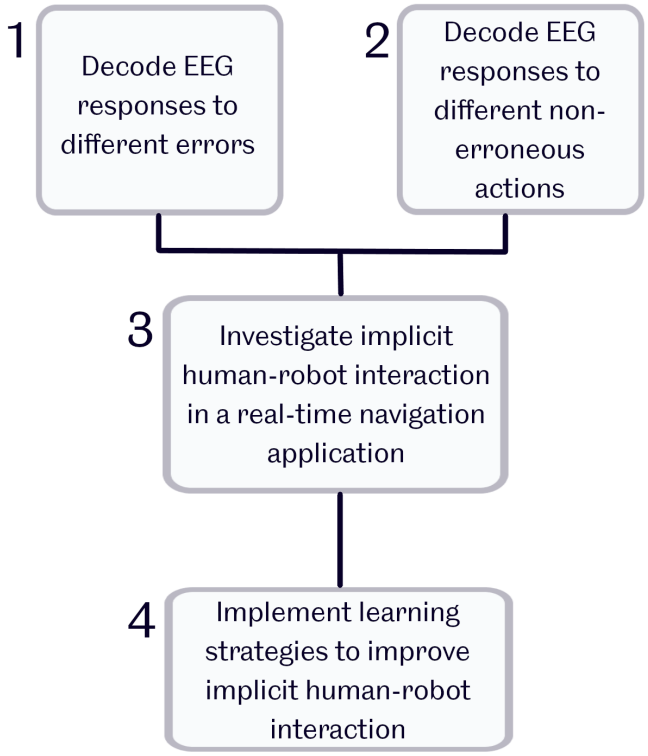

Figure 1.1: Four objectives are set out in order to achieve the overall aim of this PhD project: a new framework for implicit human-robot interaction, and thus a more autonomous BCI. Objectives 1 and 2 can be completed independently. Objectives 3 and 4 are dependent upon completion of the objectives shown above them in the figure.

1.4 Thesis Overview

This thesis describes the work carried out in order to fulfil the aforementioned objectives. The content of each chapter is as follows.

Chapter 2 provides a review of relevant literature in the research area. This begins with a background on BCI in general, and the details and challenges of the EEG modality. The chapter then discusses different types of brain signals: active, passive, and reactive, and

explores some reactive brain signals that are of key interest to this work — error related potentials (ErrP) and the P300 — in greater depth. The chapter concludes with a discussion regarding existing progress in semi-autonomous BCI, and the gaps and shortcomings that can be addressed in this field.

In chapter 3, the first objective of this project is addressed. EEG data are analysed from two tasks in which multiple error conditions occurred. Firstly, the Claw Task is introduced, in which users observe a virtual robot as it attempts to navigate towards and select a target. Two types of error are present, which differ based on the contexts in which they occur. Secondly, the Error Awareness Dot Task (EADT) is described. In this task, two different error types are committed by participants. These error types require differing cognitive processes in order to recognise that they have been committed. Neurophysiological analysis is presented, comparing the brain's responses to the various error conditions. Single trial classification analysis is then carried out. The chapter concludes with a discussion of the findings, and their implications within the broader context of BCI.

Chapter 4 addresses the second objective. EEG data are analysed from two virtual robot navigation tasks. The Cursor Task is introduced, in which a virtual robot aims to navigate towards, and identify when it has reached, a target location. Two different types of correct action are considered: actions that move towards the target but do not reach it, and actions that do reach the target. A publicly available data set based on a similar task is used to further validate the findings. Again, both neurophysiological analysis and single trial classification analysis are presented. The chapter closes with a discussion of the findings, and the new opportunities afforded in BCI by this novel investigation.

The third and fourth objectives are addressed in chapter 5. A paradigm is presented which combines the aforementioned decoding of multiple error types, and multiple types of correct action, to provide 4-way classification of robotic movements, based on the reactive brain signals produced as users merely observe the robot's actions. Additionally, error-vs-correct classification is performed on actions in which the robot identifies a location as the target. A novel application of Bayesian inference is proposed, using this detailed EEG classification as feedback. The proposed system uses the sequence of observed action classifications, combined with the confidence in the classification models, in order to iteratively update a probabilistic model to infer the most likely target location. The performance of the proposed system is rigorously compared to that of a system that uses EEG feedback to select appropriate actions in immediate response to the various classified action types, without utilising any probabilistic modelling of target likelihoods. Further, the proposed multi-way classification system is compared to one using the current state-of-the-art binary error-vs-correct movement classification. The chapter concludes with a discussion of the findings, and contextualises what this novel framework for implicit brain-machine interac-

tion could mean for future BCI users.

In chapter 6, the future outlook is explored, based on the contribution that this research has made to the field. Detailed suggestions are made regarding a protocol for carrying out real-time, in-person experiments. Challenges inherent in a human-in-the-loop scenario are discussed, as well as strategies to mitigate these challenges. Lastly, the chapter discusses future developments that could enhance and expand upon the research carried out in this project. These include: potential improvements to the BCI model; an expansion to long-term probabilistic modelling of user preferences; adaptive classification with inputs from passive brain signals such as fatigue, attention, and emotions; and extending the approach to other applications — theoretically, the framework is applicable to any task in which users select multiple preferences with varying frequency.

Finally, chapter 7 discusses the overall conclusions of the thesis. The fulfilment of the objectives is discussed, as well as the progress that this represents in the field.

1.5 Key Contributions

This thesis presents a number of advances in the field of BCI and EEG analysis. In particular:

- Classifying the EEG responses to different errors against each other, using newly-explored metrics. The differences between error types investigated in this thesis were more subtle than previously-explored differences. This contribution is examined in detail in Chapter 3.

- Showing, for the first time, that it is possible to classify the EEG responses to different correct actions against each other. This thesis presents the novel discovery that, in a navigational context, it is possible to classify responses to movements that reach a target, against other correct movements that do not reach the target, using single-trial EEG. This contribution is examined in detail in Chapter 4.

- A novel, Bayesian control system, utilising detailed feedback from reactive EEG. This thesis presents a new approach to utilising reactive EEG signals for semi-autonomous navigation. The novel system is shown to achieve faster and more accurate target identifications than existing state of the art methods. This contribution is examined in detail in Chapter 5.

1.6 Publications Based on this Thesis

1. A conference paper was published based on initial exploration of single-trial classification of different error types against each other, using data from the EADT:
   C. Wirth, E. Lacey, P. Dockree, and M. Arvaneh. Single-trial eeg classification of similar errors. InProc. 40th Engineering in Medicine and Biology Conference, Honolulu, HI, USA, July 2018.

2. A journal article was published based on neurophysiological analysis and single-trial classification analysis comparing the brain's responses to different error types against each other, as discussed in chapter 3:
   C. Wirth, P. M. Dockree, S. Harty, E. Lacey, and M. Arvaneh. Towards error categorisation in BCI: single-trial EEG classification between different errors. J Neural Eng., 2019.

3. A journal article was published based on neurophysiological analysis, and single-trial classification analysis comparing the brain's responses to different types of correct actions against each other, as discussed in chapter 4:
   C. Wirth, J. Toth, and M. Arvaneh. You have reached your destination: A single trial EEG classification study. Front. Neurosci., 2020.

4. A conference paper was published based on the investigation of four-way single-trial classification of different navigational actions — two different types of error and two different types of correct actions:
   C. Wirth, J. Toth, and M. Arvaneh. Four-way classification of eeg responses tovirtual robot navigation. In Proc. 42nd Annual International Conference of the IEEE Engineering in Medicine and Biology Society (EMBC'20), July 2020.

5. At the time of writing, a journal article is under review exploring the application of multi-way classification of navigational actions, combined with probabilistic modelling, to navigate towards and identify target loci using reactive brain signals, in simulated real-time experiments:
   C. Wirth, J. Toth, and M. Arvaneh. Bayesian Learning from Multi-Way EEG Feedback for Robot Navigation and Target Identification, under review for publication in IEEE Transactions on Systems, Man, and Cybernetics: Systems

Chapter 2

Review of the Research Area

2.1 A Background on Brain-Computer Interfaces

2.1.1 Why BCI Exist

The original intention of BCI research and development was to provide a means of communication or control to users who have severe motor disabilities, such as people with amyotrophic lateral sclerosis (ALS) [16, 17, 167].

However, more recently, the scope of uses for BCI has expanded, as researchers have realised that they could potentially be advantageous to healthy users [18, 21, 176]. For example, some studies have explored ways in which mental state monitoring could be used to assist in driving, such as by detecting mental workload and automatically removing distractions [78], or by predicting a driver's intention to brake [74] or turn in a specific direction [180].

2.1.2 Electroencephalography (EEG)

Electroencephalography (EEG), in which electrical brain activity is recorded via electrodes placed on the scalp, is the most commonly used imaging method utilised in BCI [112]. However, a number of other options have been explored. Electrocorticography (ECoG) is an invasive technology, using electrodes placed directly on the surface of the brain. It can generate signals of higher resolution, both spatially and temporally, than EEG [112]. Impressive results have been achieved in BCI using ECoG, with both human and animal users [141, 157]. However, due to its invasive nature, ECoG requires surgery, which carries risks. Some other non-invasive technologies, such as Magnetoencephalography (MEG), and Functional Magnetic Resonance Imaging (fMRI), can also generate signals with higher spatial resolution than EEG, but are not portable [112]. EEG does generate signals of high temporal resolution, and is both non-invasive and portable, as well as being available at a

relatively low cost [112]. These factors give an insight into the popularity of EEG amongst BCI researchers.

EEG electrodes are usually placed according to a standard system, known as the international 10-20 system [77]. An example of the names of electrode sites can be seen in **Figure 2.1**.

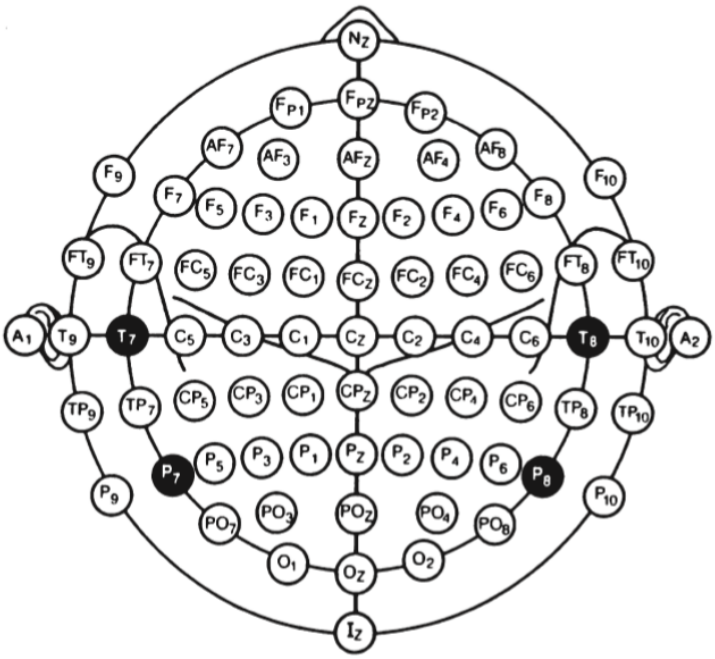

Figure 2.1: The international 10-20 system of electrode placement (Source: Klem et al., 1999 [77])

2.1.3 Signal Processing

Once raw EEG signals have been amplified, they must be processed in order to obtain meaningful information. The signal processing section of a BCI has been described as the "BCI transducer", which can be considered in three sections [44], as shown in **Figure 2.2**:

1. Artifact processing
2. Feature generation
3. Feature translation

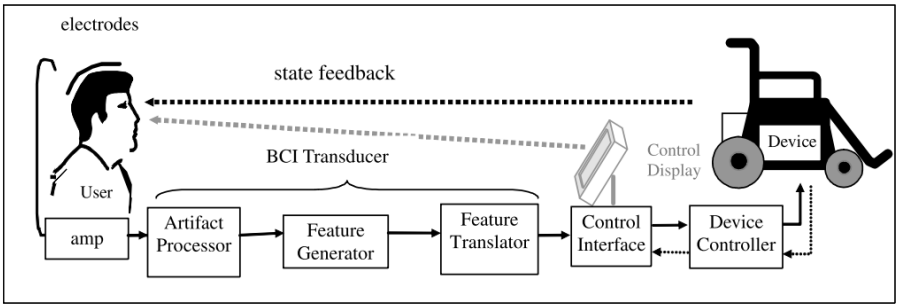

Figure 2.2: Model of a BCI system (Source: Fatourechi et al., 2007 [44], adapted from Mason and Birch, 2003 [103])

2.1.3.1 Arifact processing

Firstly, it is desirable to remove artifacts from the data. Artifacts can come from sources such as electrooculography (EOG, i.e. eye movement and blinks) and electromyography (EMG, i.e. muscle movements), and can make it more difficult to identify genuine and relevant neurological activity [44]. If data are segmented into trials, for example a given time window relative to stimuli, then one option for dealing with artifacts is to reject trials that are found to be contaminated. This can be achieved by removing any trials wherein the amplitude of the EEG signal rises above a certain threshold. If EOG or EMG signals are available, thresholds can be applied to them directly [44]. Alternatively, one can attempt to remove the artifact without rejecting the trial as a whole, using techniques such as blind source separation, or principal component analysis (PCA) [44]. Artifacts can also originate from external sources, such as power-line noise at 50 or 60Hz. This is often dealt with by applying a notch filter at the appropriate frequency [59, 115, 151].

2.1.3.2 Feature generation

After artifacts have been processed, features are extracted from the data. Many feature extraction methods have been implemented in BCI literature [10]. Features can be garnered from the time domain, frequency domain, spatial domain, or a combination of these.

In raw EEG, each measurement (i.e. each sampled time point in each channel) could be considered as a feature. In the time domain, one option to select informative features is to pre-select a specific time window, or windows, in which the signals are expected to be differentiable between classes [65, 74]. An alternative approach is to process the data in order to select such a time window [158].

Similarly, in the spatial domain, one can pre-select electrode sites in regions of the brain that are expected to be the most informative [63, 65]. More complex spatial filtering

techniques can also be applied. One such technique is the application of common spatial patterns (CSP). CSP filters aim to apply weights to each channel, such that the variance of the weighted signal is maximised for one class, whilst being minimised for another [22].

In the frequency domain, EEG signals can be broken down into different frequency bands. Some specific bands are well-established: delta (δ, <4Hz), theta (θ, 4-7Hz), alpha (α, 8-12Hz), beta (β, 12-30Hz), and gamma (γ, 30-100Hz) [112].

In a recent review of the field, Lotte et al. discuss the state-of-the-art in feature extraction methodologies for a number of different EEG-based BCI tasks [96]. They report that, for steady state visual evoked potential (SSVEP)-based BCIs, band power (i.e. frequecy domain) features are favoured. Meanwhile, they state that for event-related potential (ERP)-based studies, such as those utilising the P300 signal, time domain features are preferred. The P300 is discussed in further detail in section 2.5. The review also points out that both methods can benefit from being preceded by spatial filtering methods such as PCA or CSP (or variants thereof, such as filter-bank CSP). However, for some tasks such as those that utilise the brain's response to errors, the regions of the brain most likely to contain useful signals are widely known. As such, many studies based on these signals forego automatic spatial filtering, preferring to pre-select a small subset of electrodes [30].

Once features have been extracted, it can also be beneficial to select a subset of them, with the aim of increasing the ratio of meaningful signal to noise. As with feature extraction, a number of feature selection methods, such as genetic algorithms and PCA, have been employed in BCI [10].

The recent review from Lotte et al. also discussed the state-of-the-art in feature selection for various BCI tasks [96]. They broadly identify three subtypes of feature selection methods. Firstly, filter methods attempt to select a subset features which best discriminate between the classes, in a way that is independent from the classifier. For example, one can calculate the correlation coefficients between features and numerical representations of the classes, and then select the most highly correlated features. Secondly, wrapper methods generate a subset of features and then actively train the classifier. More feature sets are iteratively generated until a stopping criterion is met, such as high enough training accuracy, at which point the features are finalised. The third subtype of feature selection methodology discussed in the review is embedded methods. These are related to wrapper methods in that they actively evaluate the performance of features using the classification method. However, embedded methods also use feedback from the classifier to inform specific changes to the feature set. Stepwise linear discriminant analysis is identified as an embedded method that has provided "important improvements in BCI", specifically in the context of P300-based studies [38, 83, 84, 96, 148].

The most commonly used feature generation techniques used for EEG signals related to

error processing — a key aspect of this research project — are discussed in section 2.4.2.

2.1.3.3 Feature translation

The next stage is to translate the features into meaningful information that can, for example, be used to control a device, or to correct errors. The main task here is to classify the signals according to the user's intention or brain state, e.g. as imagined left hand movement vs imagined right hand movement [20, 87], or as an observed error vs non-error condition [63, 74].

A large variety of classification techniques have been applied to BCI, with some of the most commonly-used classifiers being neural networks, support vector machines (SVM), and linear discriminant analysis (LDA) [10, 97].

2.2 Challenges in Single-Trial EEG Classification

EEG classification entails a number of challenges. EEG signals tend to have a poor signal-to-noise ratio, so noise presents one challenge [97]. Another challenge is nonstationarity; EEG signals vary from session to session, and even within sessions [7]. Further to this, BCI data sets are often small, as they are usually generated in sessions with human participants, and these sessions can be fatiguing and time-consuming. As such, another challenge is often that of relatively small training sets. [97]. In many cases, many features are extracted for each trial - for example, if one were to use data from 64 electrode sites, sampled at 64Hz, and use all time points from a window of 1 second, one would have a vector of 4096 features. It is clear, then, that BCI can involve high dimensionality [97]. This leads to a challenge known as the curse of dimensionality [72]; a search space grows exponentially in relation to the growth in dimensionality. This can make classification very difficult, especially when few training data are available [72]. A review published in 2007 suggested that SVM and LDA were often appropriate classification techniques, when faced with the inherent challenges of EEG data [97]. An update to this review, published in 2018, suggested that some further techniques had been shown to handle the data well, such as Riemannian minimum distance to the mean (RMDM) classifiers and random forests, but reiterated that deep learning techniques do not appear to be effective, given these challenges [96].

2.3 Active, Reactive, and Passive BCI

Most early BCI systems were "active". In other words, users had to make a conscious effort to produce the required signals [80]. Active BCI include those which aim to classify

sensorimotor activity in order to control a device [56, 106, 174], and those which use slow cortical potentials for applications such as communication [17].

The term "passive BCI" was coined by Zander et al. in 2008 [178], and refers to BCI which use signals that are generated "spontaneously" [80]. One example of a passive BCI is a system that monitors mental workload, in order to automatically reduce distractions when necessary [78]. Systems that make use of error-related potentials (ErrP) - brain signals that are generated when a human recognises an error - have also been categorised as "passive" in some cases [80, 176]. ErrP will be discussed in further detail in section 2.4.

In 2011, Zander and Kothe expanded their definitions, and included a definition of "reactive" BCI. These are systems wherein brain signals are generated in response to external stimuli. "Reactive" BCI include those based on steady-state visual-evoked potentials - signals of a given frequency that are produced in response to a stimulus flashing at the same frequency [93], and those that utilise P300 - an aspect of the event-related potential generated when a human recognises a target stimulus [125] - for spelling applications [83,84].

The full definitions given by Zander and Kothe are as follows:

> "*Active BCI.* An active BCI is one that derives its outputs from brain activity which is directly and consciously controlled by the user, independent of external events, for controlling an application.
>
> "*Reactive BCI.* A reactive BCI is one that derives its outputs from brain activity arising in reaction to external stimulation, which is indirectly modulated by the user for controlling an application.
>
> "*Passive BCI.* A passive BCI is one that derives its outputs from arbitrary brain activity arising without the purpose of voluntary control, for enriching a human-machine interaction with implicit information on the actual user state." [176]

There is a caveat to add to this definition of passive BCI, which is pointed out in the Brain-Computer Interfaces Handbook: "A user who is aware of a passive BCI system might be influenced by the expectations they have of that system and voluntarily commit attentional resources to make sure that the 'spontaneous' activity takes place" [80]. In other words, a user's knowledge that a passive BCI is in place may, in itself, have an affect on brain state.

The role of passive BCI is considered to be somewhat different to that of active and reactive BCI. Both active and reactive BCI have been largely focused on direct control of devices, or communication [80, 167, 176]. Passive BCI, on the other hand, are commonly intended to be used alongside other activities, including other human-computer interactions, and to provide methods of improving the interactions or improving the performance of the activity [80]. However, recent uses of ErrP in conjunction with reinforcement learning have

shown that they can be used as an implicit form of device control [63,74]. Arguably, as these systems involve the user watching the device and deciding, at each movement (i.e. each stimulus), whether or not it was an error, these particular uses of ErrP could be considered as "reactive".

As the signals for passive BCI are produced spontaneously, without the need for conscious effort from the user, they can be implemented alongside other BCI, and numerous passive BCI can be implemented alongside each other [176].

2.4 Error-Related Potentials (ErrP)

2.4.1 Neurophysiology of ErrP

Error-related potentials (ErrP) are brain signals that are generated automatically when a human recognises an error [13, 51, 142]. ErrP waveforms are characterised mostly by two main features: the error-related negativity (ERN, also known as Ne), and a later error positivity (Pe) [42], as shown in **Figure 2.3**.

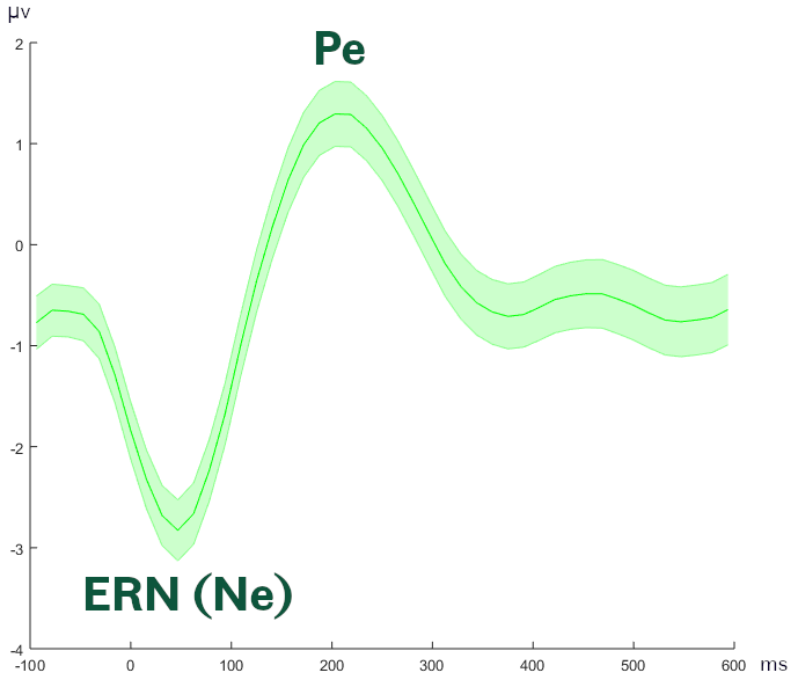

Figure 2.3: An example of an ErrP waveform at electrode site Cz. Error commission occurs at time = 0ms. This shows the mean (central green line) ± 1 standard error (green shaded area) grand average of 1002 error trials, gathered from 43 subjects.

The ERN usually occurs fronto-centrally [42, 48, 155]. The Pe has been shown to occur both fronto-centrally with a relatively sharp peak, and centro-parietally with a more sustained positivity [155].

There have been varying reports concerning the number of trials required to produce stable ErrP waveforms. In 2009, Olvet et al. found that ERN and Pe amplitudes were "fairly stable", and similar to those shown by grand averages, once 6 to 8 trials were considered. In 2010, however, Larson et al. considered the number of trials required to achieve stability between sessions. They investigated using up to a maximum of 14 trials, compared to grand averages, but found the stability "modest at best". This may be due to the nonstationarity of EEG discussed in section 2.1.3, despite reports that error-related signals are relatively stable over time [29]. Thus, they suggested that more than 14 trials may be necessary in cases where multiple sessions are to be considered. In their 2017 study, Harty et al. considered the findings of both of these studies, and elected to use a minimum cutoff of 12 trials per class, per participant [59].

2.4.2 Single-Trial Classification

A number of studies have shown that it is possible to classify errors against correct actions, using EEG, on a single-trial basis [29, 46–48, 63, 65, 75, 120, 144]. Classification accuracies have varied across these studies. For example, in a study in which users observed a robot arm making correct and erroneous movements, Kim et al. achieved classification rates of 95% in the error class and 86% in the correct class [75]. Meanwhile, a study by Charavviaga and Millán, in which users observed correct and erroneous actions of a computer-controlled cursor, showed mean classification rates of 75.8% for the error class and 63.2% for the correct class [29]. Despite the classification accuracy in this study being lower than that achieved by others such as Kim et al., it proved sufficient for its proposed purpose: facilitating machine learning. The use of ErrP as a feedback function for machine learning is discussed in greater detail in section 2.4.4. In a typing task, the best performing subject-specific ErrP classifier reported by Wang et al. had a sensitivity of 62.20% and a specificity of 51.68% [160]. It has been postulated that the relatively low performance in the latter study may have been due to a small number of errors in the training set, as only 2.28% of keystrokes were erroneous, for the average participant [30,160]. This highlights the challenge of dealing with small and imbalanced training sets.

Amongst a number of studies, a common strategy has emerged for feature extraction, prior to single-trial classification of ErrP. This current state-of-the-art strategy is to extract time domain features from a pre-selected time window (generally beginning around 100-200ms relative to error commission, and ending around 600-900ms), using data from a few pre-selected electrodes (usually fronto-central ones). These signals are usually low-pass

filtered at 10 or 20Hz [19, 29, 30, 46, 152]. The most popular classifiers used for ErrP have been LDA and SVM [30].

A few studies have compared the signals generated when users register their awareness of an error with those generated when users are unaware of an error [39, 59, 61, 110, 113]. Some of these studies showed that, while aware and unaware errors produced similar ERNs, the Pe was diminished in response to unaware errors [39, 113]. Similarly to the aforementioned studies, Harty et al. found "no evidence" of Pe in unaware error responses in either young or older age groups. Further to this, Harty et al. found the Pe to be somewhat diminished in older adults' responses to aware errors, compared to the Pe of young adults - a sign that the brain's error responses change with age [59].

The timing of a user's awareness that an error has occurred has also been shown to affect the brain's responses. Yazmir et al. found that the highest peaks in the ERP in response to success occurred significantly earlier than those for failure, in a throwing task. It was postulated that this was due to the users' ability to predict, at an earlier point, that success would occur [170]. Timing has also been shown to affect single-trial classification. Omedes et al. reported much greater success in classifying sudden errors than the gradually unfolding ones, with the expected reason being that the moment of error awareness varied more greatly for the gradually unfolding errors. Classification accuracy for gradually unfolding errors was improved by using a sliding window, trained on the sudden errors [114]. In a later study, Omedes et al. achieved higher classification accuracy on errors made during fast grasp attempts than those during slow grasps. This may, similarly, be due to awareness occurring over a broader range of time during slower grasps [115].

2.4.3 Using ErrP to Improve Existing BCI Performance

Since the revelation that ErrP could be classified on a single-trial basis, a number of studies have utilised them to improve the performance of existing BCI [30]. Some studies have applied error recognition, and immediate error correction, and have reported improved spelling speed [144] and bit rate [152]. Others have employed error correction in motor-imagery-based BCI for the control of a device, again reporting increased bit rates [47].

It should be noted, however, that the use of ErrP detection for immediate error correction may not be appropriate in all scenarios. A study presented at the International BCI Workshop in 2008 shows an example of this, in a system where ErrP feedback was used to correct errors in a P300-based spelling device [158]. The authors conclude that most of the subjects "can benefit from [error correction] when the accuracy of the P300 speller is no more than 75%." In other words, however, this means that if the intial P300 classification rates were particularly high, then applying error correction (including, of course, "correcting" in the case of some false-positive error detections) could have a detrimental affect

on the system as a whole. Similarly, while Parra et al. reported an average performance improvement of 21% across their seven subjects, a small degredation in performance was reported for two of these individuals [121]. It is important, therefore, to consider the overall system, including the classification rates of its constituent parts, when deciding whether error correction is an appropriate tool.

2.4.4 Using ErrP as a Feedback Function for Reinforcement Learning

In recent years, some studies have utilised the detected ErrP as a feedback function for reinforcement learning (RL), allowing the machine to "learn" optimal, or quasi-optimal, strategies in response to the user judging which actions are errors, and which are correct [30]. RL strategies should, theoretically, be capable of converging on (quasi) optimal strategies, using ErrP detection as a feedback function, as long as the classification rate exceeds chance level [30,63]. In 2006, Buttfield et al., in José Millán's research group, discussed ErrP, online learning, and the potential integration of the two to allow continuous adaptation in future BCI applications [25]. In 2010, Chavarriaga and Millán showed that their system could learn the optimal policy in a 1-dimensional cursor navigation task "in just a few interaction trials" [29]. Iturrate et al. applied Q-learning to a virtual basket selection task, converging on the correct basket in the vast majority of cases. Again, this showed the possibility of applying ErrP as a feedback function for RL [64].

In 2015, Iturrate et al. presented a larger study, comprising three experiments: a cursor moving 1-dimensionally, a virtual robot arm moving 2-dimensionally, and a real robot arm moving 2-dimensionally. In each task, one of several potential targets was selected at the start of each run. The user had knowledge of the target's location, but the machine did not. The machine's goal was to navigate toward the selected target. ErrPs were detected based on calibration data from a session 25 minutes long on average. In all experiments, the devices were able to converge on quasi-optimal policies after just 4 runs, and thus, most users reached significantly more targets than would be expected by chance. The strategy was also able to generalise successfully when new targets were introduced [63].

In a study in 2017, Kim et al. allowed users to control a simulated robotic arm, and a real robotic arm, using physical gestures. Since the user was observing the robot's actions, the machine learned to map each gesture to the appropriate action using ErrP as a feedback function. The authors reported a significant correlation between the true positive rate (i.e. the proportion of errors recognised) and robot performance, based on results from the real robot task. However, this claim was not substantiated by data from the simulated robot task, as the publication's supplementary materials revealed that the correlation in this case was not significant. Nevertheless, the authors were able to show a statistically significant improvement in robot performance over time, as the robot learned the relevant

mappings [75]. This provides further evidence that ErrP can be successfully used as a feedback function, allowing machines to learn appropriate actions.

2.4.5 Error Categorisation

A few studies have shown that, beyond classifying errors against correct actions, it is possible to distinguish different errors against each other based on the ErrP that they evoke. For example, in a study by Iturrate et al., a virtual robotic arm had the task of selecting a specific basket. However, there were four other baskets that the arm could erroneously select. These baskets were:

- 1 step away, left of the target basket
- 2 steps away, left of the target basket
- 1 step away, right of the target basket
- 2 steps away, right of the target basket

The study showed that there were significant differences between the ErrP for errors to the left vs those to the right, and also between those of small vs large errors. Furthermore, even with 5 classes (correct, plus both large and small errors to left and right), single-trial classification accuracies of around 60-80% were achieved for each category, for each participant [64].

In addition to comparing errors based on direction and severity, a small number of studies have considered neurophysiological differences arising from varying sources of errors. Furthermore, a study by Spüler and Niethammer showed that it is possible to classify errors committed by a human against errors committed by a machine [151]. Different ErrP and error types that have been discussed include:

- *"response ErrP"*, caused when a human recognises that they have responded incorrectly to a task [42, 46, 75].
- *"feedback ErrP"*, caused when a human is informed that they have made an error, of which they were previously unaware [46, 75].
- *"observation ErrP"*, occurring when a human observes an error committed by a machine or another human [46, 75].
- *"execution errors"*, when a machine fails to execute a command as instructed by the human (this could arguably be considered as a term for a type of error eliciting an "observation ErrP") [75, 151].

- *"outcome errors"*, when a human experiences a task failure [75, 151].

In Spüler and Niethammer's 2015 study, users played a game in which they controlled a computer cursor, using a handheld controller, to avoid virtual falling blocks. They compared execution errors - wherein the direction of the cursor would suddenly diverge from the direction specified by the user's controller - with outcome errors - when the cursor collided with a block. One confusing element of the study is that one might expect that outcome errors would often occur shortly after execution errors, as the hindrance of the user's contol may cause the cursor to collide with a block. This potential issue, and how it might affect the brain's responses, is not addressed in the publication. Even so, the authors were able to show that they could classify execution errors against outcome errors (i.e. machine errors vs human errors), using single-trial EEG, with mean accuracy of over 70%, significantly above chance level [151].

2.5 P300

Another brain signal that is produced automatically in response to certain stimuli is the P300: a positive peak in an ERP at approximately 300ms relative to a given stimulus [125,149]. This peak is known to be elicited in the brain when a subject recognises a target stimulus in a sequence containing both target and non-target stimuli [125, 128, 129]. The P300 has been successfully utilised in BCI, notably in spelling devices [43, 45, 55, 84, 148]. In these cases, the "target" stimulus is the specific character the user wishes to type. Each potentially desired character is typically highlighted a number of times, with each time being referred to as a "subtrial". These subtrials are then averaged to increase the robustness of classification [43,45,55,84,97,148]. Similar systems have also been developed for the control of robots [12, 15, 69, 100], cursors [70, 91, 130], and wheelchairs [62, 132].

Single-trial P300 classification — classifying the presence of a P300 against its absence — is challenging, due in part to the low signal-to-noise ratio of EEG data [68, 97], hence many systems presenting a number of subtrials. One study investigated the effects of different numbers of subtrials, and, while high accuracy was achieved with many subtrials, classification accuracy of less than 50% was reported based on a single subtrial, and 3 subtrials were required to achieve over 60% accuracy [89]. More recently, studies focusing on single-trial P300 classification have shown success, with some reporting accuracies over 80% [49, 79, 94].

In one previous study, one version of a task presented 80% standard stimuli and 20% target stimuli with all targets being identical to each other, while another version presented 80% standard stimuli and 20% target stimuli, with a pool of 25 different target stimuli; the latter case was found to elicit a broader P300 [24]. While the responses to the different

target stimuli were not compared to one another, this finding suggests that the P300 is affected by how often a specific stimulus appears in a task. Indeed, other literature has reported that P300 amplitude increases for larger target-to-target intervals [52]. As well as this, the P300 has been shown to be associated with positive outcomes [58], and its amplitude has been shown to be affected by reward magnitude [140, 169, 171].

2.6 BCI Control and Optimisation

Many real-time BCIs can be considered as control problems [1]. Often, the aim is to capture and interpret brain signals in order to control a cursor [168] or other neuroprosthetic device [28]. Thus, a good deal of research in BCI is related to facilitating this control, or improving some aspect of it. As one might expect, the aspect that recieves the most attention in BCI-specific research is how to improve the interpretation of brain signals [96,97]. However, other valuable contributions have been made by studies focusing on other aspects of the control problem. Shared-control systems have shown admirable performance when augmenting brain-actuated commands with reflexes from robotic sensors [73], visual feedback [12], or other environmental context [50, 156]. For example, brain signals have been combined with sensor fusion in a Bayesian system [126]. This allows prior knowledge - in this case, knowledge of the surroundings - to alleviate difficulties of EEG processing such as noisy data, in order to choose the direction that is deemed to have the highest probability of being the most agreeable. Such systems show the potential to expand BCI into complex tasks. One study showed that reliable 3D control could be achieved in a virtual environment, by imposing intelligent constraints on the commands inferred from the users' brain signals [137].

Let us consider the specific case of BCIs that utilise reactive EEG signals. These can be considered as closed-loop control systems: a machine performs a control action, receives feedback in the form of an EEG response, and updates its future actions accordingly. As discussed in section 2.4.3, one common use of reactive EEG is to classify ErrPs and use them to facilitate error correction. However, as discussed in section 2.4.4, another approach is to use EEG signals as feedback for machine learning. These systems can be considered as approaches to an optimisation problem, as they use the feedback to search for optimal or quasi-optimal solutions to a control problem. A number of these systems have employed reinforcement learning methods such as Q-learning to optimise the route from one location to another (see section 2.4.4). Also within the realm of navigation optimisation, a handful of studies have begun to investigate using EEG feedback to infer a user's preferred target destination [54, 143].

2.7 Semi-Autonomous BCI

The concept of a semi-autonomous system in general is to allow the user to make high-level decisions, but to make the machine responsible for the execution of low-level actions [30]. This has the potential to reduce the workload of the user, as discussed in section 1.1.

A small number of studies have begun to explore the possibility of developing semi-autonomous BCI. For example, Perrin et al. have presented a system in which the machine selects available navigation options for the user's wheelchair and presents them to the user, one at a time, beginning with the option deemed to be most likely. The user's task is to use motor imagery to give yes or no answers, either selecting the presented option or moving on to the next. The machine then controls the wheelchair's movements [122]. A related study from Lotte et al. allowed users to choose high-level options using motor imagery to make selections via a binary tree [98]. The low level navigational actions around a virtual environment were then controlled by the machine, although the system also offered a manual control mode. A few studies have proposed an adaptation of the P300-speller paradigm (as described in the previous section) to select high-level options. Rebsamen et al. presented what they describe as a "slow but safe and accurate" P300-based destination selection system [133]. Guger et al. used a similar P300-based approach to control various aspects of a smart home [55]. Accuracy rates in this study varied greatly between the most and least successful tasks, suggesting that such a system may be very sensitive to the specific design of the action selection screen.

Another example was presented by Lampe et al. in 2014. Here, image processing was used to identify a number of objects in view of a camera. Users were asked to imagine finger tapping to scroll through the available options, and imagine toe clenching to select the highlighted option. Reinforcement learning was then used to train the machine to perform a grasp on the object. Here, the feedback function is not based on ErrP, and is merely described as "learning from success and error" [87].

As discussed in section 2.4.4, systems using ErrP show a good deal of potential for semi-autonomous BCI, by allowing the machine to learn the user's preferences, while the user must simply have a high level goal in mind and observe the machine's actions.

The term "hybrid BCI" was coined by Pfurtscheller et al. in 2010, and defined as an overall system that is *"composed of two BCIs, or at least one BCI and another system"* [124]. As such, the semi-autonomous systems described above could be classed as "hybrid BCI". One way that semi-autonomous BCI could be developed would be to couple two BCIs together into a hybrid BCI, for example by using motor imagery to select an action, and ErrP detection to allow the machine to learn how to perform the action optimally. Alternatively, any other type of control system - if available to the user - could be employed to allow

the user to make high-level decisions, with error-driven learning again taking responsibility for the development of optimal low-level control solutions. In either case, the use of ErrP processing could provide the next step in hybrid, semi-autonomous BCI.

2.8 Gaps and Shortcomings in Existing Research

Despite a number of interesting recent studies, there are still many new avenues to be explored to advance BCI towards an autonomous system.

2.8.1 Classification of Similar Error Conditions

As discussed in section 2.4.5, recently a few studies have started to explore the single-trial classification of different errors against each other. However, in existing literature, the error conditions being compared have had clear-cut differences, such as direction [64], severity [64], or whether the error was committed by a human or by the machine [151]. However, in real-world scenarios, errors cannot always be delineated by these metrics. As such, it is important to consider whether errors that are similar in all of the aforementioned aspects, with only more subtle differences between them, can be classified against each other on a single-trial basis. The ability to do so would increase the scope of possible applications for EEG error detection, and would thus have the potential to improve brain-machine interaction.

2.8.2 Progressing Beyond Errors

Previous studies discussed in section 2.4.4, such as that of Iturratte et al. in 2015, have made interesting advances in using ErrP classification to learn how to navigate towards a target [63]. However, in these studies, classification has only been between correct actions (toward the target) and erroneous actions (away from the target). Each run automatically finished when the target was reached. The intelligent systems had no awareness that they had reached the target - only that they were moving in the correct direction. As such, in many real scenarios, a robot would have had to pass the target, at which point ErrP should inform it that this move was an error, and then return. It may then have to attempt a number of alternative directions, only to be told that all are errors, before settling on the correct location of the target. Situations such as this could be improved by considering more spontaneously generated brain signals than just ErrP. For example, instead of these systems merely considering all non-erroneous actions as one "correct" condition, it would be beneficial to be able to classify multiple different correct actions, such as moving *toward* a target vs actually *reaching* a target.

2.8.3 A Novel Framework for Implicit Human-Robot Interaction

In the existing literature, early steps have been taken in using implicit human-robot communication to allow machine-learning-based robot control [63, 75]. However, these studies have been restricted to the binary information, simply regarding each action as correct or erroneous. I believe that, building on the studies discussed in this section, addressing the research gaps outlined above, and applying learning strategies with the power of the broader and more detailed information that would be gathered, a new BCI framework could be developed. This would be manifested as a more autonomous system, achieved through implicit communication between human and machine.

Chapter 3

Classifying Different Error Conditions Against Each Other

The findings presented in this chapter have been previously published in the Journal of Neural Engineering [161], with preliminary results published in the proceedings of the 40th International Conference of the IEEE Engineering in Medicine and Biology Society (EMBC '18) [162].

3.1 Chapter Introduction

When a human recognises that an error has been committed, either by themselves or in actions that they are observing, ErrP signals are generated in the brain [51]. As discussed in section 2.4, a number of studies have shown that it is possible to differentiate between errors and correct actions, by detecting ErrP using EEG, on a single-trial basis [30, 63, 75, 179]. Interestingly, previous studies have confirmed the possibility of using single-trial error vs non-error classification as a feedback function for a reinforcement learning-based BCI [30, 63, 75, 179]. This opens up the possibility of moving toward autonomous BCI systems, allowing the machine to learn appropriate low-level actions based on the human's perceptions of which actions are correct, and which are errors. Such systems are able to learn quasi-optimal solutions in scenarios such as simple navigation tasks [63,179], and thus may reduce human mental workload. However, when tasks increase in complexity, learning will become slower if the only available information is whether a given action was correct or erroneous. Hence, if a system can be given more detailed information about the type of error that occurred, it can correct its actions more appropriately, and learn more quickly.

More recently, a handful of studies have shown that, beyond classifying errors against correct actions, it is possible to distinguish different errors against each other based on their

ErrP. For example, ErrPs have been distinguished based on the direction or severity of an erroneous action [64], and outcome errors (committed by a human) have successfully been classified against execution errors (committed by a machine) on a single-trial basis [151].

Despite these recent advances, the vast majority of literature in the field concerns the classification of errors against correct actions, rather than the classification of different error types against each other. Furthermore, different errors cannot always be categorised by previously explored metrics such as direction, severity, and whether the error was committed by the human or the machine. For example, if we are trying to navigate to a target location we could either take a wrong turn on the way, or we could reach the target but then pass it. These two errors could be of the same direction and magnitude, and therefore indistinguishable by currently explored metrics, but knowing which one had occurred would provide useful information. Therefore, it is important to consider whether there are significant neurophysiological distinctions in EEG signals between the brain's responses to very similar error conditions, even in cases where metrics explored in existing literature are not available.

To address this question, we evaluated data from two tasks. In the first task, users were presented with "go" and "no-go" stimuli and asked to respond to "go" stimuli, but withhold responses to "no-go" stimuli. All of the errors considered by this experiment were response errors committed by humans who failed to withhold responses to "no-go" stimuli, and then recognised their own errors. None of the errors had any direction associated with them, and participants were not instructed to consider any errors as more or less severe than any others. The key difference between the error conditions lay in the cognitive processes required to recognise them, with the recognition of one error condition being more memory-dependent than the other. In the second task, users observed a virtual robot attempting to navigate to, and grab, a target object. Here, we investigated users' EEG responses to two navigational errors: moving away from the target when in position and ready to grab it, and moving further away from the target object if not already in position. Errors were equally likely to be made to the left or the right. In this case, all errors were being committed by the machine. As with the first task, direction could not be used to distinguish the error conditions, and users were not told to consider either error to be more or less severe than the other. As such, the error conditions considered here could not be differentiated by metrics used in existing literature. However, the contexts in which the errors arose differed slightly: In one condition, the expected correct action would be a lateral movement towards the target. In the other condition, the expected correct action would be to grab the target. We aimed to use distinctions in the EEG signals, arising from these subtle differences of cognitive load and context, to classify the error conditions against each other.

To explore the neurophysiological distinctions between the responses to these error con-

ditions, we used time domain data to compare the latency and amplitude of key ErrP features: the error-related negativity (ERN), and the error positivity (Pe). As discussed in section 2.4, the ERN is a negative deflection, usually peaking fronto-centrally around 100ms after an error [30, 41, 51]. The Pe is a slower positive wave, often peaking centro-parietally between 200-400ms after the error [30, 41, 59, 117]. In contrast with the ERN, the Pe has been shown to depend on participants' awareness and confidence that an error has been committed [39, 110, 113, 118], suggesting that the Pe is linked to conscious processing of errors. In addition to amplitude, the "build-up rate" of the Pe (i.e. the steepness of the slope as amplitude increases to the peak) has also been identified as a marker of evidence accumulation for error detection [111]. Further to this, secondary Pe peaks have been identified, again being linked to conscious, evaluative processes [5, 40]. The ERN and Pe have been displayed in a variety of previous single-trial error classification studies [30,46,63,151].

We also investigated the spatial distribution of the brain's response to each error condition, using topographical maps. In order to distinguish between error conditions on a single-trial basis, we employed a stepwise linear discriminant analysis classification strategy, using a small, highly discriminative set of time domain features from 20 electrode sites. We tested the efficacy of this strategy using data from 20 young and 5 older adults performing one task, and 14 young adults performing the other task.

3.2 Methods

3.2.1 Participants

This study used data collected during two tasks, which we refer to as the "Error Awareness Dot Task" (EADT) and the "Claw Task". Fifty-four healthy adults were recruited for the EADT. 28 of these were young (aged 18-34) and 26 were older (aged 65-80). Seventeen healthy adults were recruited for the Claw Task.

All of these participants were included in neurophysiological analyses, but some were excluded from the single-trial classification phase of this study. 23 were excluded from the EADT (4 young, 19 older) due to not producing enough artefact-free trials for all conditions. A further 6 from the EADT (4 young, 2 older) were excluded as it may have been possible to classify their data based on motor signals, rather than ErrPs. The rationale for these exclusions is explained in further detail in section 3.2.4.1. This left 25 participants from the EADT (20 young, 5 older) to be included in the single-trial classification phase. 3 participants were excluded from the Claw Task due to not producing enough artefact-free trials for all conditions. All Claw Task participants used for single-trial classification were young (aged 18-35).

All participants for both tasks had normal or corrected-to-normal vision. They reported

no history of psychiatric illness, head injury, or photosensitive epilepsy. Written informed consent was provided before testing began. All participants of the EADT also reported that they had no history of colour-blindness. All procedures for both tasks were in accordance with the Declaration of Helsinki. Procedures for the EADT were approved by the Trinity College Dublin Ethics Committee, and procedures for the Claw Task were approved by the University of Sheffield Ethics Committee in the Automatic Control and Systems Engineering Department.

3.2.2 Experimental Setup

3.2.2.1 EEG Setup

For the EADT, 64 channels of EEG were recorded at 512Hz, using the BioSemi ActiveTwo system. Electrodes were placed using the 10-20 system. Electrooculogram (EOG) electrodes were also placed at the outer cantus of each eye, and above and below the left eye. Reference electrodes were placed on the left and right mastoid.

For the Claw Task, 20 channels of EEG were recorded at 500Hz, using an Enobio 20 5G headset. The electrode positions used were: F7, F3, Fz, F4, F8, FC1, FC2, T7, C3, Cz, C4, T8, CP1, CP2, P3, Pz, P4, PO7, PO8, and Oz. Reference electrodes were placed on the earlobe.

3.2.2.2 The Error Awareness Dot Task

The EADT was a time-critical reaction task, requiring sustained attention. The task employed a "go/no-go" paradigm, requiring participants to react to "go" stimuli with a mouse click, but withhold their reaction in the case of "no-go" stimuli.

Participants were shown a succession of randomised, differently-coloured dots on a computer screen, with a blank grey screen shown between dots, as shown in **Figure 3.1**. Participants were asked to perform a left mouse click, in a timely manner, in response to the presentation of each new dot. However, in two "no-go" scenarios, they were asked to withhold their response. These scenarios were the presentation of a blue dot, or of a dot that was the same colour as the previous dot. These are known as the "colour condition" and "repeat condition", respectively. If participants did click in either of these scenarios, they were asked to perform a second click with the right mouse button, in order to indicate their awareness of the error.

Before testing began, a practice block took place, in which participants had to respond successfully to three consecutive no-go trials, either by withholding their initial response or, if they did click erroneously, by following up with an awareness click.

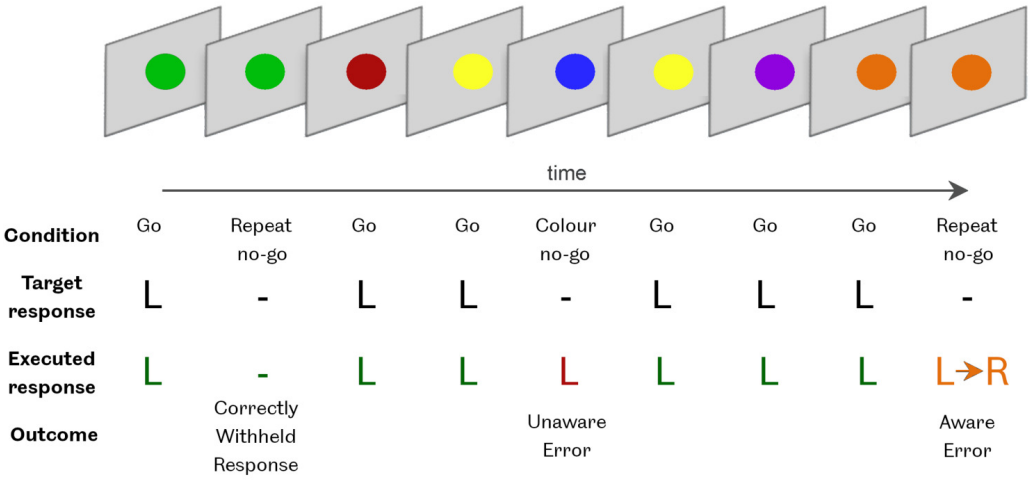

Figure 3.1: The Error Awareness Dot Task (EADT). Participants were asked to respond to "go" stimuli with a left mouse button click (L). They were asked to withold this response in the event of either a "colour no-go" stimulus (the stimulus is blue) or "repeat no-go" stimulus (the stimulus is the same colour as the previous stimulus). If participants performed a left mouse click following a no-go stimulus, they were asked to follow this with a right mouse button click (R), to register their awareness of their error.

8 blocks of trials were collected from each participant, with the exception of five, for whom 4-6 blocks of trials were collected. Each block lasted approximately 6 minutes, and contained 176 "go" trials, 16 "repeat condition" trials, and 8 "colour condition" trials.

The duration for which each stimulus was shown varied throughout the task, depending on the accuracy of the participant in performing correct responses to go and no-go trials. Initially, stimuli were displayed for 750ms. However, if the participant's accuracy were below 50%, stimulus duration would increase to 1000ms. Conversely, if the participant's accuracy were above 60%, stimulus duration would decrease to 500ms. Accuracy between 50 and 60% would result in stimulus duration remaining at, or reverting to, 750ms. Stimulus duration was updated every 40 trials. An inter-stimulus gap, in which the screen was a blank grey, remained constant at 750ms. This meant that the time period between the onset of stimulus n and the onset of stimulus $n+1$ could vary between 1250ms and 1750ms.

The EADT paradigm was previously described in the PhD thesis of Eric Anthony Lacey, entitled "Behavioural and Electrophysiological Aspects of Error Processing in Alzheimer's Disease and Healthy Ageing" [86].

Arm location	Action	Type	Probability
Not above target	Move towards target	Correct	0.7
	Move further from target	Error (FA condition)	0.2
	Grab	Error	0.1
Above target	Grab	Correct	0.65
	Step off target	Error (SO condition)	0.35

Table 3.1: Action probabilities for the Claw Task. Note that correct actions and grabbing errors were not considered as a part of this study, as the robot would always have information about whether it had performed a lateral movement or a grab action.

3.2.2.3 The Claw Task

In the Claw Task, the errors in question were committed by the machine and observed by the participants, as opposed to errors being committed by the participants themselves in the EADT. Thus, the Claw Task is similar to error-driven BCI scenarios in which users observe actions made by a machine [63, 64].

Here, participants were asked to observe a computer-controlled simulation of an arcade 'claw crane' game. Participants were shown a screen with 8 coloured circles arranged in a row and, above the circles, a virtual robotic arm, as shown in **Figure 3.2**. A single circle, selected at random at the start of each run, was designated as the target. This circle was coloured blue and marked with a score of +25 points. Every other circle was coloured red. The red circles immediately adjacent to the target were marked with a score of -10 points, and the scores marked on each circle decreased by a further 5 points with each step further from the target. The robotic arm began each run directly above a circle either 2 or 3 steps away from the target. Every 1.5s, the robotic arm would either move 1 step to the left, move 1 step to the right, or extend downward to grab the circle beneath it. Movements occurred instantaneously. The probability of each type of action occurring depended on whether or not the arm was positioned directly above the target circle. A table of action probabilities is shown in **Table 3.1**.

A score was also displayed in the top left corner of the screen. When a "grab" action was performed, the score would be updated according to the score marked on the circle that had been grabbed. After each "grab" action the run would finish and the screen would become completely black. Nine of the Claw Task participants were asked to silently count the number of times each movement error was made in each run, in an attempt

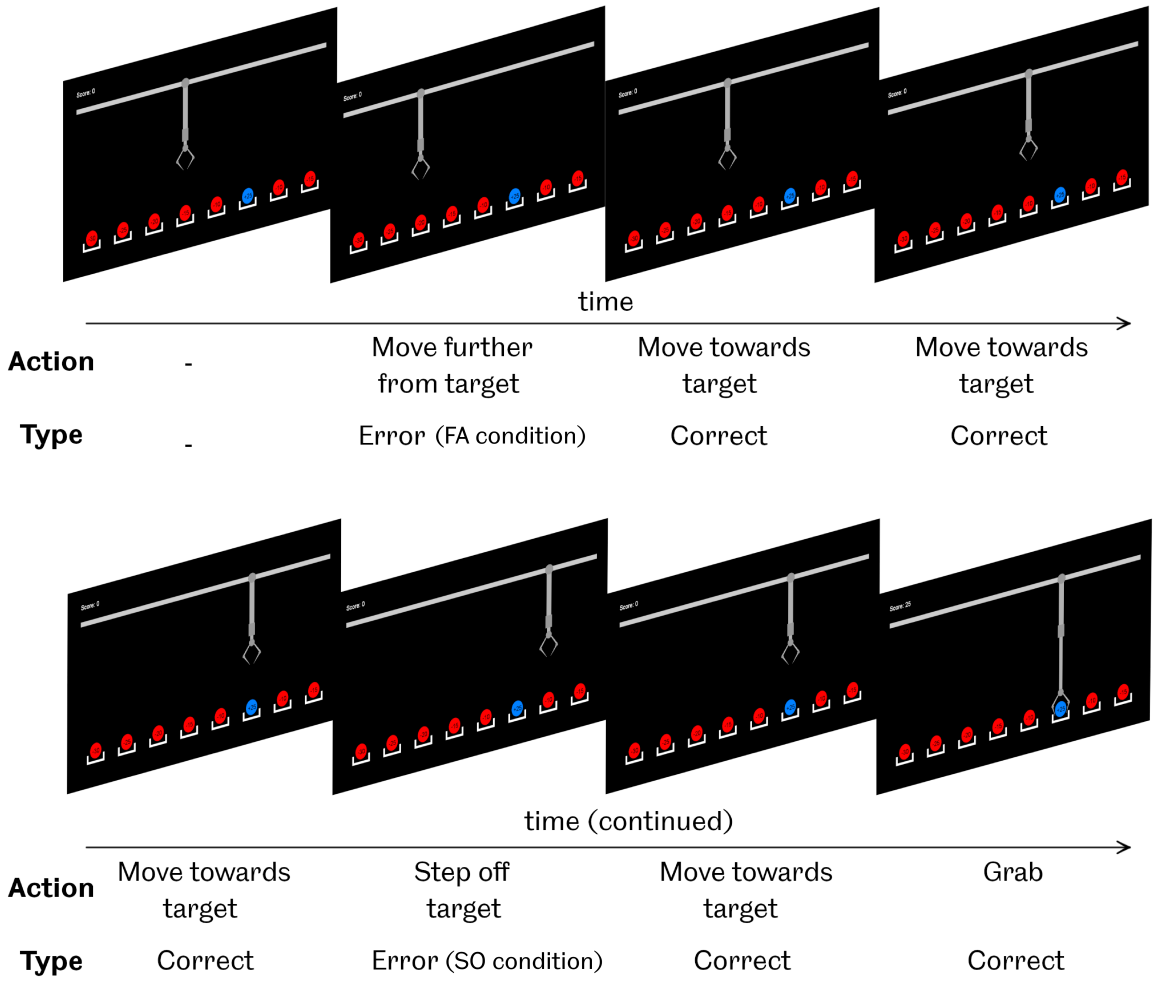

Figure 3.2: The Claw Task. Participants were asked to observe as a virtual robotic claw attempted to navigate towards, and grab, a blue target ball. If the claw was aligned over the target ball, possible actions were either to grab the ball or take 1 step away from the target. If the claw was not aligned over the target ball, possible actions were either to move 1 step towards the target, move 1 step further away from the target, or grab the red ball beneath the claw's current position.

to help them stay focused on the task. These participants were asked to write down the number of errors on a sheet provided at the end of each run. As such, the gap between the end of one run and the start of the next run was 10 seconds. The remaining eight Claw Task participants were not asked to perform the counting. For these participants, the gap between runs was 5 seconds. In either case, a beep would sound 1 second before the next run began. Participants were asked to refrain from movement and blinking during each run, but told that they could move and blink freely between runs, while the screen was blank.

This process repeated until the end of the block, with each block lasting approximately 4 minutes. The score was reset to 0 at the beginning of each new block.

The actions considered for this study were movement errors. Movements in which the virtual robot was aligned over one of the red non-target balls, and moved further away from the target, are hereafter referred to as "FA condition" errors. Movements in which the virtual robot was aligned over blue target ball, but stepped off it, are hereafter referred to as "SO condition" errors. A third error type was present in the task: a "grab error", when the robot grabbed a non-target ball. These errors occurred from a different type of movement than FA and SO condition errors, which both occurred as a result of lateral movements. The robot would always have information about whether it had made a lateral movement or a grab action. As such, in a BCI application, there would be no need to differentiate grab errors against other error types using EEG. Standard error detection applied following a grab action would be enough to identify them. For this reason, grab errors were not considered as a part of this study. The score was only updated after a "grab" action, and not after lateral movements (including either "FA condition" or "SO condition" errors), therefore no points were directly gained or lost as a result of either error condition. Considering this, together with the fact that each error was of the same magnitude (1 step), we considered them to be of similar severity.

Participants were asked to observe blocks, with breaks of as long as they wished between blocks, until they reported their concentration levels beginning to decrease. Most participants observed 6 blocks of trials. However, four participants observed 3-5 blocks, and three participants observed 7-8 blocks.

3.2.3 Data Analysis

For both tasks, EEG data were first resampled to 64Hz. In order to do this trials were first upsampled, then filtered using a least squares linear phase anti-aliasing FIR filter with a lowpass cutoff of 32Hz. The filtered data were then downsampled by averaging across data points, and initial data points from the output of filtering were removed to compensate for the delay introduced by the linear phase filter. This process was carried out using the *resample* function, from the MATLAB Signal Processing Toolbox, release 2018b [104]. After resampling, data were band-pass filtered from 1Hz to 10Hz, as ErrP components have been shown to occur at low frequencies [30, 51]. Event related spectral perturbation plots confirmed that activity for these tasks occurred predominantly in low frequencies, as shown in **Figure 3.3**. Zero-phase band-pass filters were created using the *filtfilthd* function from the MATLAB Central file exchange [92]. For the EADT, trials were included in cases where the error was followed by a secondary mouse click to indicate the participant's awareness of their error. Trials were extracted from a time window of -300ms to 700ms, relative to the

commission of each error (i.e. the initial, erroneous mouse click). Previous literature has shown evidence that participants' EEG may show signs of an error response before they commit the error [59]. As such, the EADT time window began before error commission. Errors of which the participants were unaware were not considered as part of the main investigations of this study. As the Claw Task involved errors committed by the machine, rather than the human, it would not have been pertinent to consider signals prior to error commission. Therefore, for the Claw Task, trials were extracted from a time window of 0ms to 1000ms, relative to the movement of the virtual robot. Each extracted error trial was baseline corrected relative to a period of 200ms immediately before the presentation of its related stimulus. Artefact rejection was performed by discarding any trials in which the range between the highest and lowest amplitudes, in any channel, was greater than 100μV. In EADT data, a mean of 1.9 colour condition trials and a mean of 3.0 repeat condition trials were rejected per participant, from overall means of 22.2 and 32.5 trials per participant for the two conditions respectively. In Claw Task data, a mean of 2.0 trials from the FA condition and a mean of 0.7 trials from SO condition were rejected per participant, from overall means of 48.8 and 23.4 trials per participant for the two conditions respectively. Further to this, independent component analysis (ICA) was performed on the pooled trials from all participants combined, for each task. Components resembling EOG artefacts, as identified by visual inspection of topographic maps, were filtered out of the data. Thus, one component was removed from the data related to each task, from a total of 64 components for the EADT and 20 components for the Claw Task. The remaining components for each task were then recombined. This process was carried out by running the *pop_runica*, *pop_selectcomps*, and *pop_subcomp* functions from EEGLAB in MATLAB release 2018b [34, 104]. A general visualisation of the full preprocessing methodology, applicable to both data analysis and classification, is shown in **Figure 3.4**.

Grand average time domain ErrP data were plotted using the extracted trials, showing the mean voltage $\pm$ 1 standard error of the following comparisons: EADT colour condition vs repeat condition in young adults, EADT colour condition vs repeat condition in older adults, and Claw Task FA condition vs SO condition in all participants. A small number of trials were excluded from the grand average time domain plots for the EADT, where the initial click had occurred at least 550ms after the presentation of the stimulus. This was due to the fact that longer reaction times could result in the presentation of stimulus *n+1*, which could occur 1250ms after stimulus n in the EADT, occurring within the time window (-300ms to 700ms, relative to the click) of stimulus n, and so the inclusion of these trials could have contaminated the late part of the grand average data with responses to these following stimuli. In total, 14 out of 717 colour condition trials and 12 out of 1181 repeat condition trials were excluded from these plots for this reason.

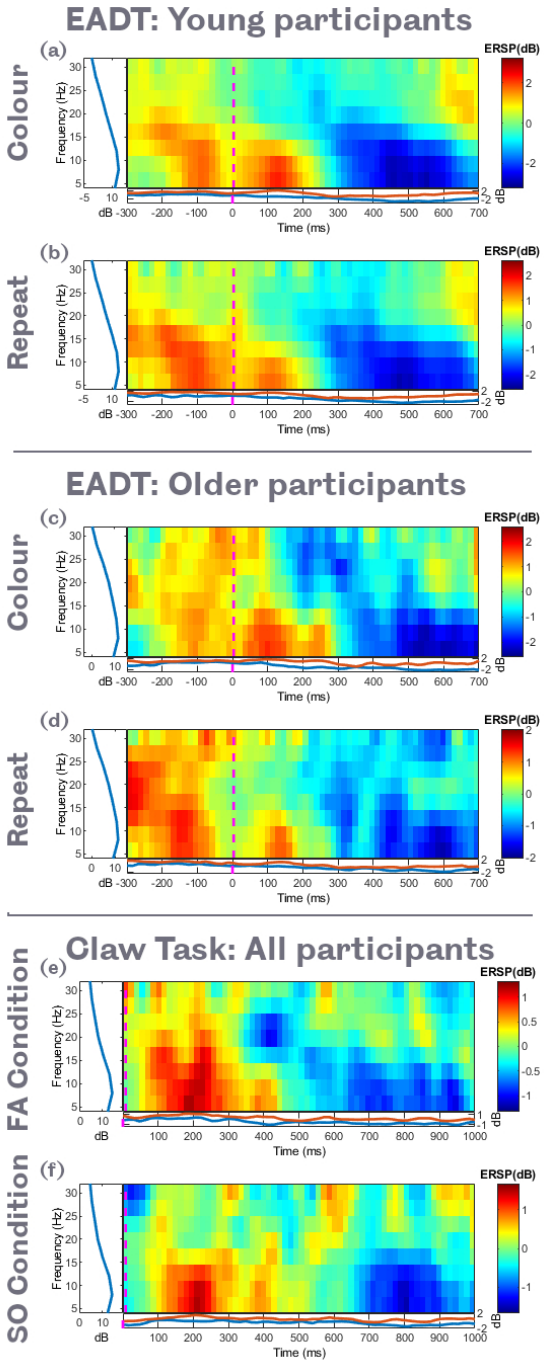

Figure 3.3: Grand average event related spectral perturbation plots, showing Cz data from (a) young EADT participants, colour condition, (b) young EADT participant, repeat condition, (c) older EADT participants, colour condition, (d) older EADT participants, repeat condition, (e) all Claw Task participants, FA condition, and (f) all Claw Task participants, SO condition.

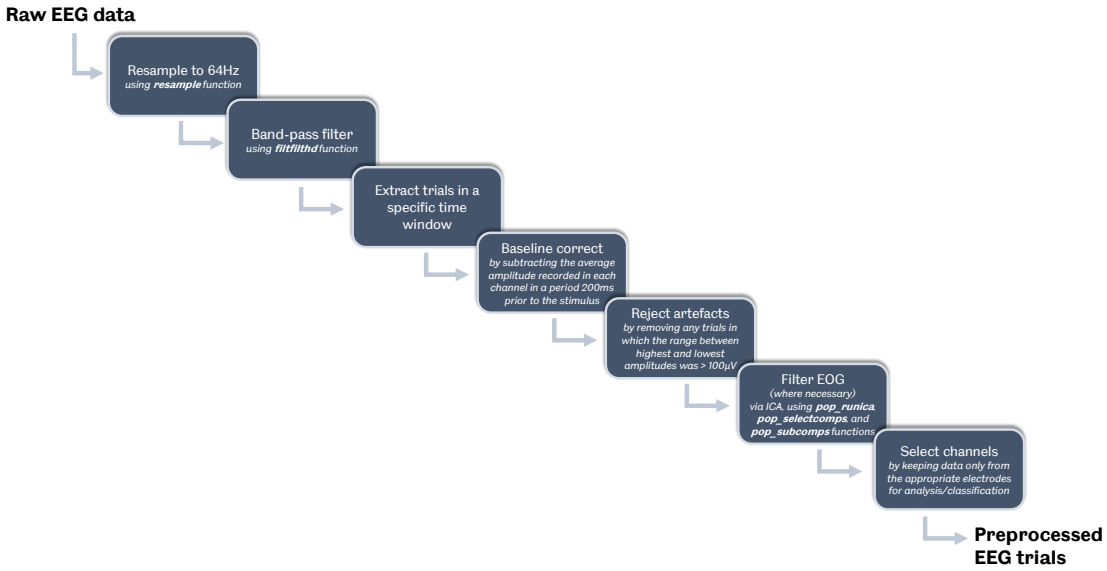

Figure 3.4: EEG data preprocessing. Band pass filter high and low frequencies, start and end time points of the time windows, and specific channels used, are all variable depending on the requirements of the analysis. For neurophysiological data analysis, artefact rejection occurred if the threshold were surpassed in any channel. For classification, artefact rejection occurred only if the threshold were surpassed in a channel that was intended to be used for classification. EOG filtering was only carried out if ICA indicated the presence of EOG artefacts.

Peak analysis was performed in order to identify the latencies at which ERN and Pe occurred in the ErrP data. This was carried out using the *findpeaks* function from the MATLAB Signal Processing Toolbox, release 2018b [104]. ErrP signals are known to be associated with midline electrodes [42]. Visual inspection of time domain ErrP and topographical plots showed high positive Pe activity around the central midline across all tasks and age groups, with the most notable amplitude difference between the classes being visible in Cz time domain data. As such, electrode site Cz was chosen as the most suitable channel for peak analysis for this study. In each task, this peak analysis was carried out on the grand average ErrP waveform related to each error condition, and also for the grand average ErrP of all trials of the two error conditions pooled together. In the EADT, the analysis was carried out seperately for each age group. For each group, the data were first averaged, and then peaks were identified in the resultant waveform. The ERN was identified as most prominent negative peak, and Pe as the highest positive peak, occurring in specific time windows. Time windows for ERN were -100ms to 200ms in the EADT, and 0ms to 300ms in the Claw Task. Time windows for Pe were 0ms to 400ms in the EADT, and 100ms to 600ms in the Claw Task. These time windows were selected based on a visual inspection of the time-domain data; ERN windows started slightly before the start of the negative deflection in grand average plots and centred on the negative peaks, and Pe windows began just before the start of the positive deflection and ended once amplitudes had returned approximately to baseline levels. As discussed earlier in this section, evidence has shown that some participants may show signs of an error response before they commit the error [59], hence the ERN time window in the EADT beginning 100ms prior to error commission. To check for statistically significant differences in peak latencies across error conditions, the same peaks were identified in the average time domain data for each individual participant with at least 12 trials per condition and at least 40 trials in total, as previous literature has suggested that a minimum of 12 trials are required to achieve a reasonable level of temporal stability of ERN and Pe, and that temporal stability increases with the number of trials [88]. Wilcoxon signed-rank tests were then carried out on these data, comparing the latencies identified in each of these participants' average time domain waveforms for the two conditions. To check for statistically significant differences in peak amplitude, the amplitude was calculated in each of these participants' average waveforms for each condition, in a 50ms window surrounding the ERN and Pe peaks identified in grand average data (from peak -25ms to peak + 25ms). Wilcoxon signed-rank tests were carried out to compare these amplitudes. Furthermore, the build-up rate of the Pe was calculated for the average waveform of each participant, in each error condition, for both tasks. This was achieved by performing a linear regression on a time window, 100ms in duration, ending at the identified Pe peak. This gives an indication of the rate at which the amplitude is

increasing up to the peak. Wilcoxon signed-rank tests were carried out to check whether the build-up rates of the different error conditions varied in a statistically significant way.

Topographical maps were then plotted for each error condition, using the same time windows. All topographical maps for a given task used the same scale, from the minimum value to the maximum values across all grand averages.

While the main focus of this study was on errors of which the participants were aware, a brief analysis was carried out to compare the number of "aware errors" (errors followed by an awareness click) vs "unaware errors" (errors not followed by an awareness click) in the EADT. The percentage of errors of which each participant was aware was calculated for each error condition in each task. Wilcoxon signed-rank tests were carried out in order to check whether there was any significant difference between awareness rates for the various conditions.

3.2.4 Classification

Broadly, the same classification protocol was followed for all participants of both tasks. However, different time windows were used to extract features for the two tasks. The protocol is described in this section.

3.2.4.1 Preprocessing

20 electrode channels were available in the Claw Task data (F7, F3, Fz, F4, F8, FC1, FC2, T7, C3, Cz, C4, T8, CP1, CP2, P3, Pz, P4, PO7, PO8, and Oz). As such, these 20 channels were used for single-trial classification of the both tasks. As with the neurophysiological analysis, data for classification were resampled to 64Hz and band-pass filtered between 1Hz and 10Hz. In the EADT, trials were extracted from -100ms to 400ms, relative to the commision of errors (i.e. the erroneous click), in cases where the participants showed awareness of the error. In the Claw Task, trials were extracted from 100ms to 700ms, relative to the virtual robot's movement. These time windows were selected based on visual inspection of grand average time domain data for each task, aiming to encapsulate the areas which indicated differences between the amplitudes of responses to the two conditions. Trials were baseline corrected to a period of 200ms immediately before presentation of the stimulus, and artefact rejection was performed to remove any trials with a range of greater than 100μV between the highest and lowest amplitude in any of the channels being used for classification. After this, remaining EOG artefacts were cleaned using ICA, as previously described in section 3.2.3.

As discussed in section 3.2.3, temporal stability of the ERN and Pe have been shown to increase with the number of trials, with a minimum of 12 trials being recommended to

achieve a reasonable level of stability [88]. As such, for the purpose of single-trial classification, we only included participants who had generated at least 12 trials per error condition, and a minimum of 40 trials overall.

Due to the experimental setup of the EADT, which involved participants clicking a mouse to confirm error awareness, motor movements would sometimes occur less than 400ms after error commission, i.e. within the classification time window. As such, it was important to ensure that the classification was based on error responses rather than sensorimotor rhythms. To this end, two analyses were carried out on the latency between error commission and awareness confirmation in the various error conditions. Firstly, for each participant, a Fisher's exact test was carried out on the number of trials that did contain awareness confirmation within the time window used for classification vs the number that did not, in each of the two error conditions. This test was to check, for each participant, whether significant classification could feasibly be achieved based on the presense or absence of sensorimotor rhythms. Secondly, for each participant in each task, Welch's t-test was carried out, comparing the latencies at which participants confirmed their error awareness, between the two error conditions. The latencies of mouse clicks, confirming error awareness, were included in the t-test if they occurred within the classification time window (-100ms to 400ms). Clicks outside this window were ignored as they were not deemed to have a potential effect on classification. The t-test was automatically marked as not significant if there were no awareness confirmations within the classification epoch. The purpose of this test was to act as a guide, for each participant, as to whether significant classification could feasibly have been achieved based on differences in the time at which awareness-based sensorimotor rhythms occurred. We were mindful that the classification results of this study could have been unfairly biased if we had included any participants for whom classification may have been possible due to differences between motor signals across the two conditions. Therefore, participants for whom a significant result ($p < 0.05$) was recorded, in either the Fisher's exact test or the t-test, were discarded from the classification phase.

After preprocessing, 25 participants remained to be used in the classification phase from the EADT (20 young, 5 older), and 14 remained from the Claw Task (8 asked to count errors, 6 not asked to count errors).

3.2.4.2 Feature Extraction

Our EEG data, having been resampled at 64Hz, contained 33 time points per trial in the EADT and 40 time points per trial in the Claw Task. If we were to consider all available time domain data, there would have been a total of 660 features (20 channels $\times$ 33 time points) or 800 features (20 channels $\times$ 40 time points) to describe each trial. Although we employed a minimum cutoffs of 12 trials per condition and 40 overall trials, many participants still had

relatively few trials per class. With the number of features given by the full time domain data greatly outweighing the number of trials per condition, it was clear that the curse of dimensionality could cause problems if we attempted to classify based on all available time domain data [72].

Our classification was performed using stepwise linear discriminant analysis (SWLDA), as described in section 3.2.4.3. However, the feature selection inherent in SWLDA is relatively sophisticated, and less complex methods are known to be less susceptible to overfitting [90]. Therefore, we opted to reduce the dimensionality by using a simpler first step for preliminary feature extraction. This allowed the SWLDA to be applied to a small number of highly discriminative selected features.

For each participant, the preliminary step was carried out as follows: For each time-domain feature (i.e. each time point in each channel), there were a set of training data points. Each point had an amplitude and an associated class label. A linear correlation coefficient was calculated between these amplitudes and class labels, resulting in each feature having an associated correlation coefficient. The correlation coefficients acted as a simple indication of how strongly related the amplitude was to the class labels in a given feature, and thus how separable the classes may be based on the amplitude. In each channel, the feature with the largest absolute correlation coefficient was selected. This meant that each trial was represented by 20 features.

3.2.4.3 Stepwise Linear Discriminant Analysis Implementation

In order to classify the data based on the most pertinent subset of the extracted features, SWLDA was chosen as our classification approach, since it has previously been shown to perform well in feature selection and classification of EEG data [38, 84, 148]. Stepwise regression was performed to select which features would be included in the model. Initially, an empty model was created. At each step, a regression analysis was performed on models with and without each feature, producing an F-statistic with a p-value for each feature. If the p-value of any feature was < 0.025, the feature with the smallest p-value would be added. Otherwise, if the p-value of any features already in the model had risen to > 0.075 at the current step, the feature with the largest p-value would be removed from the model. This process continued until no feature's p-value reached the thresholds for being added to, or removed from, the model. If no features were added to the model at all, a single feature with the smallest p-value would be selected. This feature selection process was performed using the *stepwisefit* function from the MATLAB Statistics and Machine Learning Toolbox, release 2018b [104]. Training and test trials were then reduced to the selected features. The class with the fewest training trials was oversampled in order to ensure that training occurred with an equal number of trials per class. A linear classification model was then trained and

tested. The model was trained using the *fitcdiscr* function, and each trial tested using the *predict* function, both from the MATLAB Statistics and Machine Learning Toolbox, release 2018b [104]. The SWLDA algorithm is visualised as a flowchart in **Figure 3.5**.

All classifiers were trained and tested using leave-one-out cross validation. For each iteration, one trial was selected as the test sample, and all the other trials were used as the training samples. Feature extraction and training of the stepwise linear model were then performed on the training samples. The model was then tested on the test sample. This process was repeated until each trial had been selected as the test sample. To test statistical significance of the classification, a right-tailed Fisher's exact test was performed on the confusion matrix of each participant's results. As the individual participants were independent, no p-value adjustments were necessary [136]. Therefore, classification for an individual was deemed to be significant if the p-value was less than 0.05. In order to test the significance at a group level, individual p-values were combined into a group p-value using Fisher's method [60, 99]. To test whether there was any difference in the efficacy of the classification strategy across age groups, Welch's t-test was carried out comparing the overall accuracies of all young adults with those of older adults in the EADT.

3.3 Results

3.3.1 Neurophysiological Analysis of Error-Related Potentials

Peak analysis was used to identify ERN and Pe latencies based on the grand average Cz time domain waveform for each combination of task, condition, and age group. The identified latencies are shown in **Table 3.2**.

Wilcoxon signed-rank tests were carried out to check for statistically significant differences in the ERN and Pe amplitudes and latencies generated in response to the different error conditions, as discussed in section 3.2.3. The results of these tests are shown in **Table 3.3**.

3.3.1.1 Error Awareness Dot Task

In the grand average ErrP of young adults in the EADT, responses to both conditions showed ERN with latencies of 44ms, as can be seen in **Figure 3.6** (blue and red lines). Wilcoxon signed-rank test showed no significant difference between the amplitudes of these ERNs (see **Table 3.3**), and showed no significant difference between the ERN latencies related to the two conditions, based on peaks identified in Cz data of each participant's average waveform ($p = 0.42$). However, there was a clear difference between the error conditions in the Pe. While the latencies of the Pe in response to the two conditions showed no

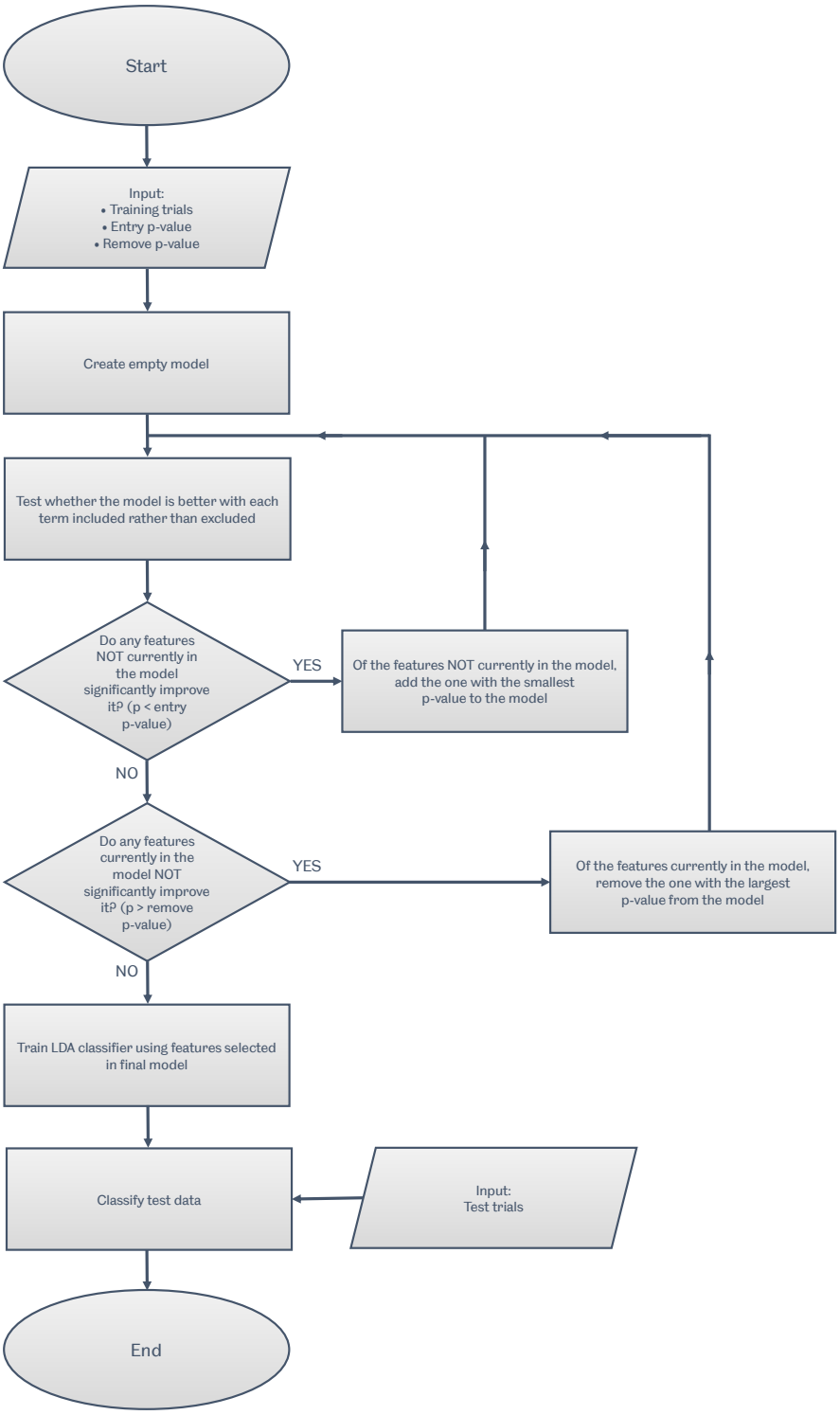

Figure 3.5: Stepwise Linear Discriminant Analysis flowchart.

Grand Average Peak Latency Identification			
ERN			
	Colour Condition	**Repeat Condition**	**Pooled Trials**
EADT, young	44ms	44ms	44ms
EADT, older	59ms	59ms	59ms
	FA condition	**SO condition**	**Pooled Trials**
Claw Task	78ms	141ms	78ms
Pe			
	Colour Condition	**Repeat Condition**	**Pooled Trials**
EADT, young	216ms	247ms	231ms
EADT, older	200ms	247ms	215ms
	FA condition	**SO condition**	**Pooled Trials**
Claw Task	281ms	344ms	328ms

Table 3.2: ERN and Pe latencies, relative to error commission, as identified by peak analysis on the grand average channel Cz time domain waveform. The most prominent negative peak, between -100ms and 200ms in the EADT, or between 0ms and 300ms in the Claw Task, relative to error commission, was selected as the ERN. The highest positive peak, between 0ms and 400ms in the EADT, or between 100ms and 500ms in the Claw Task, relative to error commission, was selected as the Pe.

Condition Comparisons				
	ERN Amplitude		**ERN Latency**	
	p-value	**Significant**	**p-value**	**Significant**
EADT, young	0.42	No	0.91	No
EADT, older	0.94	No	0.69	No
Claw Task	0.22	No	0.72	No
	Pe Amplitude		**Pe Latency**	
	p-value	**Significant**	**p-value**	**Significant**
EADT, young	*0.003*	*Yes*	0.47	No
EADT, older	*0.016*	*Yes*	0.15	No
Claw Task	0.19	No	*0.032*	*Yes*

Table 3.3: Wilcoxon signed-rank test results from comparisions of peak amplitudes and latencies of colour condition vs repeat condition (EADT) and FA condition vs SO condition (Claw Task). Comparisons were performed at ERN and Pe sites, in young adults and older adults, using electrode site Cz. Amplitude comparisons were based on the mean amplitude recorded, for each subject, in ERN and Pe time windows 50ms in duration, from -25ms to 25ms relative to the peak latencies identified by grand average peak analysis. Latency comparisons were based on the peak latencies identified from each participant's average time domain data for each condition.

significant difference ($p = 0.47$), the amplitudes of the Pe were increased in the colour condition, compared to the repeat condition ($p = 0.003$). The build-up rate of the Pe was also greater in the colour condition than the repeat condition, and a Wilcoxon signed-rank test showed that this distinction was statistically significant ($p = 0.001$). Topographical maps confirmed negative fronto-central activity during the ERN, and positive centro-parietal activity during the Pe, in response to both error conditions, as shown in **Figure 3.7 a, b, e, and f**.

Participants of all ages indicated awareness of a higher proportion of colour condition errors (mean 89.3%, SD 17.7%) than repeat errors (mean 76.4%, SD 23.5%). A Wilcoxon signed-rank test showed that this difference was significant ($p = 8.7 \times 10^{-8}$).

In the older adults' EADT data, early positivity stalls the ERN, and some differences between the error conditions can be seen in the time domain data prior to error commission, as shown in **Figure 3.6** (green and brown lines). However, the difference between responses to the conditions was not found to be significant in older adults at the ERN. As with younger adults, the latencies of the ERN and Pe showed no significant difference ($p = 0.69$ and $p = 0.15$, respectively). While the build-up rate of the Pe was appeared to be steeper in response to the colour condition than the repeat condition, a Wilcoxon signed-rank test did not find this to be significant in older EADT participants ($p = 0.25$). Again, the most notable difference between the two error conditions was the greater amplitude of the Pe in the colour condition, as compared to the repeat condition ($p = 0.016$).

Both ERN and Pe peaks were observed to be more positive in older adults than young adults, in response to both error conditions. Welch's t-tests confirmed that that these age-related amplitude differences were statistically significant ($p = 2.1 \times 10^{-15}$ for colour condition related ERN amplitudes, $p = 5.4 \times 10^{-8}$ for colour condition related Pe amplitudes, $p = 3.1 \times 10^{-20}$ for repeat condition related ERN amplitudes, and $p = 5.4 \times 10^{-13}$ for repeat condition related Pe amplitudes).

The typical fronto-central negativity cannot be identified by visual inspection of the topographical maps of the ERN in response to either error condition for older adults' EADT data (**Figure 3.7 c-d**). A posterior-anterior shift in aging (PASA) has been reported in previous literature [33, 53] and is evident here in the Pe related to both conditions of the EADT. As discussed previously, the most positively active areas during the Pe are centro-parietal in young adults, as shown in **Figure 3.7 e-f**. In older adults, this shifts toward more fronto-central activity, in both the colour condition and the repeat condition, as can be seen in **Figure 3.7 g-h**. Indeed, the electrode sites with the highest grand average Pe amplitudes in young adults were CPz & Cz for the colour condition, and CPz & Pz in the repeat condition. In older adults, the highest grand average Pe amplitudes were found at electrode sites FCz and FC1, for both error conditions.

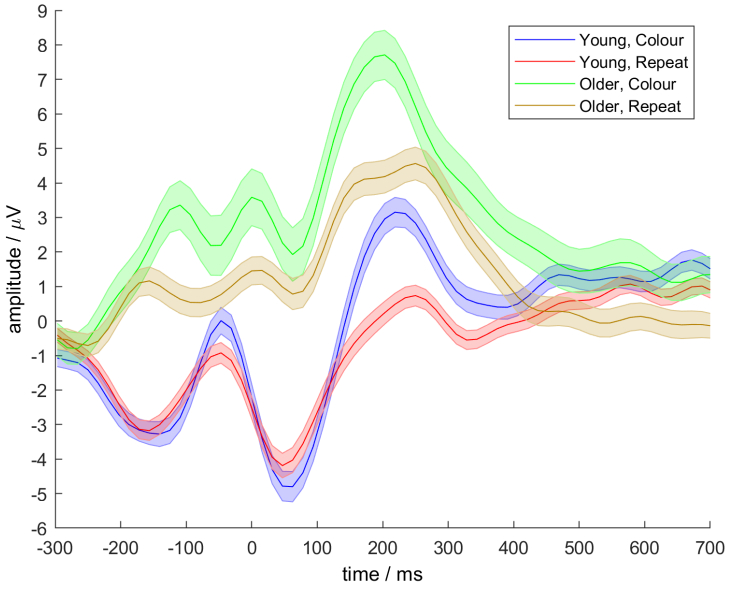

Figure 3.6: Grand average time domain EADT data at electrode site Cz. Time shown is relative to error commission. Central lines represent mean signals. Shaded areas cover 1 standard error. Blue lines show colour condition data from young adults. Red lines show repeat condition data from young adults. Green lines show colour condition data from older adults. Brown lines show repeat condition data from older adults.

Across all EADT participants, mean amplitudes for individual channels in the selected time windows ranged from $-11.1\mu V$ to $8.1\mu V$, and their associated standard deviations ranged from $0.04\mu V$ to $1.3\mu V$. Further topographical maps showing the standard deviation from the mean at each channel in the EADT are shown in **Figure 3.8a-h**.

3.3.1.2 Claw Task

Time domain data related to responses to the Claw Task can be seen in **Figure 3.9**. Here, no statistically significant difference was found between either the latency or amplitude of the ERN ($p = 0.72$ and $p = 0.22$, respectively). In contrast to the EADT, neither the amplitude of the main Pe peak, nor the build-up rate of the Pe showed signifigant differences ($p = 0.19$ and $p = 0.60$, respectively). However, the latencies of the Pe peaks, at their highest points, were found to be significantly different ($p = 0.032$), with the Pe in responses to the SO condition peaking later than that related to the FA condition.

A secondary component of the Pe also appeared to be present in the grand average Claw Task data, and appeared to be more prominent in response to the SO condition than the FA condition, followed by a difference in grand average amplitudes. We identified that

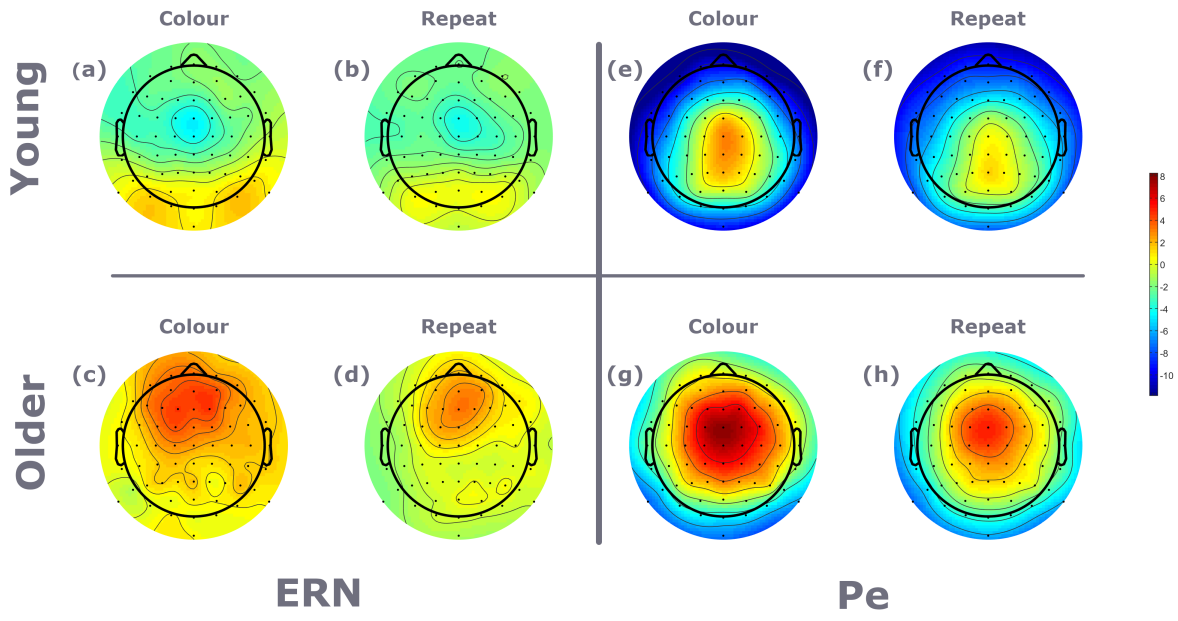

Figure 3.7: Grand average topographical maps of EADT data. Maps were plotted based on a 50ms window surrounding the peaks identified as ERN and Pe from grand average data across all participants. Plots shown represent (a) ERN in the colour condition in young adults, (b) ERN in the repeat condition in young adults, (c) ERN in the colour condition in older adults, (d) ERN in the repeat condition in older adults, (e) Pe in the colour condition in young adults, (f) Pe in the repeat condition in young adults, (g) Pe in the colour condition in older adults, and (h) Pe in the repeat condition in older adults.

the maximum difference here occurred at 538ms (see **Figure 3.9** for illustration), and performed a further Wilcoxon signed-rank test on the amplitudes of the two conditions in the 50ms window surrounding this latency. The difference in amplitudes at this point was found to be statistically significant ($p = 6.1 \times 10^{-4}$).

Topographical maps showed broad, slightly negative amplitudes across the brain during the ERN of the Claw Task, in response to both error conditions, as shown in **Figure 3.10 a and c**. Slightly more positive amplitudes can be seen in fronto-central regions in response to the FA condition. During the Pe, strong positive activity can be seen in central and centro-parietal regions, as shown in **Figure 3.10 b and d**.

Mean amplitudes for individual channels in the time window ranged from $-1.1\mu V$ to $5.4\mu V$, and their associated standard deviations ranged from $0.01\mu V$ to $0.8\mu V$. Further topographical maps showing the standard deviation from the mean at each channel in the Claw Task are shown in **Figure 3.8i-l**.

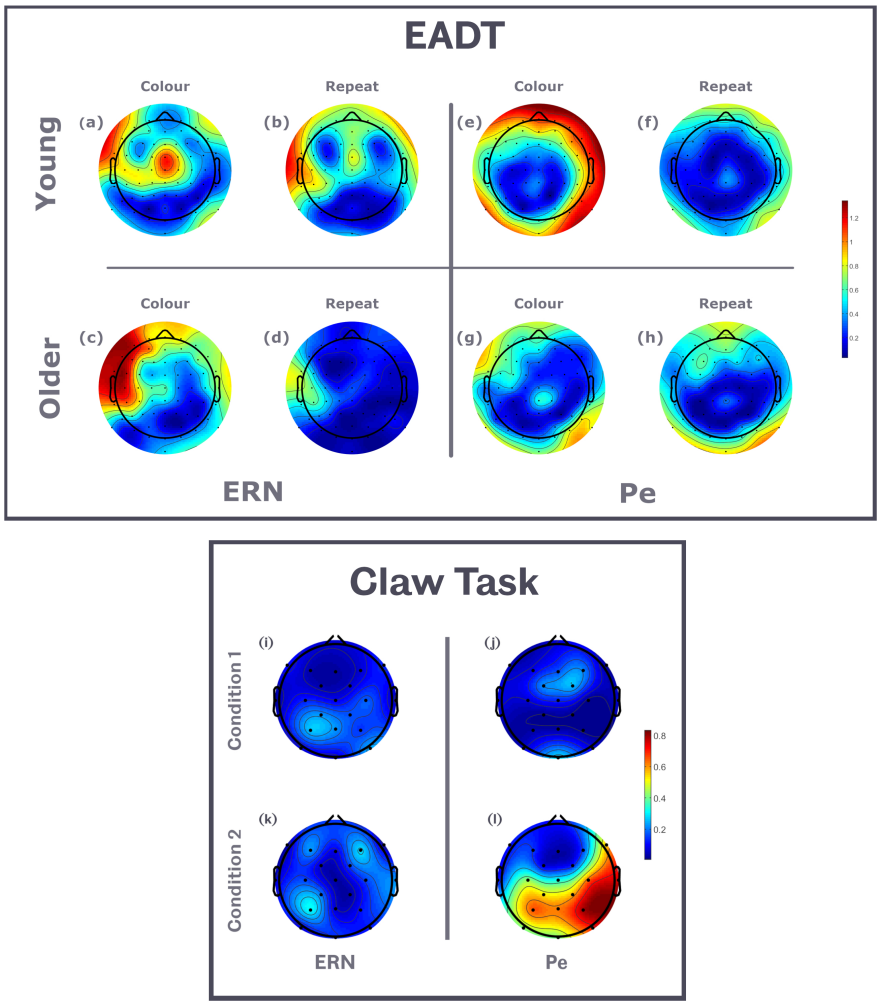

Figure 3.8: Topographical maps showing the standard deviation from the mean amplitude at each channel, during a 50ms window surrounding the latencies identified as the ERN and Pe. Subfigures represent the following: (a) Young EADT participants at the ERN for the colour condition, (b) young EADT participants at the ERN for the repeat condition, (c) older EADT participants at the ERN for the colour condition, (d) older EADT participants at the ERN for the repeat condition, (e) young EADT participants at the Pe for the colour condition, (f) young EADT participants at the Pe for the repeat condition, (g) older EADT participants at the Pe for the colour condition, (h) older EADT participants at the Pe for the repeat condition, (i) all Claw Task participants at the ERN for the FA condition, (j) all Claw Task participants at the Pe for the FA condition, (k) all Claw Task participants at the ERN for the SO condition, (l) all Claw Task participants at the Pe for the SO condition.

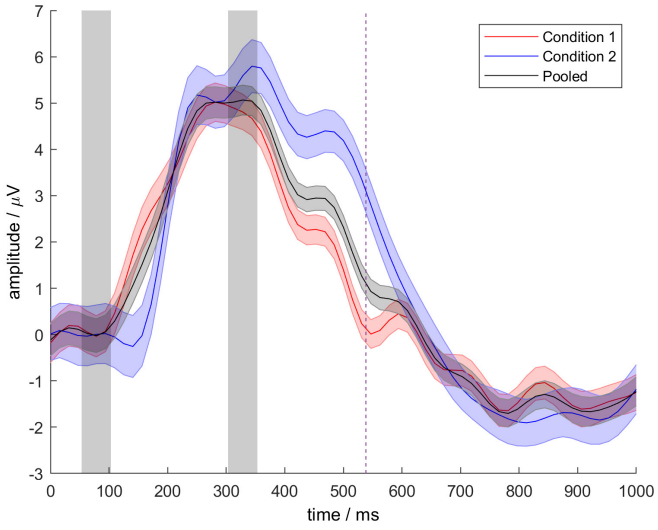

Figure 3.9: Grand average time domain Claw Task data at electrode site Cz. Time shown is relative to the erroneous movement of the robot. Central lines represent mean signals. Shaded areas cover 1 standard error. Red line shows FA condition data from all participants. Blue line shows SO condition data from all participants. Black lines represent data from both conditions pooled together. Translucent grey vertical bands represent the time windows identified as ERN and Pe by peak analysis on pooled data. Windows show 50ms, from -25ms to 25ms relative to the identified peaks. Dashed purple line at 538ms represents latency of largest difference between conditions following the secondary component of the Pe.

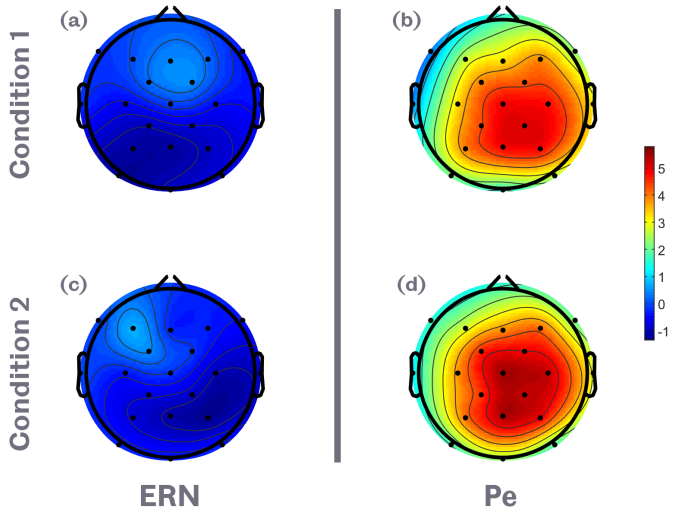

Figure 3.10: Grand average topographical maps of Claw Task data. Maps were plotted based on a 50ms window surrounding the peaks identified as ERN and Pe from grand average data across all participants. Plots shown represent (a) ERN in the FA condition, (b) ERN in the SO condition, (c) Pe in the FA condition, and (d) Pe in the SO condition.

3.3.2 Reporting of Classification Accuracy

There are two common ways in which system-wide classification accuracy is reported in studies such as this. One option is to report the overall accuracy, i.e. the percentage of trials, of any class, that were classified correctly. This provides a good overview of how the system performs in the true context of the trials with which it is presented. However, one drawback is that it can be misleading if performance is very strong in one class but weak in others. For example, a system faced with 80% of trials from class 1 and 20% of trials from class 2 could achieve high overall accuracy simply by classifying every trial as class 1, but this would not be a useful classifier. An alternative is to report the balanced accuracy, i.e. the accuracy is recorded for each class, and the mean of these is reported. Conversely, this approach does take into account the performance on all classes, but loses some information regarding the true context in which the classifier operates.

Here, for a full picture of the classifier's performance, we present the overall accuracy, but also report the accuracy in each class separately. Furthermore, statistical significance of the classification for each subject is tested via a Fisher's exact test on the confusion matrix of true and classified labels for each subject. Therefore, this is not unduly influenced by the majority class.

3.3.3 Classification of EADT Errors

The classification accuracies achieved for each individual participant in the EADT are shown in **Table 3.4**. The mean overall accuracy for all EADT participants was 65.2%. Amongst young adults, mean overall accuracy was 63.7%, and for older adults it was 71.3%. Mean colour condition accuracy was 60.4% for all participants, 59.4% for young adults, and 60.4% for older adults. The mean accuracy of the repeat condition was 67.6% for all participants, 66.0% for young adults, and 74.0% for older adults. Trained classification models for the EADT included a mean of 3.7 ± 1.3 features. Generally, more features were selected from posterior regions of the brain than anterior regions, echoing the heightened activity, varying in amplitude across the two classes, that was shown in these regions. A Wilcoxon signed-rank test was used to compare the average number of features selected per channel, for each participant, in more anterior channels (fronto-central channels and further anterior) against those in more posterior channels (centro-parietal channels and further posterior). The results showed the average number of selected features per channel was significantly higher in the posterior region compared to those in the anterior region ($p = 4.9 \times 10^{-4}$). At an individual level, features were often selected where the subject-average amplitude displayed a relatively large differences between the two classes. **Figure 3.11** contains a further breakdown of feature selection rates, including an example for an individual EADT participant.

Statistically significant separation of the error conditions ($p < 0.05$) was found, using Fisher's exact tests, for 17 of the 25 participants overall (68.0%). Statistical significance was achieved for 13 of the 20 young adults (65.0%), and 4 of the 5 older adults (80.0%). At a group level, the classification results were found to be statistically significant in each age group ($p = 1.6 \times 10^{-16}$ for young adults and $p = 3.2 \times 10^{-11}$ for older adults) and overall ($p = 2.7 \times 10^{-25}$).

The overall accuracies of young adults were compared with those of older adults using Welch's t-test. The result did not show any significant difference ($p = 0.16$). While Welch's t-test is considered to be reliable in dealing with unequal sample sizes [35,138], it should be noted that only 5 older adults remained in the single-trial classification, which may mean that this finding should be treated with a measure of caution.

3.3.4 Classification of Claw Task Errors

The classification accuracies achieved for each individual participant in the Claw Task are shown in **Table 3.5**. The mean overall accuracy for all Claw Task participants was 65.6%. Mean accuracy for the FA condition was 69.5%, and the mean accuracy for the SO condition was 57.4%. Welch's t-test compared the overall accuracy achieved for participants who were

Age Group	**Subject**	**# Colour Trials**	**# Repeat Trials**	**Colour Accuracy**	**Repeat Accuracy**	**Overall Accuracy**	**Significant**	**p-value**
Young	1	27	27	55.6%	48.1%	51.9%	No	0.5
	2	34	42	58.8%	69.0%	64.5%	Yes	0.014
	3	15	35	60.0%	74.3%	70.0%	Yes	0.024
	4	29	55	65.5%	70.9%	69.0%	Yes	0.0014
	5	21	26	57.1%	61.5%	59.6%	No	0.16
	6	30	38	50.0%	60.5%	55.9%	No	0.27
	7	14	31	42.9%	58.1%	53.3%	No	0.60
	8	17	57	58.8%	74.6%	71.1%	Yes	0.012
	9	41	53	64.3%	63.0%	63.5%	Yes	0.0071
	10	33	43	57.6%	65.1%	61.8%	Yes	0.041
	11	22	34	72.2%	70.6%	71.4%	Yes	0.0017
	12	26	42	50.0%	64.3%	58.8%	No	0.16
	13	32	51	75.0%	76.5%	75.9%	Yes	4.5×10^{-6}
	14	25	46	52.0%	76.1%	67.6%	Yes	0.017
	15	25	51	68.0%	72.5%	71.1%	Yes	8.7×10^{-4}
	16	20	29	55.0%	75.9%	67.3%	Yes	0.029
	17	30	30	46.7%	56.7%	51.7%	No	0.50
	18	42	45	61.9%	51.1%	56.3%	No	0.16
	19	33	58	66.7%	67.2%	67.0%	Yes	0.0017
	20	28	45	69.0%	64.4%	66.2%	Yes	0.0049
Older	21	17	47	41.2%	61.7%	56.3%	No	0.52
	22	*45*	*33*	*80.0%*	*81.8%*	*80.8%*	*Yes*	4.8×10^{-8}
	23	21	47	76.2%	63.8%	67.6%	Yes	0.0024
	24	19	35	63.2%	80.0%	74.1%	Yes	0.0021
	25	13	46	61.5%	82.6%	78.0%	Yes	0.0034
Young	**Mean**	**27.2**	**41.9**	**59.4%**	**66.0%**	**63.7%**	**65.0%**	**Group p-value**
	SD	*7.7*	*10.3*	*8.6%*	*8.3%*	*7.2%*		$\mathbf{1.6 \times 10^{-16}}$
Older	**Mean**	**23.0**	**41.6**	**64.4%**	**74.0%**	**71.3%**	**80.0%**	**Group p-value**
	SD	*12.6*	*7.0*	*15.3%*	*10.3%*	*9.8%*		$\mathbf{3.2 \times 10^{-11}}$
All	**Mean**	**26.4**	**41.8**	**60.0%**	**67.6%**	**65.2%**	**68.0%**	**Group p-value**
	SD	*8.7*	*9.6*	*10.1%*	*9.1%*	*8.2%*		$\mathbf{2.7 \times 10^{-25}}$

Table 3.4: Single-trial classification results of EADT data. Overall accuracy calculated as the percentage of trials, of either class, correctly classified. SD refers to standard deviation. The participant for whom the highest overall accuracy was achieved is highlighted in italics. Group p-values were calculated by combining p-values using Fisher's method.

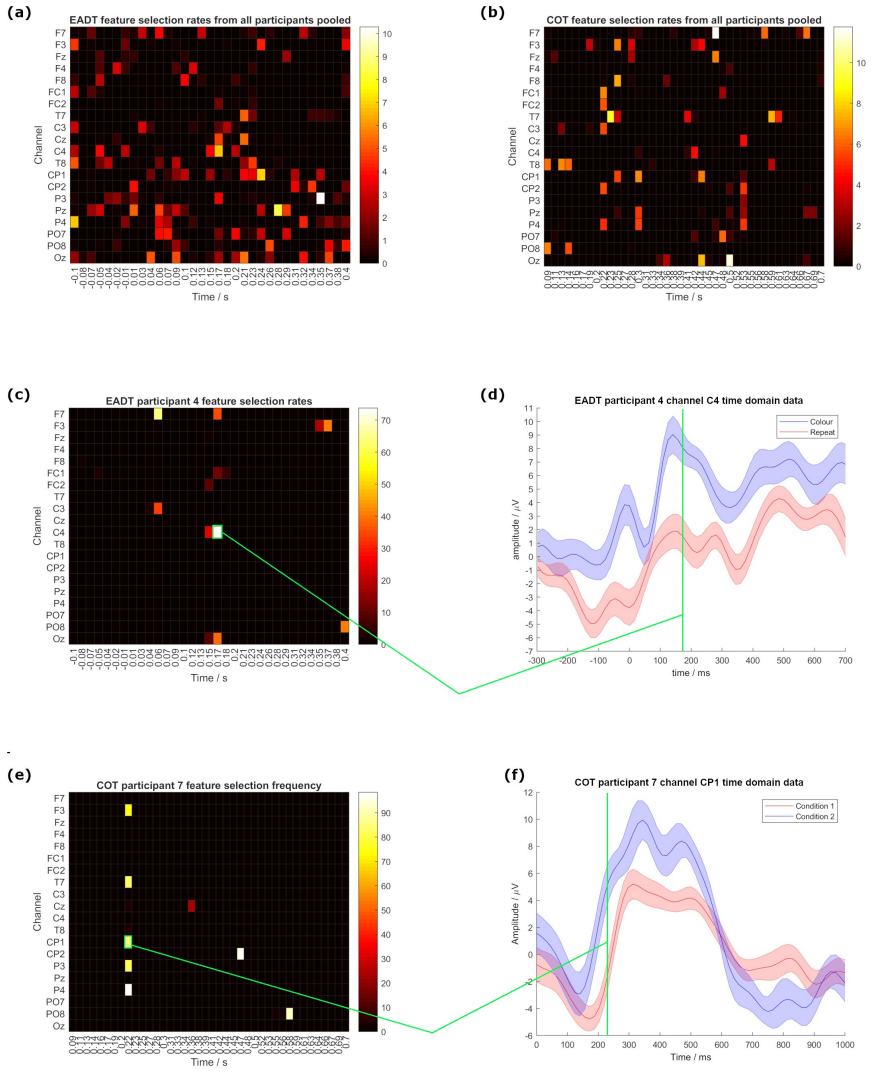

Figure 3.11: Heatmaps showing the percentage of trials in which each feature (i.e. combination of time point and channel) was selected in classification models, and time domain data related to commonly-selected features. Heatmap x-axes show time points, y-axis show channels, and colour represents the percentage of classification models for which each feature was selected during the leave-one-out cross validation procedure. (a) shows feature selection data from all EADT participants pooled together. (b) shows feature selection data from all Claw Task participants pooled together. (c) shows individual feature selection data from participant 4 of the EADT. (d) shows time domain data from EADT participant 4, channel C4, with green highlighting showing the link between a commonly selected feature in the heatmap, and the corresponding time-domain data. (e) shows individual data from participant 7 of the Claw Task. (f) shows time domain data from Claw Task participant 7, channel CP1, with green highlighting showing the link between a commonly selected feature in the heatmap, and the corresponding time-domain data.

Subject	# FA condition Trials	# SO condition Trials	FA condition Accuracy	SO condition Accuracy	Overall Accuracy	Significant	p-value
1	42	27	66.7%	63.0%	65.2%	Yes	0.015
2	92	30	72.8%	53.3%	68.0%	Yes	0.0088
3	69	22	58.0%	40.9%	53.8%	No	0.63
4	43	23	65.1%	52.2%	60.6%	No	0.13
5	46	29	73.9%	65.5%	70.7%	Yes	8.2×10^{-4}
6	*30*	*14*	*86.7%*	*64.3%*	*79.5%*	*Yes*	*0.0011*
7	48	18	79.2%	72.2%	77.3%	Yes	1.8×10^{-4}
8	46	29	69.6%	62.1%	66.7%	Yes	0.0069
9	49	21	77.6%	47.6%	68.6%	Yes	0.036
10	33	19	63.6%	52.6%	59.5%	No	0.20
11	34	21	58.8%	42.9%	52.7%	No	0.56
12	39	26	64.1%	61.5%	63.1%	Yes	0.038
13	44	13	70.5%	61.5%	68.4%	Yes	0.040
14	32	22	65.6%	63.6%	64.8%	Yes	0.032
Mean	**46.2**	**22.4**	**69.4%**	**57.4%**	**65.6%**	**71.4%**	**Group p-value**
SD	*16.4*	*5.4*	*8.0%*	*9.2%*	*7.6%*		**1.9×10^{-11}**

Table 3.5: Single-trial classification results of Claw Task data. Overall accuracy calculated as the percentage of trials, of either class, correctly classified. SD refers to standard deviation. The participant for whom the highest overall accuracy was achieved is highlighted in italics. The group p-values was calculated by combining p-values using Fisher's method.

asked to keep count of the errors (subject IDs 7-14) against those who were not (subject IDs 1-6). No significant difference was identified ($p = 0.80$). Trained classification models for the Claw Task included a mean of 2.9 ± 1.5 features. At a population level, it was difficult to discern clear patterns of which features were selected. However, as in the EADT, an individual level features were often selected where there was a relatively large difference between the subject-average amplitudes of the classes. **Figure 3.11** contains a further breakdown of feature selection rates, including an example for an individual Claw Task participant.

Statistically significant separation of the error conditions ($p < 0.05$) was found, using Fisher's exact tests, for 10 of the 14 participants (71.4%) in the Claw Task. At a group level, the classification results were found to be statistically significant ($p = 1.9 \times 10^{-11}$).

3.4 Discussion

3.4.1 Distinctions in Responses by Condition and Age

Previous literature has shown that different tasks can elicit differing ErrP waveforms [173]. In some cases, distinctions have been shown in ErrPs even when the errors are committed during variants of the same task [66,115]. Indeed, our findings are aligned with those of the previous literature on this point. Interestingly, when comparing the error conditions within

each task, the key neurophysiological distinctions that we were able to identify were found in different components of the ErrP for the two tasks in this study.

In the EADT, the clearest distinction shown between the error conditions was in the amplitude of the Pe. We witnessed greater amplitudes of Pe in the colour condition than the repeat condition for both young and older adults. Previous studies, including some which were based on error awareness tasks, have shown a diminished Pe in errors of which participants are unaware, compared to errors of which they are aware [39, 110, 113, 118]. Here, in the case of the colour condition, all necessary information for the participant to know whether they have committed an error is present, on-screen, in the current stimulus. With the repeat condition, however, participants are relying on their memory of the previous stimulus to determine whether or not they have committed the error. Indeed, Wilcoxon signed-rank tests found that participants were significantly more likely to be aware that they had committed a colour condition error than a repeat condition error. While this study was focused on trials in which participants signified awareness of their errors, it is possible that participants could be more confident in their assertion of the error for some trials than others. It is possible, therefore, that the higher amplitude of the Pe in the colour conditions, compared to the repeat conditions, is due to greater certainty and confidence that an error was committed. Previous studies have also identified the build-up rate of the Pe as a marker of evidence accumulation for error detection [111]. In young adults, the build-up rate to the Pe was found to be significantly greater in the colour condition than the repeat condition. This is a further indication that a greater degree of awareness may be present in the case of colour condition errors than repeat condition errors.

Some distinctions were also noted between the different age groups in the EADT. Older participants' responses were found to generate more positive amplitudes at both the ERN and Pe latencies, for both error conditions. A posterior-anterior shift in aging was also identified in the spatial distribution of the Pe.

In the Claw Task, the most notable difference in time domain data appeared to result from a secondary component of the Pe. This occurred at around 500ms, causing an increase in the amplitude of responses to the SO condition compared to those of the FA condition in the grand average signals. This gap remained until beyond 600ms. A Wilcoxon signed-rank test found the amplitude difference, at its widest point (538ms) to be statistically significant ($p = 6.1 \times 10^{-4}$). As discussed in section 3.1, secondary Pe components have previously been identified, and have been linked to conscious, evaluative processes [5,40]. This suggests that the SO condition, in which the virtual robot steps off the target, having been aligned above it, elicits stronger responses in the aware aspect of the error response.

3.4.2 Single-Trial Classification

Across all participants who were included in the classification stage, we achieved a mean overall accuracy of 65.2% for the EADT data, and 65.6% for the Claw Task data. The associated standard deviations were relatively high (8.2% and 7.6% respectively) as, although statistically significant classification was not possible for some participants, high classification rates were achieved for others. Indeed, in the best cases, for both tasks, the error conditions were classified against each other with around 80% overall accuracy. Group p-values calculated using Fisher's method showed that, at a population level, statistically significant separation of the error conditions was achieved ($p = 2.7 \times 10^{-25}$ for the EADT and $p = 1.9 \times 10^{-11}$ for the Claw Task). As a proof of concept, these classification accuracies show that it is possible to classify these subtly different error conditions, which could not be differentiated by previously explored metrics such as direction or severity, against each other using single-trial EEG.

A Welch's t-test, comparing the results of young adults with those of older adults, returned non-significant results. Though this finding should be taken tentatively, due to the small number of older participants included in the classification phase, it suggests that our chosen classification strategy is robust across different age groups, despite some age-related neurophysiological differences.

In previous literature regarding error decoding, a wide variety of classification accuracies have been reported. When classifying errors against non-errors, some studies have been able to achieve very high single-trial classification rates. For example, SVM-based classification models have been used to achieve average accuracies of 80% [6] or even above 90% [75], deep learning approach achieved average accuracy of 84% [159], and Gaussian models have been reported to achieve a high of around 90% [121].

Classification of different error conditions against each other can be considered more challenging than error vs non-error classification as the EEG signals in response to errors are expected to be more similar to each other than to the signals of non-errors. Nonetheless, some errors have been classified against each other on a single trial basis with a high level of success. In a virtual robot reaching task, performed by 2 participants, Iturrate et al. reported correct classification of left vs right sided errors with an impressive 90% accuracy [64]. Furthermore, in the same study, they were able to distinguish small vs larger errors with around 75% accuracy. Spüler and Niethammer reported an overall accuracy of 75.5% for the classification of execution errors against outcome errors (i.e. errors committed by a machine vs errors committed by a human) during a computer game task [151]. However, they did not find significant differences between movement errors occurring at different angles, highlighting the potential difficulty of differentiating errors based on subtle differences.

One of the challenges in error decoding is that data sets for error trials may be small, as errors often occur more rarely than correct actions, both in real-world scenarios [75] and experimental paradigms [123]. Small sample sizes are known to be challenging in classification problems [67, 131]. This is exacerbated when attempting error vs error classification, as the error trials are divided into still smaller groups. Indeed, for both tasks of the present study, we were able to achieve higher classification accuracy for the class with more training samples, on average.

Given the challenges of comparing such similar error conditions as the ones in this study, we believe that the results are encouraging. Separation of the error conditions was above chance level for most participants across both tasks. While mean overall classification rates did not reach the accuracy of the most successful studies discussed above, this study has shown that it is indeed feasible to classify ErrPs of different error conditions against each other based on differences in cognitive process, or in the context of differing expected actions. The fact that overall accuracy of around 80% was achieved for some participants is particularly encouraging. In future, it may be interesting to investigate the use of other classification techniques such as those discussed above, especially if larger training sets are available, with the aim of increasing classification accuracy further.

3.4.3 Implications for BCI

Error detection is becoming an increasingly useful aspect of BCI [30]. It has proven to be utilisable in increasing the accuracy of existing BCI control techniques, such as motor imagery [47] and P300 [144], by performing immediate error correction [177]. Furthermore, error detection has been successfully integrated into various BCI systems as feedback for reinforcement learning (RL) strategies, allowing the systems to gradually improve over time [25,63,75,179]. As discussed in section 3.1, this creates the possibility of BCI becoming more autonomous [63, 179]. RL-based systems such as these can work effectively as long as the classification accuracy exceeds chance level [30, 63].

It has been shown, in previous literature, that different errors can elicit different ErrP waveforms [13, 150]. Recently, a few studies have begun to classify different errors using single-trial EEG, based on aspects such as the direction of the error [64], the severity of the error [64], or whether the error was committed by the human themselves or by a machine [151].

In the Claw Task, we presented a scenario in which a virtual robot was attempting to navigate towards, and grab, a target object among several non-target objects. This scenario could be used in an error-driven BCI. Each robot action would be followed by single-trial EEG classification, to tell the robot what kind of action the human had observed. If we employed simple error detection, we would be able to tell the robot when it had made an

incorrect move. However, with the error categorisation displayed in this study, an extra layer of detail could be switched on for participants with statistically significant separation. In the case of FA condition errors, we could tell the robot that the target is in the other direction, but is not in the adjacent location. In the case of the SO condition errors, we could tell the robot precisely that the target is in the location it just stepped away from. These principles could be applied to a number of BCI-based navigation or target selection scenarios.

Investigating the EADT allowed us to provide further evidence that errors can be categorised in the absence of previously used metrics, with only subtle difference between error conditions.

Statistically significant classification accuracy was achieved for the vast majority of the participants included in the classification phase in our study. Thus, the error categorisation displayed here is accurate enough to be utilised in a BCI, for immediate and specific error correction, or as an integral part of a learning system. This opens up the potential for more detailed information to be garnered about the category of error that has occurred, thus allowing for a BCI with more effective error correction and more efficient error-driven learning.

3.5 Conclusion

The error conditions considered in this study were very similar to one another. Nevertheless, due to the different cognitive processes required to recognise the errors in the EADT, and the different contexts in which the errors occurred in the Claw Task, we were able to identify differences between the grand average ErrP waveforms of the different error conditions. In the EADT, the clearest distinction between the error conditions was found in the amplitude of the Pe. The colour conditions generally elicited greater amplitudes than the repeat conditions, leading us to speculate that the increased Pe in these conditions could be due to greater certainty that an error had been committed. In the Claw Task we found distinctions in a secondary component of the Pe. These distinctions led us to speculate that participants may have had a heightened anticipation of a correct action when the virtual robot was aligned above the target, ready to grab it.

Interestingly, we were able to classify the error conditions of both the EADT and the Claw Task, the latter of which could be directly applied in a BCI, with over 65% mean overall accuracy, and around 80% in the best cases. Classification rates were above chance level ($p < 0.05$) for most participants, of those included in the classification phase of the study, for both tasks, and group-level analysis showed the single-trial separation of the different error conditions to be highly significant overall ($p = 2.7 \times 10^{-25}$ for the EADT

and $p = 1.9 \times 10^{-11}$ for the Claw Task). The ability to classify such similar errors using single-trial EEG, as we have shown here, is very promising for the future prospect of making error-driven BCI more efficient through the acquisition of more detailed information.

I believe that the findings of this chapter uncover new opportunities in brain-machine interaction, pushing towards a more autonomous BCI.

Chapter 4

Classifying Different Correct Actions Against Each Other

The findings presented in this chapter have been previously published in Frontiers in Neuroscience [163]

4.1 Chapter Introduction

In the previous chapter, I concluded that it is possible to classify different error conditions against each other, even when the different conditions have only subtle differences such as the context in which they occur, and the cognitive load required to recognise them. As such, the first objective of this project has been achieved. The next objective is to move beyond errors, and to investigate the possibility of distinguishing the brain signals generated in response to different correct actions. This objective is explored in the current chapter.

As discussed in previous chapters, studies concerning robotic movement and navigation tasks have previously used EEG to investigate the brain's responses to observing correct and erroneous movements. These studies have shown that it is possible to classify the responses to correct movements against erroneous ones on a single-trial basis [30,63,75,179], and to subclassify different types of erroneous conditions [64, 151, 161], as well as showing that correct-vs-error classification can be used as feedback for reinforcement-learning-based BCI [63,75,179]. These interesting advances have created the possibility of systems in which machines can control the low-level action decisions in order to navigate semi-autonomously towards a target, with feedback provided via implicit communication with a user through brain signals spontaneously generated while observing the task [63, 179].

However, none of these previous studies have investigated whether it is possible to classify EEG responses to different types of correct actions against each other. In most

navigation tasks, it is crucial not only to know that you are moving in the correct direction, but also to recognise when you have reached your destination. As such, it is highly important to consider whether there are significant neurophysiological differences between the brain's responses to observing different correct movements: those that get closer to a target, compared to those that actually reach it.

To address this question, we evaluated data from a virtual robotic navigation task. Participants were asked to observe a virtual robot, represented by a cursor, navigating in a 1-dimensional space and attempting to reach a target. We then investigated the EEG responses to movements that reached the target (hereafter referred to as the "TR condition", short for "target reached"), in contrast to the responses to movements towards the target, but not reaching it (hereafter referred to as the "TT condition", short for "towards target").

To explore neurophysiologicial distinctions between the TT condition and the TR condition, we used time domain features to compare the latency and amplitude of key features of the event related potentials (ERPs). We also examined the spatial distribution of EEG responses to each condition, using topographical maps.

Our main focus was on the P300. As discussed in section 2.5, P300 peaks are known to be generated when an observer notices a target stimulus in a sequence containing both target and non-target stimuli.

Unlike many previous studies utilising the P300 for robotic control, and similar applications, in our study each stimulus (i.e. each movement) was only presented once, and so our classification phase required single-trial classification. Single trial classification of the presence of a P300 signal, versus its absence, is challenging in itself. Our goal was to differentiate the P300s elicited in response to two slightly different desired actions. This presents an extra challenge, as we can expect the signals of the conditions to be more similar to each other.

In this study, the desired stimulus is either a movement towards the target or, in cases when the virtual robot is adjacent to the target location, a movement that reaches the target. We hoped to identify and exploit differences between responses to these stimuli, arising from both the experimental differences and the participants' cognitive response to the two conditions. With regard to experimental differences, actions reaching the target occur less frequently than other correct moves, and target-to-target interval is known to affect P300 amplitude [52]. With regard to cognitive responses, reaching the target may be considered more important than other correct moves — the P300 may therefore be affected as it has been shown to be associated with positive outcomes [58], and its amplitude has been shown to be affected by reward magnitude [140, 169, 171]. We then aimed to use the identified neurophysiological differences in order to classify the EEG responses to the two conditions against each other on a single-trial basis.

In order to classify responses to the conditions against each other, we implemented a stepwise linear discriminant analysis strategy, using time domain features from 6 electrode sites to generate subject-specific classification models. A second publicly available data set [29], gathered from participants observing a similar 1-dimensional navigation paradigm, was used to further validate the efficacy of the classification strategy. We tested our approach using data from 10 healthy young adults from the first task, and a further 5 healthy young adults from the second task.

4.2 Methods

This study uses data from two tasks. Neurophysiological analysis and single-trial classification were performed on data from a task we refer to as the Cursor Task. These data were recorded at the University of Sheffield, UK. Data from a a similar task, referred to as the Publicly Avaliable Cursor Task (PACT), were used in order to further validate the single-trial classification section of the study. This was an open access data set, obtained under a Creative Commons Attribution - Non Commercial - No Derivatives 4.0 International licence, based on a study by Chavarriaga and Millán [29].

4.2.1 Participants

10 healthy adults (4 female, 6 male, mean age 27.30 $\pm$ 8.31) were recruited to participate in the Cursor Task. All of these participants were included in all aspects of the study. All participants had normal or corrected-to-normal vision. They reported no history of psychiatric illness, head injury, or photosensitive epilepsy. Written informed consent was provided by all participants before testing began. All procedures were in accordance with the Declaration of Helsinki, and were approved by the University of Sheffield Ethics Committee in the Automatic Control and Systems Engineering Department.

6 healthy adults (1 female, 5 male, mean age 27.83 $\pm$ 2.23) performed the PACT. 1 participant was excluded from this study as too few trials were available after artefact rejection.

4.2.2 Experimental Setup

4.2.2.1 EEG Setup

For the Cursor Task, 8 channels of EEG were recorded at 500Hz using an Enobio 8 headset. The electrode sites recorded were Fz, Cz, Pz, Oz, C3, C4, P07, and PO8. A further reference electrode was placed on the earlobe.

For the PACT, 64 channels of EEG were recorded at 512Hz using a BioSemi ActiveTwo system, and were referenced to the common average. Electrodes were placed using the 10-20 system.

4.2.2.2 The Cursor Task

In the Cursor Task, participants were seated in front of a screen and asked to observe a computer controlled cursor. Participants were presented with 9 squares, arranged in a horizontal line, on a black background, as seen in Figure 4.1. The cursor's current square was coloured blue. The target square was identified by a red bullseye symbol on a white background. All other squares were plain white.

At the beginning of each run, the cursor appeared 2 or 3 squares away from the target location, either to the left or the right. Every 2 seconds, either the cursor would move to an adjacent square, or a yellow box would be drawn around the cursor's current position in order to identify that the computer believed that it had reached the target. Such target identification could occur correctly or erroneously. Actions occurred with preset probabilities, which depended on whether or not the cursor was on the target. These probabilities are shown in Table 4.1.

After the target was identified, either correctly or erroneously, the run finished and the screen was cleared. After 5 seconds, the next run began. A beep sounded 1 second before the start of each run. Participants were asked to refrain from movement and blinking during each run, but told that they could move and blink freely between runs, while the screen was blank. This process repeated until the end of the block, with each block lasting approximately 4 minutes.

Each participant performed a single session of observations. Participants were asked to observe blocks, with breaks of as long as they wished between blocks, until they reported their concentration levels beginning to decrease. Most participants observed 6 blocks of trials. However, two participants observed only 2 blocks. On average, Cursor Task participants observed a total of 149.2 $\pm$ 40.0 (mean $\pm$ standard deviation) TT condition trials, and 82.3 $\pm$ 20.0 TR condition trials.

4.2.2.3 The Publicly Avaliable Cursor Task

In the Publicly Avaliable Cursor Task (PACT), participants were similarly asked to observe the 1-dimensional movement of a computer-controlled cursor. 20 locations were arranged in a horizontal line across a screen. The cursor was displayed as a green square. The target was displayed as a blue square when it appeared to the left of the cursor, or a red square when it appeared to the right of the cursor.

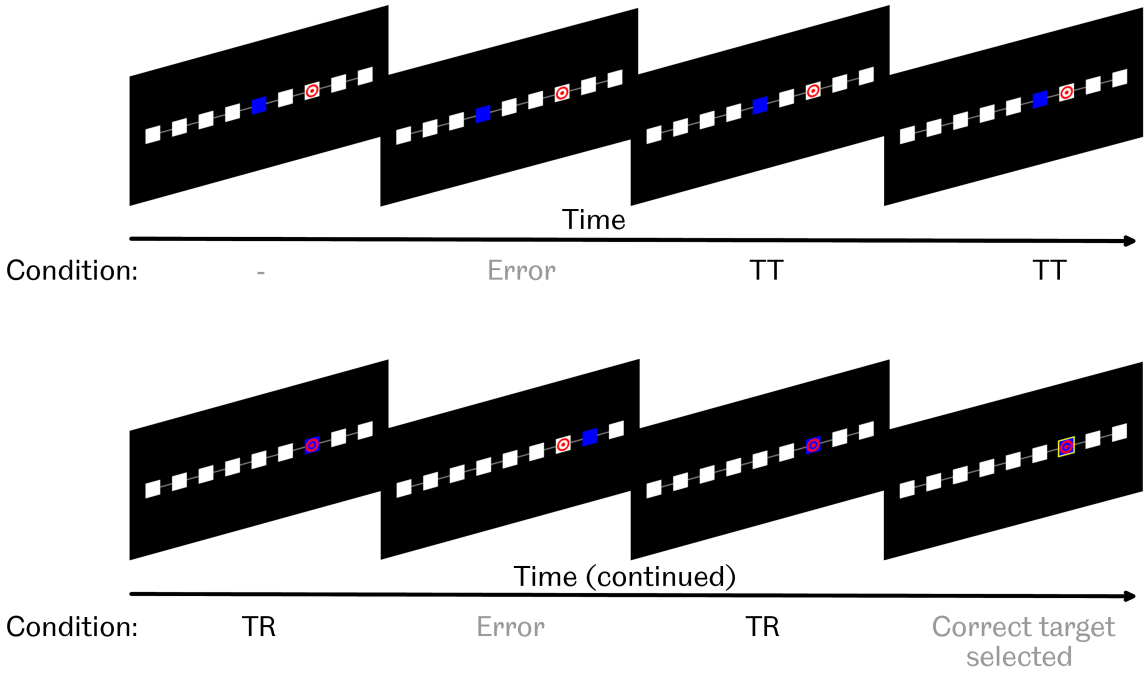

Figure 4.1: The Cursor Task paradigm. Participants were asked to observe as a blue cursor attempted to navigate towards, and select, a marked target square. If the cursor was on the target, possible actions were either to select it by drawing a yellow box around the square, or take 1 step away from the target. If the cursor was not on the target, possible actions were either to move 1 step towards the target, move 1 step further away from the target, or erroneously select the current square as the target by drawing a yellow box around it. "TT" condition refers to "towards target" i.e. movements towards, but not reaching, the target. "TR" condition refers to "target reached" i.e. movements that did reach the target.

At the beginning of a run, the target was drawn no more than 3 positions away from the cursor. Every 2 seconds, the cursor would move either towards or away from the target with preset probabilities, shown in Table 4.1. Unlike the Cursor Task, no target identification was required by the computer. Instead, each run ended when the cursor reached the target. After this, the cursor stayed in its existing location, and a new target was drawn, again no more than 3 positions away from the cursor. This process repeated until the end of the block, with each block lasting 3 minutes.

Participants each performed two sessions of observations. Each session consisted of 10 blocks. The number of days between sessions varied between participants, from a minimum of 50 days to a maximum of more than 600 days. On average, PACT participants observed a total of 620.2 $\pm$ 10.6 TT condition trials, and 277.7 $\pm$ 14.1 TR condition trials.

Task	Cursor location	Action	Probability
Cursor Task	Not on target	Move towards target	0.7
		Move further from target	0.2
		Identify location as target	0.1
	On target	Identify location as target	0.67
		Step off target	0.33
Publicly Avaliable Cursor Task	Not on target	Move towards target	0.8
		Move further from target	0.2

Table 4.1: Action probabilities for Tasks 1 and 2. Note that each run in the PACT ended once the cursor reached the target. As such there were no moves from an on-target position in the PACT. In both tasks, both TT and TR conditions occurred as a result of "move towards target" actions. If these actions occurred when the cursor was adjacent to the target, the result would be reaching the target (i.e. TR condition). If the cursor was not adjacent to the target prior to the action, the result would be moving closer to the target, but not reaching it (i.e. TT condition).

4.2.3 Neurophysiological Analysis

Data from the Cursor Task were used for neurophysiological analysis. As we did not have control over the experimental paradigm for the PACT, and so did not have a precisely detailed picture of how the stimuli were presented, we opted not to perform neurophysiological analysis on PACT data, instead using these only to further validate the classification phase of this study.

Raw data from the Cursor Task were resampled to 64Hz, using the *resample* function, from the MATLAB Signal Processing Toolbox, release 2018b [104]. Data were then band-pass filtered from 1Hz to 10Hz, using a zero-phase Butterworth filter, created using the *filtfilthd* function from the MATLAB Central file exchange [92]. TT and TR Trials were extracted from a time window of 0ms to 1000ms, relative to the movement of the cursor. All extracted trials were baseline corrected relative to a period of 200ms immediately before the movement of the cursor. Artefact rejection was performed by discarding any trials in which the range between the highest and lowest amplitudes, in any channel, was greater than 100μV. A general visualisation of the full preprocessing methodology, applicable to both data analysis and classification, can be seen in the previous chapter, in **Figure 3.4**. Note that the EOG filtering phase was not performed for this data set, as ICA did not reveal any clear EOG artefacts that would be necessary to filter out. This is most likely due to the lack of anterior electrodes used for this experiment.

Grand average time domain event related potential (ERP) data were plotted using the extracted trials, showing the mean voltage $\pm$ 1 standard error, comparing responses to the

TT condition with those to the TR condition.

Peak analysis was performed in order to identify the latencies at which the P300 occurred in the ERP data. This was carried out using the *findpeaks* function from the MATLAB Signal Processing Toolbox, release 2018b [104]. Visual inspection of time domain ERP and topographical plots indicated that the highest P300 amplitude in this study occurred at electrode site Cz, and that there was a difference in P300 amplitudes in response to the two conditions at this site. As such, Cz was chosen as the most suitable channel for peak analysis. This peak analysis was carried out on the grand average ERP for responses to each condition. Subsequently, the P300 was identified as the highest positive peak, occurring between 200ms and 500ms. This time window was selected based on a visual inspection of the grand average time-domain data. To check for statistically significant differences in peak latencies, the same analysis was carried out to find the P300 peak in the average responses of each individual participant, for both conditions. According to one-sample Kolmogorov-Smirnov tests, we could not assume the data to be normally distributed. Therefore, a Wilcoxon signed-rank test was performed to compare the peak latencies identified for the two conditions.

To check whether there was a statistically significant difference in peak amplitude between responses to the two conditions, the mean amplitude was calculated in the responses the average responses of each individual participant, in a time window from 200ms to 500ms in order to encapsulate the full breadth of the P300. According to one-sample Kolmogorov-Smirnov tests, we could not assume the data to be normally distributed. Therefore, a Wilcoxon signed-rank test was performed to compare the amplitudes identified for the two conditions.

Topographical maps were then plotted for responses to each condition, using a 50ms window surrounding the P300 latency (from peak - 25ms to peak + 25ms) as identified in the pooled data from all trials of both conditions combined. All topographical maps used the same scale, from the minimum value to the maximum values across all grand averages.

4.2.4 Single-Trial Classification

Single-trial classification was performed on data from both tasks. The same classification protocol was followed for both data sets, and is described in this section.

4.2.4.1 Preprocessing and Feature Extraction

Data from 6 electrode sites were used for single-trial classification: Fz, Cz, Pz, Oz, PO7, and PO8. These channels were selected based on visual inspection of grand average time domain ERPs, and considering prior knowledge related to these sites. The P300 has shown

to peak in midline electrodes [127], and posterior sites such as PO7 and PO8 are associated with visual processing [37, 145, 165]. As with the neurophysiological analysis, data were resampled at 64Hz, trials were baseline corrected to a period of 200ms immediately before presentation of the stimulus, and artefact rejection was performed to remove any trials with a range of greater than 100μV between the highest and lowest amplitude in any channel. For the classification phase, data were band-pass filtered between 1Hz and 32Hz. This band was selected after visual inspection of event-related spectral perturbation (ERSP) data which showed that, while most activity occurred at low frequencies, some potentially useful activity was also present in higher frequencies. Trials were extracted from 200ms-700ms relative to the movement of the cursor. This window was selected based on visual inspection of grand average time domain ERPs. Selecting this window results in 33 samples per channel. Thus, in total, each trial was represented by 198 (6×33) features.

Previous literature has suggested that a minimum of 20 trials are required to provide stability in the P300 [31]. As such, we implemented a minimum cut-off of 20 artefact-free trials per class, in order to ensure we had enough data to produce a reliable training set. 1 participant was excluded from the single-trial classification phase of this study due to this cutoff.

4.2.4.2 Classification with Stepwise Linear Discriminant Analysis

In order to classify the data based on the most relevant subset of features, stepwise linear discriminant analysis was chosen as our classification approach, as previous literature has shown this strategy to be effective at both feature selection and classification of both P300 [38, 83, 84, 96, 148] and motion-onset visual evoked potential (mVEP) EEG data [57]. An individual classification model was generated for each participant, using only the data from that individual participant's responses to the task. Firstly, for a given participant, an initial subset of features was selected. The amplitudes of the training trials for each condition were compared in each feature (i.e. each combination of channel and time point) using an unequal variances t-test. Features whose p-value was less than 0.05 were included in the initial feature set. The stepwise procedure was then performed to select which features would be included in the final model. At each step, a regression analysis was performed on models with and without each feature, producing an F-statistic with a p-value for each feature. If the p-value of any feature was less than 0.05, the feature with the smallest p-value would be added. Otherwise, if the p-value of any features already in the model had risen to > 0.10 at the current step, the feature with the largest p-value would be removed from the model. This process continued until no feature's p-value reached the thresholds for being added to, or removed from, the model. This feature selection process was performed using the *stepwisefit* function from the MATLAB Statistics and Machine Learning Toolbox,

release 2018b [104] If no features were added to the model at all, a single feature with the smallest p-value would be selected. Training and test trials were then reduced to the selected features. A flowchart visualising the SWLDA algorithm can be seen in the previous chapter, in **Figure 3.5**.

The training set for the condition with the fewest training trials was oversampled in order to ensure that training occurred with an equal number of trials per condition. A linear classification model was then trained and tested. The model was trained using the *fitcdiscr* function, and each trial tested using the *predict* function, both from the MATLAB Statistics and Machine Learning Toolbox, release 2018b [104]. All classifiers were trained and tested using leave-one-out cross validation. To test statistical significance of the classification, a right-tailed Fisher's exact test was performed on the confusion matrix of each participant's results. In order to test whether the classification was significant at a group level, individual p-values were combined into a group p-value using Fisher's method [60, 99].

4.3 Results

4.3.1 Neurophysiological Distinctions

In the responses to both conditions, grand average time domain ERPs showed a broad P300 peak, as can be seen in Fig. 4.2 a. Fig. 4.2 b and c show examples of time domain ERPs from individual participants (1 and 10, respectively). In both conditions, the shape of the broad P300 featured a peak shortly prior to 300ms, followed by a slight drop in amplitude, and then a secondary peak, shortly after 400ms. In responses to the TR condition, the earlier peak was found to have the highest amplitude, at a latency of 265ms. The secondary peak marked the highest amplitude in grand average responses to the TT condition, with a latency of 420ms. However, the Wilcoxon signed-rank test did not find a significant difference between the P300 peak latencies of responses to the two conditions ($p = 0.81$).

A distinction was seen between the P300 amplitudes of responses to the two conditions. The TR condition was observed to elicit a P300 with a greater amplitude than that generated in response to the TT condition. The Wilcoxon signed-rank test comparing the amplitudes of the two conditions, based on a time window from 200-500ms in order to encapsulate the breadth of the P300, found this difference in amplitude to be statistically significant ($p = 0.004$).

Topographical maps plotted at the P300 peak latency showed the main activation to occur in the central midline, in response to both conditions, as can be seen in Fig. 4.3.

We observed some features in the ERP responses to both conditions which may be related to motion-onset visual evoked potentials (mVEP). Such mVEPs occur when users percieve the beginning of movement of an object or symbol on a screen [14,57,85,102]. Three

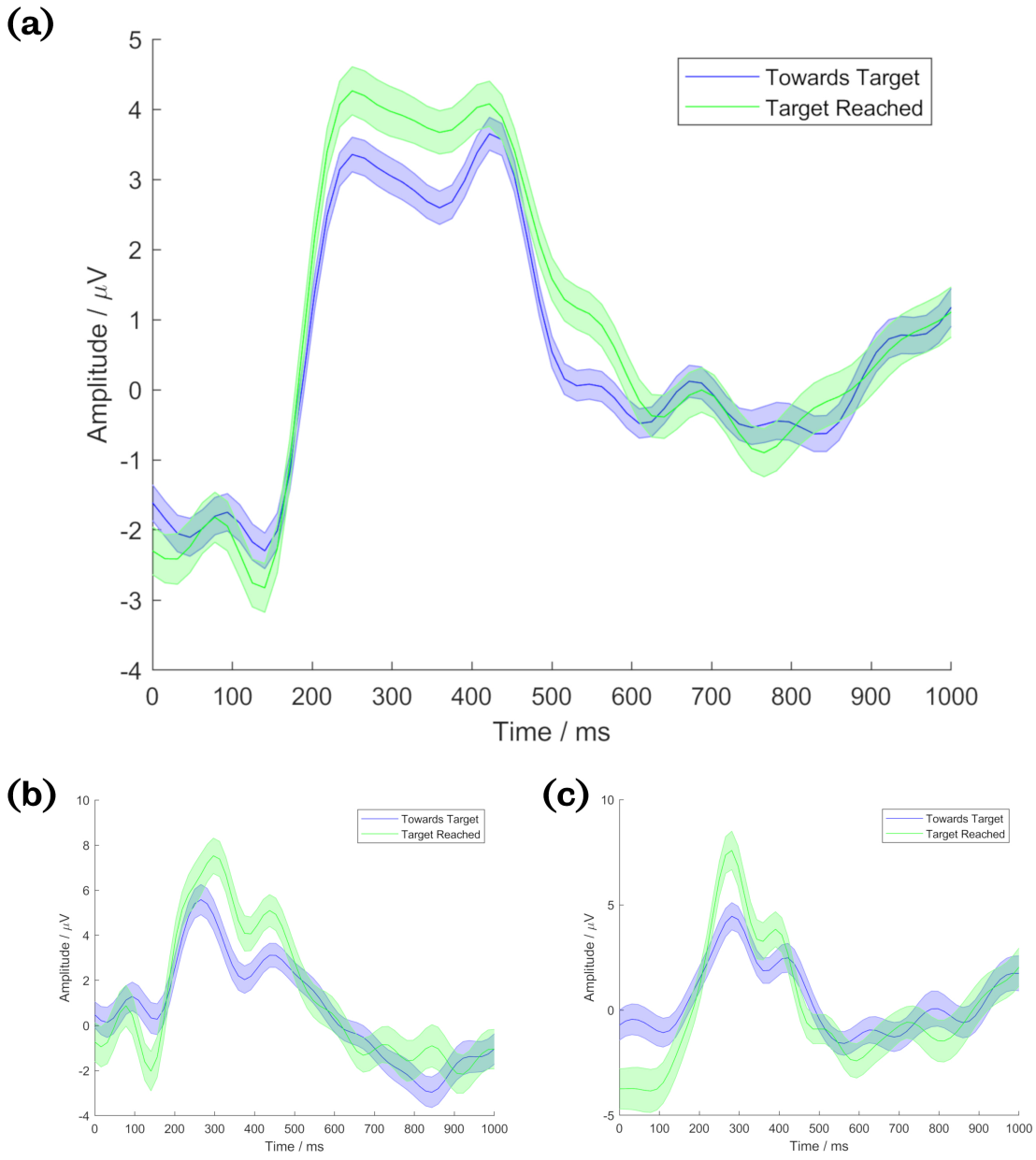

Figure 4.2: Time domain ERPs at electrode site Cz, from the Cursor Task. Time shown is relative to movement of the cursor. Central lines represent mean signals. Shaded areas cover 1 standard error. Blue lines show TT condition data. Green lines show TR condition data. (a) shows grand average data from all Cursor Task participants, (b) shows data from participant 1, and (c) shows data from participant 10.

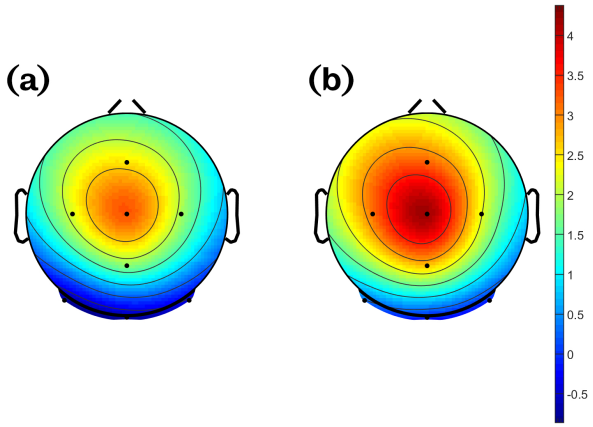

Figure 4.3: Grand average topographical maps of Cursor Task data. Maps were plotted based on a 50ms window surrounding the peaks identified as P300 from grand average data across all participants, and both conditions. Plots shown represent (a) responses to the TT condition, and (b) responses to the TR condition.

main peaks have been identified in mVEP: a positive peak (P1), followed by a negative deflection (N2), then another positive peak with a latency of 240-500ms [14, 57, 85, 102], which has been described as a P2 [57, 85, 102] or P300 [14]. The movements considered in this study were instantaneous steps from one location to the next. However, along with the P300, small P1 and N2 peaks were visible, with latencies of 78ms and 125ms respectively, relative to the movement of the cursor. These peaks did not appear to differ between responses to the two conditions.

4.3.2 Classification

4.3.2.1 Classification of Cursor Task data

The classification accuracies of each individual participant of the Cursor Task are shown in Table 4.2. As previously discussed in section 3.3.2, here we present the overall accuracy, as well as the accuracy obtained for each class. The mean overall accuracy for all Cursor Task participants was 66.5%. The mean accuracy for the TT condition was 68.8%, and the mean accuracy for the TR condition was 62.4%. Statistically significant separation of the conditions ($p < 0.05$) was found for all Cursor Task participants. At a group level, the classification results for the Cursor Task were found to be statistically significant ($p = 2.8 \times 10^{-54}$).

Subject	# TT Trials	# TR Trials	Mean # Features Selected	TT Accuracy	TR Accuracy	Overall Accuracy	p-value
1	162	86	35.0	64.8%	55.8%	61.7%	1.4×10^{-3}
2	73	40	44.8	68.5%	60.0%	65.5%	3.1×10^{-3}
3	157	93	10.3	60.5%	51.6%	57.2%	4.2×10^{-2}
4	163	89	50.9	76.1%	70.8%	74.2%	4.1×10^{-13}
5	63	39	30.4	65.1%	53.8%	60.8%	4.7×10^{-2}
6	155	88	6.3	67.7%	63.6%	66.3%	1.9×10^{-6}
7	154	85	16.6	59.7%	52.9%	57.3%	4.0×10^{-2}
8	156	81	15.9	67.3%	61.7%	65.4%	1.7×10^{-5}
9	145	76	40.0	73.1%	72.4%	72.9%	7.5×10^{-11}
10	169	89	37.7	85.2%	80.9%	83.7%	5.0×10^{-26}
Mean	**139.7**	**76.6**	**28.8**	**68.8%**	**62.4%**	**66.5%**	**All** < 0.05**, group p-value:** $p = 2.8 \times 10^{-54}$

Table 4.2: Single-trial classification results of Cursor Task data. Overall accuracy calculated as the percentage of trials, of either class, correctly classified. Number of features selected calculated as the mean of all iterations of leave-one-out cross-validation.

4.3.2.2 Classification of Publicly Avaliable Cursor Task data

The classification accuracies of each individual participant of the PACT are shown in Table 4.3. The mean overall accuracy for all PACT participants was 68.0%. The mean accuracy for the TT condition was 70.5%, and the mean accuracy for the TR condition was 61.0%. As with the Cursor Task, statistically significant separation of the conditions ($p < 0.05$) was found for all PACT participants. At a group level, the classification results for the PACT were found to be statistically significant ($p = 9.6 \times 10^{-62}$).

4.4 Discussion and Conclusion

4.4.1 Neurophysiological Distinctions Between The Conditions

In this study, the key neurophysiological difference that we identified between the two conditions was in the amplitude of the P300. The amplitude of the P300 was found to be greater in response to the TR condition (i.e. movements that reached the target) than the TT condition (i.e. movements that were correct, but did not reach the target). This distinction was found to be statistically significant ($p = 0.004$).

As discussed in section 4.1, a number of studies have reported that P300 amplitude

Subject	# TT Trials	# TR Trials	Mean # Features Selected	TT Accuracy	TR Accuracy	Overall Accuracy	p-value
1	448	105	44.3	75.0%	60.0%	72.2%	1.9×10^{-11}
2	585	180	89.2	74.2%	66.7%	72.4%	7.3×10^{-23}
3	259	128	64.7	67.6%	60.9%	65.4%	8.4×10^{-8}
4	201	93	31.5	61.7%	51.6%	58.5%	2.2×10^{-2}
5	603	250	71.8	74.0%	66.0%	71.6%	1.4×10^{-27}
Mean	**419.2**	**151.2**	**60.3**	**70.5%**	**61.0%**	**68.0%**	**All** < 0.05**, group p-value:** $p = 9.6 \times 10^{-62}$

Table 4.3: Single-trial classification results of PACT data. Overall accuracy calculated as the percentage of trials, of either class, correctly classified. Number of features selected calculated as the mean of all iterations of leave-one-out cross-validation.

is affected by reward magnitude [140, 169, 171]. It should be noted that, in this study, participants were not directly rewarded based on the virtual robot's performance. However, it is certainly feasible that they regarded moves that reached the target as being more important than moves that did not reach it, which could be considered analogous to the TR condition having a higher reward magnitude. Reports have been mixed regarding the effects of valence on the P300. Some studies have reported amplitude being affected by positive valence [26, 169], while others have reported valence either having no effect [27, 171], or an effect only in the case of negative valence [32]. P300 amplitude has also been shown to be dependent on whether feedback was expected or unexpected [58], and on target-to-target interval, with amplitude increasing when targets appeared less frequently [52].

Taking into consideration previous findings on the P300, and the experimental setup of our task, there are a number of potential causes of this increase in amplitude for responses to the TR condition, compared to the TT condition. It may represent a cognitive response recognising that a move that reaches the target is a more important step than other correct moves. Alternatively, while this study was designed as a navigation observation task, it could also conceptually be considered as an oddball paradigm. That is to say, the TR condition occurs less frequently than the TT condition. Therefore, it is possible that the increased P300 amplitude is due to the relative rarity of the TR condition. It is quite possible that the difference in amplitude may be the result of a combination of these factors.

We also briefly investigated frontal theta power, and asymmetry in alpha power, as these have been reported to vary with regard to valence [134]. However, no significant differences in these markers were identified between the conditions. It is certainly feasible that participants would not have had a strong emotional reaction to reaching the target.

In the Cursor Task, the goal was not fully achieved until the target was not only reached but also identified. Furthermore, users knew they were not controlling the virtual robot, and were not rewarded if it performed well. It may be interesting to investigate whether these valence markers indicate different reactions in future on-line experiments, in which participants' responses affect the actions of the virtual robot.

4.4.2 Single-Trial Classification

Previous studies have successfully classified the brain's responses to correct movements against responses to erroneous movements in navigation tasks such as the ones explored in this study. The original study for which the data of the PACT were generated reported classification accuracy of 75.8% and 63.2% for the correct and erroneous movement classes respectively [29]. Another study reported correct vs erroneous movement classification accuracy, in three similar navigation tasks, of 73.8%, 72.5%, and 74.3% [63]. It is reasonable to expect that the classification of two different correct movements against each other would be more challenging than the classification of correct movements against erroneous ones; we would expect to see more pronounced differences in the brain's responses in the latter case.

In this study, classifying EEG responses to correct movements towards the target (but not reaching it) against responses to movements that reached the target, we achieved mean overall classification accuracy of 66.5% and 68.0% for the two tasks. Indeed, these were only slightly below the levels previously reported for erroneous versus correct movements in similar tasks. Interestingly, overall accuracy reached a high of 83.7% in the best case. Crucially, statistically significant separation of the two conditions ($p < 0.05$) was achieved for all participants from both tasks, and highly significant separation of the classes was shown at the group level ($p = 2.8 \times 10^{-54}$ and $p = 9.6 \times 10^{-62}$ for the Cursor Task and the PACT, respectively).

As a proof of concept, we have shown that it is possible to classify responses to these two classes of correct movement against each other using single-trial EEG. As discussed in section 4.2.4.2, we chose to apply stepwise linear discriminant analysis in this study, as it has previously been shown to be successful in classifying similar data types [38,57,83,84,96,148]. However, it is possible that other methodologies, which could be explored in future, may be able to provide further increases in classification accuracy. In potential future systems, classifications of the human observer's EEG responses could be used to guide the movement of a real or virtual robot, with the user being explicitly rewarded for good performance of the robot. In such systems, adding information from more frontal electrodes may be able to provide an increase in classification accuracy, as the frontal cortex has been shown to code prediction and reward [105, 146, 147].

4.4.3 Implications for BCI

The P300 has a history of successful use in BCI, as discussed in section 4.1. In particular, there have been many studies, dating back over 30 years, regarding the use of P300 signals in BCI spelling devices [43, 45, 55, 84, 148]. These systems have often been able to improve the robustness and accuracy of their classifications by using paradigms that allowed each stimulus to be presented multiple times, and the responses to be averaged. P300-based BCIs have also been created for other applications such as video games [49, 71], virtual reality [11], and control of robots [12, 15, 69, 100], cursors [70, 91, 130] and wheelchairs [62, 132]. Furthermore, the P300 has been utilised alongside other modalities such as motor imagery [154] and steady-state visual evoked potentials (SSVEP) [172] to create hybrid BCIs [3, 109, 124]. The navigation scenarios presented in this study provided a further challenge compared to many previous P300-related systems, as each stimulus (i.e. movement) was only presented once. This was an important aspect of the paradigm, as we wished to simulate the observation of real navigation, with a view to future applications in which classifications could be made solely based on users' responses to the actions they observe. In such real navigation, each action occurs only once. While accurate single-trial P300 classification is challenging due to the low signal-to-noise ratio of EEG [68, 97], some recent studies have shown that it can be achieved. One study using a video game context reported mean offline classification accuracy of 85%, and online accuracy of 66% [49]. Another study reported single trial P300 classification accuracy of 70% [68]. In other cases, the area under the receiver operating characteristic curve (AUC) was reported for various possible classifier parameters, rather than the classification accuracy for a specific trained and optimised model. An AUC of over 0.8 has been reported for many participants [79, 94]. In this study, rather than classifying a condition eliciting a P300 against a condition that did not elicit a P300, we were classifying two P300-generating conditions against each other. As such the fact that statistically significant separation of two different correct conditions was achieved for all participants is encouraging for the use of the P300 in single-trial BCI scenarios.

In recent years, there have been interesting advances in BCIs based on signals that are generated spontaneously in the brain, without the need of a conscious effort to generate them on the part of the user. These systems, making use of implicit communication, have been described in two groups, referred to as "reactive BCI", in which a spontaneous response is triggered by a stimulus, and "passive BCI", whereby arbitrary mental states are measured [175–177]. Some particularly interesting recent studies have been those exploring reactive BCI in robotic movement and navigation tasks. Classification of error-related potentials (ErrP) in order to differentiate correct movements from erroneous ones has been combined with reinforcement learning in order to allow machines to perform a desired action [75] or navigate towards a desired target [29, 63, 179]. By obtaining more detailed

information from spontaneously generated signals, we can provide these systems with more context, and allow them to learn more efficiently and act more appropriately. The ability to classify when a target has been reached specifically and separately from other correct movements, as has been demonstrated in this study, would be an important aspect of a navigation system, and thus could enhance the usability and effectiveness of navigation-based BCI.

4.4.4 Conclusion

In this chapter, we compared the ERPs generated in EEG data, in response to observing two types of correct movements by a virtual robot: those that moved the robot closer to the target without reaching it, and those in which the robot reached the target. We were able to show that both correct movement conditions elicited a P300, and we identified a significantly higher P300 amplitude in cases in which the target was reached.

Interestingly, we were able to classify the responses to these two types of correct actions against each other with mean overall accuracies of 66.5% and 68.0% for two tasks, achieving statistically significant separation of the conditions for all participants. This single-trial classification could be used as part of a learning-based BCI, and opens a new door toward a more autonomous BCI navigation system.

Chapter 5

Simulated Learning in Semi-Autonomous Robot Navigation

At the time of writing, the findings presented in this chapter are under review for publication in IEEE Transactions on Systems, Man, and Cybernetics: Systems, with preliminary results published in the proceedings of the 42nd International Conference of the IEEE Engineering in Medicine and Biology Society (EMBC '20) [164]

5.1 Chapter Introduction

In the previous chapter, I showed that it is possible to use single trial EEG to classify the brain's responses to different correct navigational actions against each other. This fulfilled the second objective of this project. When combined with the findings of chapter 3, it has now been established that detailed subclasses of action can be identified from brain signals generated spontaneously while users merely observe the actions of a machine. This paves the way for a more efficient semi-autonomous system, in which the machine can use these detailed classifications as feedback to improve its performance, via machine learning. This chapter explores a system in which multiple types of navigational actions are classified in real time, and the classifications are used to inform the machine's future actions, thus addressing the third objective of the project. Finally, in order to address the fourth objective, a straightforward approach, simply using the classifications for immediate error correction, is compared to an approach that uses the classifications for a machine learning-based approach.

There is a performance bottleneck in many BCIs, as users are required to control each

low-level action in order to achieve a high-level goal. For example, users may need to consciously generate brain signals to move a cursor, prosthesis, or assistive robot, step-by-step to a desired location. This places a high mental workload on the user.

Machine learning provides the potential to alleviate this mental burden. Recent studies have shown the possibility of using "cognitive probing" — monitoring reactive brain signals in response to certain machine actions [81], and using these signals as feedback for reinforcement learning (RL), thus allowing robots to learn to perform tasks [64, 75]. In these systems, users must still focus on the task. However, we can postulate that mental workload may be reduced, as users are merely observing the task rather than consciously generating signals to control it. These studies have mostly been based on distinguishing correct actions from erroneous ones, by detecting error-related potentials (ErrP) — characteristic signals that are spontaneously produced in the brain in response to an error recognised by the human [30, 51]. Indeed, previous studies achieved encouraging results for robot path planing using ErrP detection combined with RL [2,63,66,143,179]. However, there are other options for route planning without the need for human intervention. In outdoor scenarios, satellite navigation is available. For smaller scale or indoor scenarios, there are myriad methods for robot path planning without the need for EEG feedback [23, 36, 101, 107, 139]. One thing that cannot be inferred without feedback from the human, is which target they wish the robot to travel towards. Arguably, therefore, "target identification" is the more important piece of information to learn from the EEG.

A few studies have begun to tackle this problem. Chavarriaga and Millán used EEG-based RL to choose between whether a target was on the left or the right of the machine's current location [29]. Some have indicated the possibility of using EEG rewards to infer which specific location, from a subset on a grid, was the target. In a recent study, Schiatti et al. had the machine converge upon optimal routes to each potential target via Q-learning, and then implemented a second layer of Q-learning to choose between possible targets [143]. However, in this paradigm, the robot received an environmental reward and stopped automatically when the target was reached, assuming that there was an external way to know the target was correct, rather than inferring this information purely from EEG feedback. Iturrate et al. showed that it is possible to converge on targets without the need for such external validation — their approach similarly used Q-learning to find optimal routes, and then compared feedback rewards with expected Q-values [66]. However, it has been stated that Q-learning suffers from poor scalability [63] and, indeed, these studies each had only a small subset of potential target loci in relatively small areas. Iturrate et al. recently stated, "It is then an open question how the proposed [brain-machine interface] paradigm may generalize across tasks or scale to more complex scenarios" [63]. Furthermore, all of these studies used binary classification of robotic actions, classifying each movement

simply as correct or erroneous.

Grizou et al. presented an unsupervised method to use reactive EEG for semi-autonomous navigation [54]. Their method did not use a calibration phase to learn the classification model. Instead, the machine considered all possible intended targets, and calculated which of the observed actions would be correct - and which would be erroneous - for each potential target. The system then inferred the most likely intended target based on the best separation of these classes. When a new target was chosen by the user, the system retained its inferred model of the user's previous EEG responses, but attempted to identify the most likely new target by using a Gaussian Bayes classifier to evaluate new EEG signals. As with the above methods, this study focused on binary, error-vs-correct classification

In the previous chapters, we showed that it is possible to subclassify different navigational errors, and different correct navigational actions, against each other. In this chapter, we utilise this, and propose a system 4-way EEG-based feedback for learning in robot navigation and target identification, rather than binary EEG feedback used in previous studies. The 4 classes of movements are: towards the target but not reaching it (TT condition), reaching the target (TR condition), moving from an off-target location to a location even further away from the target (FA condition), and stepping directly off the target location (SO condition). In this study, the user's intended target will be inferred from reactive brain signals, generated spontaneously as the user merely observes the robot's actions. Importantly, the target could be any location in the space. In order to overcome the scalability issues of RL, our approach reframes the challenge of how to utilise reactive EEG to achieve semi-autonomous navigation. Instead of attempting to learn the route from A to B, we assume that the route is known. Rather, the key information that we need to infer from the user is the intended target. We propose a learning system featuring a novel implementation of Bayesian inference, utilising prior knowledge of classification contingency tables to contextualise EEG feedback, and build a probabilistic model in order to learn the most likely target location. In order to test both efficiency and scalability, we investigate our strategy's effectiveness in both small (9×1, i.e. 9 spaces) and large (20×20, i.e. 400 spaces) grids using EEG data recorded from 10 participants. Furthermore, we investigate the trade-off between speed and accuracy, using an adjustable parameter to control the level of evidence that must be accumulated before converging on a particular target.

5.2 Experimental Design

5.2.1 Datasets

In the present study, we used real EEG data from the Cursor task, as described in detail in the previous chapter, and shown in Fig. 4.1. As previously discussed, ten healthy adults

(4 female, 6 male, mean age 27.30 ± 8.31) had merely observed a virtual robot navigation paradigm. The brain signals were recorded at 500Hz, at electrode positions Fz, Cz, Oz, Pz, C3, C4, PO7, and PO8, using an Enobio 8 headset. The paradigm consisted of a cursor, representing the virtual robot, moving left and right in a 1-dimensional space on a screen. The robot's goal was to reach, and correctly identify, a target location. However, erroneous movements and erroneous target identifications occurred with preset probabilities.

5.2.2 Simulations Using Real EEG Feedback

The goal of this study was to simulate a real-time implicit human-machine interaction. In order to achieve this, while being able to explore a variety of scenarios, running through each a large number of times, we used previously-recorded real EEG data as feedback. This approach has recently proven useful in exploratory studies [108].

Of the ten participants who observed the Cursor Task, two did not produce enough artefact-free trials in each class, and were excluded. Therefore, simulations were performed using feedback generated by the remaining eight participants. For this purpose, for each participant, 85% of the EEG trials from each class were randomly selected as training samples, with the remaining 15% being reserved as test samples.

In the simulation phase, two different grids were used. Firstly, the virtual robot navigated in a 1-dimensional space made up of 9 squares. Secondly, the virtual robot navigated in a 2-dimensional space made up of 400 squares, arranged in a 20×20 square. The target could be randomly positioned in any location (i.e. any square in the grid) at the start of each run. The robot began the run at a randomly selected location a minimum of 2 moves away from the target, with no maximum distance imposed other than the boundaries of the space. Each action consisted of either (a) a discrete movement from the robot's current square to an adjacent square, or (b) identifying the robot's current square as the target location.

Three navigation strategies were tested, namely our proposed "Bayesian Inference", "Random" and "React". The precise details of these navigation strategies are described in section 5.3.2. Generally, an initial action was selected. Then, after each action was performed by the robot, a test EEG trial from a participant who had previously observed the experiment (as described in section 5.3.1) was retrieved. The trial was classified as if it were being processed in real time. The classification outputs provided by the trained model was used to inform future actions of the robot. This continued, using trials from the same participant as feedback, until the navigation strategy determined that the target had been reached. Each navigation strategy was run 1000 times per participant on each grid size.

5.3 Methods

5.3.1 Multi-Way Classification of Robotic Actions

For each participant, a four-way classification model was trained to distinguish four classes of observed movement:

- "TT condition": Towards target (but not reaching it)
- "TR condition": Target reached
- "FA condition": Further away (when moving from an already off-target location, to a location further away from the target)
- "SO condition": Stepped off target

Classification of movement actions, — hereafter specified as "movement classification" — was achieved via a 2-stage binary tree. Firstly, EEG trials were classified as responses to either correct (TT and TR condition) or erroneous (FA or SO condition) movements. They were then subclassified as one of the specific conditions. Classification inputs were time domain EEG samples from 200ms to 700ms relative to the robot's action, from the 8 electrodes. Data were bandpass filtered, and downsampled to 64Hz. For the first stage of classification (error vs correct), a passband of 1 to 10Hz was used, as low frequencies have generally proven fruitful in error detection studies [30]. For the second stage (subclassification), a passband of 1 to 32Hz was used, as the inclusion of information at higher frequencies has previously proven successful in subclassifying similar navigation observations [164].

Stepwise Linear Discriminant Analysis (SWLDA) was selected as the classification strategy for each stage of the class, as this has previously been shown to be effective in selecting features and classifying event related potentials [83], including in our previous work with observed robot navigation [161, 164]. Features were selected iteratively. Beginning with an empty feature set, regression analysis was performed on models created with and without each feature, providing a p-value for each one. If the p-value of any features not already in the model were below 0.025, the feature with the lowest p-value would be added to the model. If no p-values were below this threshold, then the feature in the model with the highest p-value, if above 0.075, would be removed from the model. Iterations continued until no features reached the thresholds to be added to, or removed from, the model. Linear classification models were then trained and tested, using the selected features.

A minimum of 12 trials are recommended to achieve a reasonable level of stability in the ERN and Pe [88], and literature suggests that a minimum of 20 trials are required for a stable P300 [31]. Therefore, in line with our previous studies [161, 164], participants were only included in the classification phase if they had produced at least 12 trials in each of

the FA and SO error conditions, at least 40 trials from error conditions combined, and at least 20 trials in each of the TT and TR correct conditions. This meant that classification analysis was performed using data from 8 participants.

Additionally, binary classification of target identification actions — hereafter referred to as "TI classification" — was carried out for each participant, in attempt to gather further information about whether the identified location was the correct target. For all EEG trials in which the robot identified its current location as the target, a classification model was built to classify correct target identifications — hereafter referred to as the "CTI" condition, against false ones — the "FTI" condition. EEG trials were processed in a similar manner to observed movement trials, and were extracted from 200ms to 700ms relative to the yellow box appearing around the robot's location. Trials for this model were filtered between 1 and 10Hz. Similarly to the movement classification, an SWLDA classifier was used. This TI classification was used as an extra layer of feedback in the simulated experiments, giving the robot a chance to undo a target identification, if the TI classification output indicated that it was false.

5.3.2 Navigation Strategies

In this study, we assumed that the robot knew the map perfectly — it knew the shortest path between any two locations. We could imagine that the robot had a satellite navigation system for any route it might need to take. However, the robot did not know which location was the target - this is what the robot needed to learn from the EEG feedback. Given this assumption, three navigation strategies were used.

5.3.2.1 Proposed Bayesian Inference

Kruschke and Liddell describe Bayesian analysis as "reallocation of credibility across possibilities" [82]. In this case, each location on the grid represented a possible target. At the start of each run, each location could be considered to have an equal probability of being the target, but as we gathered more information in the form of EEG feedback, we could infer that some locations are more credible targets than others. As such, we deemed Bayesian inference to be an appropriate strategy for this scenario of learning to navigate and identify targets.

Let us present the action performed by the robot at time step t as U_t, where $t \in [1, 2, .., l]$ and l denotes the last time step in a given run. U_t can be considered as the control state of the model representing that the robot either moved to a neighbouring location, or identified its current location as the target. Subsequently, S_t represents the participant's interpretation, at time step t, of what has occurred as a result action U_t. In this study, for

movement actions $S_t \in \mathcal{S}$=[TT, TR, FA, SO], and for target identification actions $\mathcal{S}$=[CTI, FTI]. This interpretation was not seen directly by the robot, and so can be considered as the hidden state of the model. However, the participant's interpretation of U_t could be reflected in the recorded EEG signals. Thus, EEG signals resulting from interpretation S_t were classified, providing observation $\boldsymbol{O_t} \in \mathcal{O}$ as the classification output at time step t. In this study, each observation was represented as a binary vector with length equal to the number of possible classification outputs. For movement actions, $\boldsymbol{O_t} = \mathcal{O}(1)$ =[1 0 0 0] represented a classification output of TT, $\boldsymbol{O_t} = \mathcal{O}(2)$ =[0 1 0 0] represented TR, $\boldsymbol{O_t} = \mathcal{O}(3)$ =[0 0 1 0] represented FA, and $\boldsymbol{O_t} = \mathcal{O}(4)$ =[0 0 0 1] represented SO. For target identification actions, $\boldsymbol{O_t} = \mathcal{O}(1)$ =[1 0] represented CTI, and $\boldsymbol{O_t} = \mathcal{O}(2)$ =[0 1] represented FTI. Theoretically, our proposed approach could be extended, such that $\boldsymbol{O_t}$ could represent the likelihood of each class, rather than being binary.

Fig. 5.1(a) shows a representation of the way that each action U_t influenced the participant's interpretation S_t, which lead to a classifier output $\boldsymbol{O_t}$. The probability of each grid location being target was updated as explained below, thus influencing the following action. Depending on the classification output and the updated probabilities, the following action would be either identifying the current location as the target or making the next movement action.

Defining the Next Movement Action: Let's define $P(T^t_{i,j})$ as the probability of a given grid location (i, j) being the target at time step t. Similarly, $P(T^t_c)$ is defined as the probability that the robot's current location is the target. At the start of each run, these probabilities were equal to $P(T^1_{i,j}) = 1/(n \times m)$ for every location of a grid with n rows and m columns. When a new classification output $\boldsymbol{O_t}$ was observed following a robot action U_t, $P(T^{t+1}_{i,j})$ at time step $t+1$ were updated according to Bayes theorem [153], using (5.1) and (5.2);

$$P(T^{t+1}_{i,j}) = \frac{P(T^t_{i,j}|\boldsymbol{O_t})}{\sum_{j=1}^{m}\sum_{i=1}^{n} P(T^t_{i,j}|\boldsymbol{O_t})}, \tag{5.1}$$

$$P(T^t_{i,j}|\boldsymbol{O_t}) = \frac{P_{\mathbf{A}}(\boldsymbol{O_t}|T_{i,j})P(T^t_{i,j})}{P(\boldsymbol{O_t})}. \tag{5.2}$$

In (5.2), $P_{\mathbf{A}}(\boldsymbol{O_t}|T_{i,j})$ was calculated using the likelihood matrix $\mathbf{A}$, representing the likelihood of observations given the hidden states. In this study, for the movement actions $\mathbf{A} \subset \mathbb{R}^{4\times4}$, whereas for the target identification actions, $\mathbf{A} \subset \mathbb{R}^{2\times2}$. The elements of $\mathbf{A}$ were calculated as

$$\mathbf{A}(i, j) = P(\mathcal{O}(i)|\mathcal{S}(j)). \tag{5.3}$$

In fact, using $\mathbf{A}$ the robot could estimate the reliability of each classification output. $\mathbf{A}$ was subject-specific, and calculated using leave-one-out cross validation on the classification

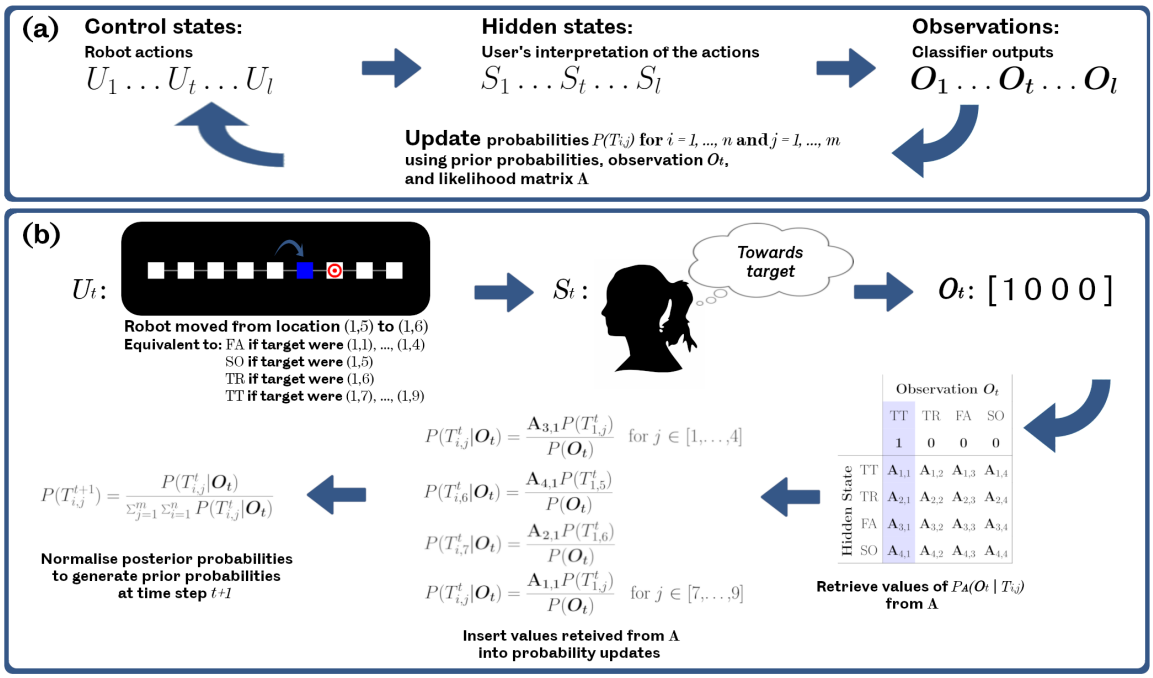

Figure 5.1: Formulation of the proposed Bayesian inference strategy. (a) shows the general case. Robot actions lead to interpretations by the user. These resulted in EEG signals which were given classification outputs. These observations, along with existing target location probabilities and the likelihood matrix $\mathbf{A}$, determined updated target location probabilities. Probabilities informed the next robot actions. (b) shows an example of how the Bayesian inference strategy updated the target location probabilities after one movement action, thus influencing future actions. The action U_t was that the robot moved from location $(1, 5)$ to $(1, 6)$. The user saw that this resulted in the robot moving towards the target. The classifier correctly produced the observation representing the TT condition. Values from the appropriate column were extracted from $\mathbf{A}$ and used to update probabilities. If any of locations 1-4 were the target, the action would have represented the FA condition. For location 5, the action would have represented the SO condition. For location 6, the action represented the TR condition. For locations 7 (the actual target), 8, and 9, the action would have represented the TT condition. All probabilities were updated accordingly. The robot would then go on to select the next action, U_{t+1}. Depending on the latest classifier output $\boldsymbol{O}_t$ and the updated target location probabilities, action U_{t+1} would either be to select the current location as the target, or to perform another movement action.

training EEG data. Subsequently, $P_{\mathbf{A}}(\boldsymbol{O_t}|T_{i,j})$ was extracted from $\mathbf{A}$, by retrieving the value in the column corresponding to $\boldsymbol{O_t}$, and the row corresponding to what the participant's perception S_t would have been, if (i, j) were the target. $P(\boldsymbol{O_t})$ could be also calculated using $\mathbf{A}$, as the sum of the elements in the column corresponding to $\boldsymbol{O_t}$, divided by the sum of all the elements of $\mathbf{A}$. In other words, $\boldsymbol{O_t}$ could be calculated using the following

equation:

$$P(\boldsymbol{O_t}) = \frac{\sum_{j=1}^{k} P(\boldsymbol{O_t}|\mathcal{S}(j))}{\sum_{i=1}^{k}\sum_{j=1}^{k} P(\mathcal{O}(i)|\mathcal{S}(j))}, \tag{5.4}$$

where k was the total size of $\mathcal{S}$ which is 4 for the movement actions and 2 for the target identifications.

Fig. 5.1(b) shows an example of how the probabilistic model was updated using the proposed Bayesian inference strategy, after an individual movement action.

After calculating $P(T_{i,j}^{t+1})$ for all the grid locations, the robot identified the location with the highest probability of being the target, and then calculated the shortest path to reach it. The virtual robot then took the first step on this path as U_{t+1}. If multiple locations were tied for the highest probability, one was selected at random.

Identifying the Current Location as Target: In order to determine whether the robot's current location c was the target, after the target location probabilities had been updated following each movement action, algorithm 1 was run. *stringency* is a predefined variable to determine the level of certainty the system required before identifying the robot's current location as the target. In this study, values between 0.1 and 0.9 were used.

Algorithm 1 Method to determine when to identify the current location as the target

if ($\boldsymbol{O_t} = [0100](i.e. TR)$ **and** $P(T_c^t) > stringency$)
or $P(T_c^t) > \frac{stringency+0.1}{stringency+0.2}$ **then**
  Identify c as the target
end if

According to algorithm 1, there were two scenarios in which the robot could select a target:

(a) The current movement classification output $\boldsymbol{O_t}$ represented TR and a lower probability threshold was met.

(b) The current movement classification output $\boldsymbol{O_t}$ did not represent TR but a higher probability threshold was met.

At the lowest *stringency* value of 0.1, this meant a movement classification output of TR resulted in the target being identified as long as the probabilistic model believed there to be more than a 10% chance of the current location c being the target. Alternatively, without a movement classification output of TR, the current location c would still be identified if it was considered more than twice as likely to be the target as all other loci combined. As *stringency* increased, the required probabilities — and thus the strength of evidence that had to be accumulated in support of a given location being the target, either with or without a classification output of TR — increased.

The proposed Bayesian inference strategy allowed the possibility of deselecting targets. Following a target identification action, if the TI classification output was FTI, the target was deselected. Thereafter, all probabilities $P(T_{i,j}^t)$ were updated using (5.1) and (5.2), with the likelihood matrix of target identification actions, $\mathbf{A} \subset \mathbb{R}^{2\times 2}$. The run continued until a target identification action was followed by a TI classification output of CTI.

5.3.2.2 React

The next strategy, *React*, used EEG feedback to inform immediate moves, but did not involve any broader learning. This strategy effectively put 100% trust in the most recent EEG classification output.

If the classifier had not identified the robot's current location c as the target, the robot would move to a neighbouring location, selected at random from a list of eligible neighbours of the robot's current location. For the first action of each run, all neighbours were eligible. After action U_t, a pre-recorded EEG trial from the appropriate class was processed, and classification output $\boldsymbol{O_t}$ was produced by the trained model. If $\boldsymbol{O_t}$ suggested that the action was the TT condition (moving towards the target but not reaching it), then the robot's previous position would be ruled out from the list of eligible neighbours. Locations were only ruled out for a single action, as the most recent classification output superseded previous ones. If $\boldsymbol{O_t}$ suggested that the action was an erroneous movement (FA or SO condition), the list of eligible neighbours would be reduced to only the previous position, and therefore action U_{t+1} would be to move back to the robot's previous location, undoing the error. Finally, if $\boldsymbol{O_t}$ suggested the target had been reached (TR condition), then the robot's position c would be identified as the target location.

When the yellow box was drawn to identify the target, TI classification was performed in order to classify the identification as either correct (CTI) or false (FTI). If the classification output was FTI, the identification would be undone, and the run would continue. The run would end when a movement action received a TR movement classification output, then the yellow box was drawn around the robot's location, and the TI classification output was CTI.

5.3.2.3 Random

As a performance baseline, a random strategy was implemented. For each action, with probability of $1/(n\times m)$ (i.e. $1/9$ on the 9×1 grid, $1/400$ on the 20×20 grid), the robot's current position c would be identified as the target location. Otherwise, a neighbouring position would be selected at random, and the robot would move there. The process would repeat until the target was identified, at which point the run would end. While this strategy did

not require EEG feedback, 1000 runs were still simulated for each participant.

5.3.3 Assessing the Effect of Detailed EEG Feedback

In this study, our proposed Bayesian inference strategy made use of detailed EEG feedback. We implemented 4-way classification of movement actions, as opposed to the state-of-the-art approach using binary classification. Furthermore, we included the classification of target identification actions.

In order to investigate the effect of TI classification, we compared our proposed Bayesian inference strategy to an equivalent system which had the TI classification feature switched off. In this case, each run ended as soon as the first target identification action was performed.

We also compared proposed system to one using state-of-the-art, binary error vs correct movement classification. The binary system was equivalent to the Bayesian inference strategy, with two key changes. Firstly, the likelihood matrix $\mathbf{A}$ for movement classifications was reduced from a 4×4 matrix (TT, TR, FA, and SO) to a 2×2 matrix (correct and erroneous movements). Secondly, as specific TR classification outputs were no longer available, the target would simply be identified if $P(T_c^t) > \frac{stringency+0.1}{stringency+0.2}$. For both of these alternative systems, 1000 simulations were run for each participant, and for each of the small and large grids, with *stringency* values ranging from 0.1 to 0.9.

5.4 Results

5.4.1 Classification of Movement and Target Identification Actions

Four-way movement classification accuracies of the test samples for each individual participant are shown in Table 5.1. As previously discussed in section 3.3.2, here we present the overall accuracy, as well as the accuracy obtained for each class. The mean overall accuracy was 48.7%, well in excess of the 25% baseline for four classes. The overall movement classification accuracy for each participant was over 40%. Average classification accuracies of each condition were also all well over 40%, with the exception of the FA condition, at 39.9%. Results for the first stage of movement classification: error vs correct, are also shown. The mean error vs correct accuracy was 71.3%.

Classification accuracies of target identification (TI) action, based on the test samples for each individual participant, are shown in Table 5.2. The mean overall accuracy of TI classification was 73.5%. The accuracy for each individual participant was well in excess of 60%. Mean accuracy was strong in both the classification of both correct and erroneous target identifications, with the two conditions being correctly classified in 73.4% and 74.4%

Subject	Condition				Error vs Correct	Overall
	TT	TR	FA	SO		
1	41.7%	53.9%	50.0%	20.0%	71.2%	44.2%
2	70.8%	50.0%	16.7%	50.0%	77.1%	56.3%
3	58.3%	61.5%	28.6%	33.3%	76.6%	53.2%
4	43.5%	46.2%	80.0%	66.7%	77.3%	50.0%
5	52.2%	30.8%	50.0%	100.0%	64.4%	48.9%
6	47.8%	33.3%	42.9%	33.3%	68.9%	42.2%
7	45.5%	45.5%	22.2%	40.0%	59.6%	40.4%
8	52.0%	61.5%	28.6%	100.0%	75.0%	54.2%
Mean	**51.5%**	**47.8%**	**39.9%**	**55.4%**	**71.3%**	**48.7%**

Table 5.1: Four-way movement classification results.

of cases, respectively.

Subject	Correct	Error	Overall
1	85.7%	60.0%	75.0%
2	66.7%	80.0%	71.4%
3	80.0%	80.0%	80.0%
4	70.0%	80.0%	73.3%
5	80.0%	80.0%	80.0%
6	87.5%	60.0%	76.9%
7	57.1%	80.0%	66.7%
8	60.0%	75.0%	64.3%
Mean	**73.4%**	**74.4%**	**73.5%**

Table 5.2: Target identification (TI) classification results.

5.4.2 Evaluation of Navigation Strategies in Small and Large Grids

Navigation strategies were compared using two metrics, namely $PTCI$ and MNS. To assess accuracy, we calculate the percentage of targets correctly identified ($PTCI$). Higher $PTCI$ represents greater accuracy. To assess speed, we calculate the mean normalised number

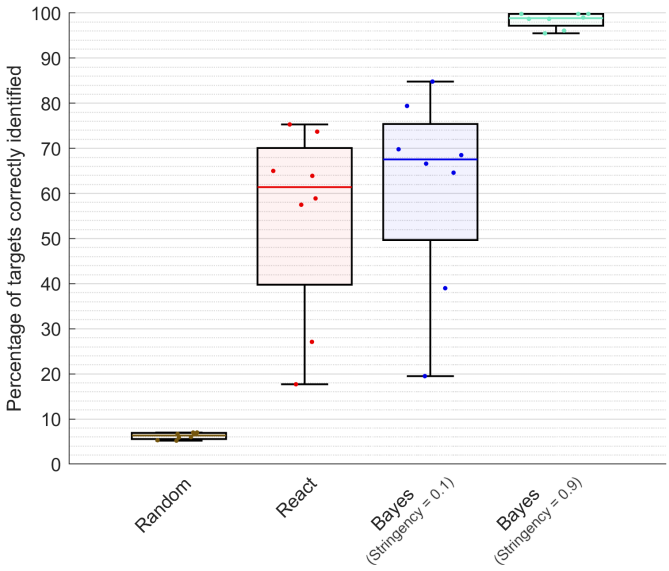

Figure 5.2: PTCI (percentage of targets correctly identified) performance of each navigation strategy on the small (9×1) grid, across the 8 participants. Higher PTCI represents greater accuracy.

of steps (MNS) taken to achieve correct target identifications. Steps are normalised to represent the efficiency of the path taken, accounting for the fact that the virtual robot starts each run a variable number of steps away from the target.

5.4.2.1 Percentage of Targets Correctly Identified (PTCI)

A comparison of the strategies' $PTCI$ on the small, 9×1 grid across the 8 participants is shown in Fig. 5.2. The *Random* strategy achieved a mean $PTCI$ of only 6.2% (s.d. 0.7%). The PTCI increased to a mean of 54.9% (s.d. 21.2%) for the *React* strategy, and increased further to a mean of 61.5% (s.d. 21.7%) for the proposed Bayesian inference strategy with a *stringency* value of 0.1. At the highest *stringency* level of 0.9, a mean $PTCI$ of 98.4% (s.d. 1.7%) was achieved.

In the large, 20×20 grid, the $PTCI$ for the *Random* and *React* strategies were effectively negligible, at just 0.2% (s.d. 0.1%) and 6.4% (s.d. 4.7%), respectively. Conversely, our proposed Bayesian inference strategy retained strikingly high $PTCI$ when scaling to the large grid. At a *stringency* level of 0.1, a mean $PTCI$ of 62.0% (s.d. 19.0%) was achieved in the large grid. At a *stringency* level of 0.9, very nearly all targets were correctly identified: the mean $PTCI$ was 98.03% (s.d. 1.8%). Indeed, for one participant at this highest *stringency* setting, 100% of the 1000 targets in the large grid were identified correctly.

A 2 (grids: small and large) × 3 (navigation strategies: *Random*, *React*, and Bayesian inference with a *stringency* level of 0.1) repeated measures ANOVA was performed on the

$PTCI$ results. The statistical results revealed significant main effects of grid size ($p = 0.001$) and navigation strategy ($p < 0.001$) on the $PTCI$. Moreover, a significant interaction between the grids and the navigation strategies were observed, regarding $PTCI$ ($p < 0.001$).

Post hoc analysis revealed that, after Bonferroni correction, the proposed Bayesian inference strategy significantly outperformed both *Random* ($p < 0.001$) and *React* ($p < 0.001$) strategies in terms of $PTCI$. The *React* strategy also significantly outperformed the random strategy ($p = 0.001$). Interestingly, when comparing the proposed Bayesian inference strategy with the *React* strategy, a significant interaction was revealed between grid size and navigation strategy ($p < 0.001$). This shows that the *React* strategy's $PTCI$ is much more negatively affected by the change from small to large grid than the proposed Bayesian inference strategy. In fact, the proposed Bayesian inference strategy was quite robust to the increase in grid size. Therefore, the proposed Bayesian inference strategy not only provided the best target recognition accuracy of all the tested strategies, but was also shown to be a scalable approach.

5.4.2.2 Mean Normalised Steps (MNS)

Violin plots comparing the strategies' MNS on the 9×1 grid are shown in Fig. 5.3. The distributions for these plots are based on all runs in which the target was correctly identified, from all participants, combined. Using the *Random* strategy, the MNS was 4.4 (s.d. 0.4). With the *React* strategy, the MNS, calculated across the averages for each participant, was reduced to 3.9 (s.d. 1.5). This reduced further for the Bayesian inference strategy with *stringency* level of 0.1, to 3.3 (s.d. 0.9).

An increase in MNS (i.e. decrease in speed) was observed when expanding to the large grid, which is to be expected as there is a change from 1 dimension to 2. With the *Random* strategy, the increase in MNS was very large, to a mean of 72.4 (s.d. 76.4). With both the *React* and Bayesian inference (*stringency* = 0.1) strategies, the change in MNS was much smaller, increasing to 6.4 (s.d. 3.6) and 7.8 (s.d. 3.7), respectively.

A 2 (grids: small and large) × 3 (navigation strategies: *Random*, *React*, and Bayesian inference with a *stringency* level of 0.1) repeated measures ANOVA was performed on the MNS results. Again, significant main effects of both grid size ($p = 0.031$) and navigation strategy ($p = 0.040$) were reported, as well as a significant interaction between grid size and navigation strategy ($p = 0.045$). This further substantiates the point that, while the *Random* strategy's MNS was severely affected by an increase in grid size, this change had a significantly smaller effect on both the *React* strategy and the proposed Bayesian inference strategy.

Post hoc analysis, after Bonferroni correction, did not show any significant pairwise differences between navigation strategies in terms of MNS.

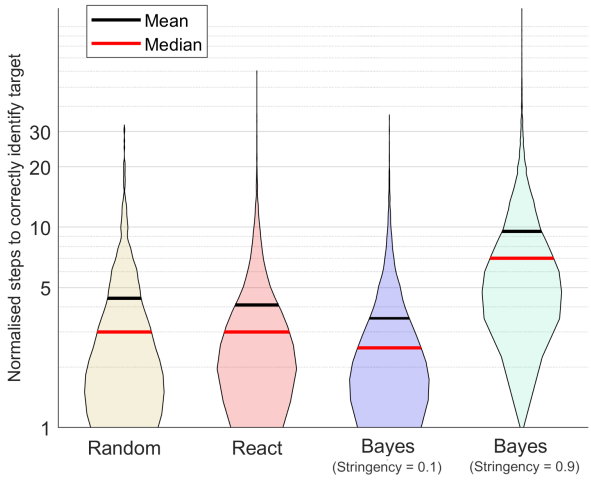

Figure 5.3: MNS (mean normalised steps) performance of navigation strategies on a small (9×1) grid. Violin plots show the smoothed distribution of normalised number of steps to correctly identify targets. *React* and Bayesian strategy distributions are based on data from all participants, combined. Lower MNS represents greater speed. The y-axis is plotted on a logarithmic scale.

5.4.3 The Speed-Accuracy Trade-Off

By changing the *stringency* setting, we can choose to put more focus on either the speed (MNS) or the accuracy ($PTCI$) of the system. There is a trade-off — generally, increasing performance in one of these metrics means decreasing performance in the other.

Using the Bayesian inference strategy, we calculated $PTCI$ and MNS, in both small and large grids, with *stringency* values in increments of 0.1 between 0.1 and 0.9. The results of these calculations are shown in Table 5.3. The trade-off is demonstrated by the high correlation coefficients between $PTCI$ and MNS: $r = 0.94$ in the 9×1 grid and $r = 0.95$ in the 20×20 grid ($p = 1.6 \times 10^{-4}$ and $p = 6.2 \times 10^{-5}$, respectively). A visualisation of this trade-off is shown, for both the small and large grids, in Fig. 5.4 (solid lines).

On average, it was possible to achieve a $PTCI$ of over 90% with a *stringency* setting of 0.6 in the small grid, and 0.5 in the large grid. These settings afforded a mid-range MNS, at an average of 6.9 and 10.9 in the small and large grids, respectively. For applications where the very highest $PTCI$ (i.e. the highest accuracy) is required, we can achieve this in either the small or large grid by setting the *stringency* to 0.9. Of course, this does require more steps in order to attain the higher threshold of confidence that the target has been reached. With this very high *stringency* value, the MNS increased to an average of 9.6 and 12.6 in the small and large grids, respectively. The reward is near-perfect accuracy: In both grids, an average $PTCI$ of over 98% was achieved, with $PTCI$ of over 95% for every single participant.

Table 5.3: Percentage of targets correctly identified (PTCI), and the mean normalised number of steps taken in order to identify them (MNS), using the Bayesian inference strategy, with various values of the stringency variable, on both the small and large grids. Results shown represent mean ± standard deviation across all participants

Stringency	9 × 1 Grid		20 × 20 Grid	
	PTCI	MNS	PTCI	MNS
0.1	61.5% ± 21.7%	3.3 ± 0.9	62.0% ± 19.1%	7.8 ± 3.7
0.2	68.6% ± 17.5%	3.8 ± 0.9	77.9% ± 13.8%	9.0 ± 4.9
0.3	77.2% ± 13.2%	4.4 ± 0.9	85.4% ± 10.3%	9.6 ± 5.1
0.4	84.6% ± 10.1%	5.3 ± 1.1	88.4% ± 8.4%	10.3 ± 6.1
0.5	88.8% ± 8.0%	6.2 ± 1.3	91.6% ± 6.3%	10.9 ± 6.1
0.6	92.7% ± 5.2%	6.9 ± 1.7	93.6% ± 5.1%	11.2 ± 6.2
0.7	94.9% ± 3.8%	7.5 ± 1.8	95.5% ± 3.9%	11.3 ± 5.3
0.8	96.4% ± 3.1%	8.5 ± 2.2	96.8% ± 2.8%	12.1 ± 6.2
0.9	98.4% ± 1.7%	9.6 ± 2.8	98.0% ± 1.8%	12.6 ± 6.4

There was also a high negative correlation between *stringency* and the standard deviation from the mean $PTCI$ ($r = -0.97$, $p = 1.4 \times 10^{-5}$ in the small grid; $r = -0.95$, $p = 6.2 \times 10^{-5}$ in the large grid). Conversely, there was a very high positive correlation between *stringency* and the standard deviation from the mean MNS ($r = 0.95$, $p = 1.1 \times 10^{-4}$ in the small grid; $r = 0.78$, $p = 0.01$ in the large grid). In other words, as we require more evidence in order to identify each target, $PTCI$ gets more consistent across participants. Meanwhile, MNS is more consistent across participants when the *stringency* is lower, and becomes more varied as *stringency* increases. Therefore, if an application were to require consistency across users in either speed or accuracy, these features can also be controlled by tuning the *stringency* parameter.

5.4.4 The Effect of Classifying the Target Identification Action

As discussed in section 5.3.3, simulations were also run with the TI classification feature switched off. The results of these simulations are shown as the dashed lines in Fig. 5.4.

Paired samples t-tests found the $PTCI$ achieved with TI classification to be significantly higher ($p < 0.05$) than that achieved without TI classification at every *stringency* level in the small grid, and all but the highest *stringency* level in the large grid. As we might expect, targets are generally identified slightly faster on average without TI classification, as no extra steps can be taken after an initial target identification action. This difference

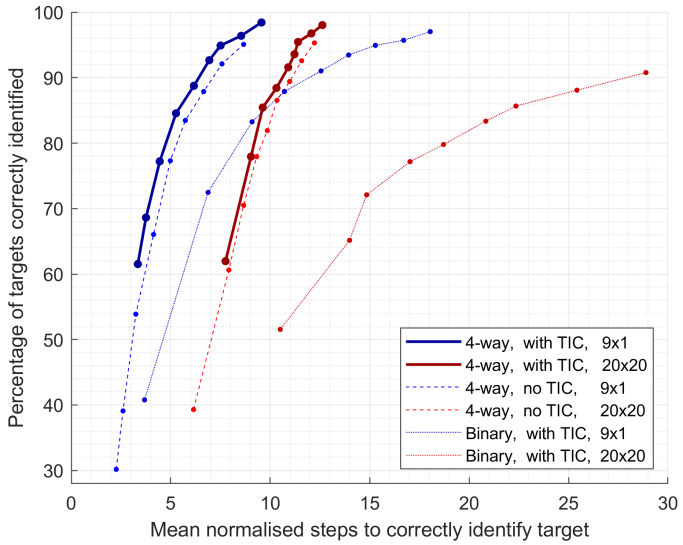

Figure 5.4: Speed and accuracy trade-off. MNS and PTCI results at various *stringency* values, from 0.1 (lowest point of each line on both axes) to 0.9 (highest point of each line on both axes). Lower MNS represents greater speed. Higher PTCI represents greater accuracy. Bold, solid lines represent data generated using the proposed Bayesian inference system (with 4-way movement classification, and TI classification, here abbreviated to "TIC"). Dashed lines represent data generated using a system without target identification classification. Dotted lines represent data generated using a system with binary movement classification (i.e. correct versus error). Blue lines represent data from the small, 9×1 grid. Red lines represent data from the large, 20×20 grid. All lines show average results across all participants.

in MNS was found to be significant ($p < 0.05$) at all but the highest *stringency* level in the small grid. However, in the large grid, the difference in MNS was only found to be significant at 3 of the 9 *stringency* levels.

The most notable effect of TI classification occurs at the lowest *stringency* levels. In these cases, we can reasonably expect more false target identifications to occur, as less evidence needs to be accumulated in order to perform a target identification action. In the 9×1 grid, $PTCI$ of 61.5% was achieved with TI classification, as opposed to just 30.2% without TI classification ($p = 0.0006$). In the 20×20 grid, 62.0% $PTCI$ was achieved with TI classification, compared to 39.3% without ($p = 0.005$). This indicates that TI classification strongly improves the robustness of the system.

5.4.5 Comparison of 4-Way vs Binary Classification

We compared the efficiency of the system using the proposed 4-way movement classification against one using the existing state-of-the-art, binary error vs correct movement classification. The results of the simulations using binary movement classification (as discussed in

section 5.3.3) are shown as the dotted lines in Fig. 5.4.

Paired t-tests on each *stringency* level of each grid revealed that only in the small grid with *stringency* of 0.1 were the $PTCIs$ significantly different. In this case, 4-way classification achieved a higher $PTCI$.

The more striking effect of 4-way classification is on the speed of the system. As can be seen in Fig. 5.4, 4-way movement classification allows convergence on correct targets in fewer steps, on average, than binary movement classification. This difference in MNS was statistically significant ($p < 0.05$) in the small grid at 5 out of 9 *stringency* levels, and tending to be statistically significant ($0.05 < p < 0.07$) in a further 3 cases. In the large grid, the increases in speed using 4-way movement classification were not found to be statistically significant ($0.08 < p < 0.18$). This may be due to the high standard deviation of MNS between participants, when using binary movement classification. At a *stringency* of 0.9, the standard deviation was 36.3 when using binary movement classification, compared to 6.4 when using 4-way movement classification.

Therefore, when using 4-way movement classification, we have seen some significant improvements in speed, as well as increased consistency of speed between participants.

5.5 Discussion & Conclusion

This study has presented a scalable approach that makes it possible to use reactive EEG feedback not only to navigate towards target locations, but also to accurately identify the correct targets once they have been reached. All strategies using EEG feedback correctly identified several times more targets than the *Random* approach. The EEG feedback strategies were also capable of identifying these targets in fewer steps than the *Random* approach. Our proposed Bayesian inference strategy, which iteratively updated a probabilistic model to learn the most likely target location, proved to be the most efficient of the navigation strategies tested in this study. The Bayesian strategy also maintained very high accuracy — here defined as the percentage of targets correctly identified ($PTCI$) — when expanded to a large grid, in which any of 400 spaces could be the target.

For the first time, we have shown that it is possible to perform 4-way single-trial classification of different types of navigational actions, based on automatically generated EEG signals as participants only had to observe the virtual robot tasks. Furthermore, we have shown a system that uses this 4-way classification of EEG responses to robotic movements as feedback for learning-based navigation. This provided contextualised feedback to the robot, including specific information regarding when the target location had been reached. Our results demonstrate that such detailed classification can lead to a more efficient semi-autonomous robot navigation than can be achieved with binary, error vs correct EEG

classification alone. We therefore recommend the use of detailed EEG classification where possible in reinforcement learning-based BCIs.

Additionally, binary classification was performed on target identification actions, classifying them as either correct or false. Reliable classification of target identification actions provides the system with an increased level of robustness, due to ability to undo false identifications.

Our proposed Bayesian inference strategy includes an adjustable parameter: *stringency*. By tuning this parameter, we can make the system require a higher or lower threshold of certainty to be met before identifying a target. As such, we can amend the strategy to focus on reaching targets more quickly, or identifying them with greater accuracy, making this approach applicable in a wide range of scenarios. In the fastest case, targets were correctly identified after a mean of 3.3 normalised steps, indicating that a small number of errors can be enough to teach the robot. Interestingly, in the most accurate case, an average of more than 98% of targets were identified correctly.

We have shown the capability for a robot to learn user intentions from reactive EEG signals in a more efficient and scalable manner than ever before. These signals are obtained while users simply observe the robot's actions, providing a form of implicit communication. We therefore believe that the mental workload of the user would be reduced. Such capability could be extremely useful for assistive robotics. Therefore, this study represents important steps forwards for semi-autonomous BCIs, and for efficient, user-friendly human-machine interaction.

Chapter 6

Future Outlook: Towards Real-Time Semi-Autonomous Navigation

6.1 Chapter Introduction

In the previous chapter, I showed that it is possible to use detailed EEG feedback, combined with a machine learning model, to navigate towards targets and identify when they have been reached in an efficient manner. In order for a system such as this to be fully usable, the next required development would be to implement the system with a human-in-the-loop in real time. As such, the proposed approach for including the human-in-the-loop is discussed in this chapter.

In the field of BCI, considerably more attention has been paid to the training and adaptation of classifiers and machine learning systems than the training and adaptation of users [95, 135]. Nonetheless, the effects of different training and feedback approaches on the human-in-the-loop have been investigated in some depth in active BCI [135]. For example, a variety of different feedback modalities have been shown to improve user performance in BCI for stroke rehabilitation [4]. Meanwhile, biased feedback has been shown to reduce classification accuracy for users who already proficiently control a BCI, but can improve accuracy for users who were previously performing at or near chance level [9]. In BCI based on mental tasks, adaptive feedback methods have been recommended to enhance performance [95].

Comparatively little is known about the effects of feedback, or user adaptation, in passive or reactive BCI systems. However, it has been shown that appropriate and timely feedback can modulate ERP responses in a P300-based BCI, and thus improve performance [8].

Therefore, these factors are important considerations with a human-in-the-loop reactive BCI.

6.2 A Real-Time Paradigm

Preliminary real-time piloting began prior to being curtailed due to COVID-19 related restrictions.

Initial piloting was carried out using a 1-dimensional implementation of the Cursor Task. This was selected as strong results were previously reported in the 1-dimensional Cursor Task, and the task would allow straightforward expansion to more complex scenarios such as a 2-dimensional space, and the inclusion of obstacles.

The proposed EEG setup was the same as had been implemented in offline sessions of the Cursor Task, as previously described in section 4.2.2.1. 8 channels of EEG were to be recorded at 500Hz using an Enobio 8 headset. The electrode sites recorded were Fz, Cz, Pz, Oz, C3, C4, P07, and PO8. A further reference electrode was to be placed on the earlobe. This setup was selected due to this relatively small number of electrodes providing key data and proving fruitful in our simulated outcomes, as discussed in the previous chapter.

At the beginning of each session, a number of calibration blocks would be carried out, each lasting approximately 4 minutes. These blocks would follow a similar protocol to that of the offline Cursor Task sessions, descried in section 4.2.2.2. Participants would then be given a brief break in order for the subject-specific classification models to be trained. These would consist of:

1. A four-way classification model of movement actions
2. A binary classification model of target selection actions

All classifiers would be implemented using stepwise linear discriminant analysis (SWLDA) as previously described in section 5.3.1.

Online blocks of trials, again lasting approximately four minutes per block, would then be carried out. These would follow a similar protocol to the simulated real-time experiments discussed in the previous chapter: after each action performed by the virtual robot, an EEG trial would be extracted from 200ms to 700ms relative to the movement. This trial would immediately be preprocessed and classified according to the appropriate model, depending on the type of action that had been performed. The virtual robot would navigate and identify target loci according to the Bayesian inference navigation strategy described in section 5.3.2.1.

6.3 Overcoming Challenges of a Human-in-the-Loop Scenario

A number of potential challenges are involved in performing real-time experiments with immediate EEG feedback from participants.

One such challenge is to achieve the correct balance in selecting the number of calibration blocks. Of course, the first priority is to obtain enough trials of each class, in order to properly train the models and achieve accurate classification. However, long calibration sessions are undesirable in practice, as users generally will not wish to be required to calibrate a system for a long time each time they need to use it.

In the offline Cursor Task experiments, most participants recorded 6 blocks of trials (approximately 24 minutes in total), and this proved enough to provide accurate and usable 4-way classification. For a system employing binary, error-vs-correct movement classification, Chavarriaga and Millán used 10 blocks of approximately 3 minutes each (approximately 30 minutes in total) to collect training data [29]. In a study by Iturrate et al., also using binary error-vs-correct movement classification, blocks of 100 actions were observed, and a classifier was trained after each block [63]. Training continued until classification accuracy reached 80%, or until four training blocks had been completed, resulting in a mean training time of 25 minutes. A similar approach may be advisable here, with the model being trained after each 4 minute run. Training blocks could then continue until 4-way movement classification accuracy and binary target identification classification, assessed via leave-one-out cross validation, reached 45% and 70% respectively (mean accuracies by these metrics in the data used for simulated experiments were 48.7% and 73.5% respectively, and the minimum for individual participants were 40.4% and 64.3% respectively — see tables 5.1 and 5.2), or until a maximum of six blocks of trials had been recorded.

Another consideration is whether the reactive EEG signals will remain consistent between calibration blocks and online blocks. There are some factors that could affect this. Firstly, it has been shown that differing rates at which erroneous actions occur can affect the ErrP response and, in turn, classification accuracy [29]. Similarly, P300 amplitude has been shown to be affected by target-to-target interval [52]. Therefore, it may be desirable — at least in early experiments — that the rate at which each action type occurs aligns as closely as possible between the calibration and online sessions. A suggested strategy to mitigate this challenge would be similar to that discussed above. Error rates in calibration sessions could be set according to known data regarding average classification accuracy. Training could then be curtailed when the trained models reached the equivalent accuracy levels.

It has been shown that factors that are intrinsic to the user, such as motivation, can modulate the brain's response to stimuli in a BCI [76]. It is feasible that signals may

also be affected by participants' perceived difference in valence between calibration sessions (where their observation has no effect on the system) and online sessions (where their observation does affect the performance). For example, one piloting participant appeared to display a larger P300 peak in response to the TR condition — albeit based on a relatively small number of calibration samples — resulting in this becoming conflated with the error conditions. Related studies that have included both training and online sessions have not reported notable differences between responses across the sessions [29, 63]. However, it should be noted that these studies dealt only with binary movement classification, and each run automatically ended when targets were reached, and so trials equivalent to the TR condition were not considered. In order to mitigate this challenge, it would be advisable to duplicate scenarios as closely as possible between the calibration and online sessions. One way to achieve this would be to tell participants that their responses were influencing the performance from the beginning of the calibration session.

6.4 Further Proposed Developments

In the approach explored in this thesis, users merely have to observe the actions of a machine, which is then controlled semi-autonomously, using implicit human-machine communication as feedback to guide it. This approach has the potential to make BCI more user-friendly by reducing the mental workload required by users. In order to make such a system as efficient and effective as possible, there are a number of further developments that we would recommend.

6.4.1 Improvements to the BCI Model

New or updated machine learning strategies could be researched and implemented in order to improve the generalisability from small and imbalanced training data. Transfer learning algorithms could be explored in order to further improve both calibration time and classification accuracy.

6.4.2 Expansion upon the User Behaviour Model

The current system treats each run as a standalone navigational task, and as such each run begins with every available location having an equal probability of being the user's desired target. However, whether we are navigating about a room or a city, there are some locations we are likely to visit more often than others. For example, we are more likely to need to navigate to our own workplace than another office building. Therefore, a natural extension to this research would be to develop long-term, adaptive probabilistic modelling. As well as

updating target probabilities in the short term for each run — that is, for each journey — such a system would also update long-term probabilities of a user's preferences and target locations after each successful target identification. This would inform the initial prior probabilities at the beginning of future journeys, making it more likely that the machine would immediately set out on the correct path, but still allowing the user to choose a less common target, or even one that had not previously been visited.

6.4.3 An Intelligent Interaction between the BCI Model and User Model

With the BCI model and user model both in place and working efficiently, the overall system could be further improved via the research and development of an intelligent interaction between the two models. Confidence in the accuracy of both models could be continually assessed, and used to inform the machine's predictions and actions. Factors such as fatigue, workload, emotions and alertness, could be considered, by using passive brain signals as further inputs to monitor the user model. To maintain a high level of performance over time, the system must consider changes in brain signals as the human adapts to using the BCI. The system should itself be adaptive, promoting long-term, mutual learning.

6.4.4 Extending to Other Tasks and Applications

Virtual robot navigation has been the primary exemplar for the concepts shown in this thesis, and we would propose that they would also make an appropriate exemplar for the extensions and developments discussed above. A natural next step would then be to apply these techniques with a real robot navigating in a physical space. However, these techniques could be applicable to any scenario in which users select a number of preferences at varying rates.

Chapter 7

Conclusions

7.1 Key Achievements

This thesis presented several research achievements, which have contributed new and important knowledge to the fields of EEG analysis and BCI.

- The thesis successfully showed that it was possible to classify new and more subtle subclasses of errors against each other, using single-trial EEG.
- The thesis successfully showed, for the first time, that it is possible to classify different types of correct actions against each other, using single-trial EEG.
- The thesis successfully showed that the above information could be combined as inputs for a novel Bayesian learning system, for efficient semi-autonomous navigation.

These contributions are detailed further in the following sections.

7.2 Decoding EEG Responses to Different Errors

The first objective of this research project was to investigate the possibility of decoding EEG responses to different types of errors. As discussed in chapter 3, this project has successfully shown that it is possible to decode these signals, classifying them against each other on a single-trial basis. This was shown to be possible even when the differences between conditions were relatively subtle, in metrics that had not previously been explored.

In a navigational context, we explored the Claw Task - a virtual robotic claw crane game in which the robot's aim was to move towards, and select, a target object. As a proof of concept, we showed that it is possible to use single trial EEG to distinguish between the brain's responses to two different types of erroneous movement:

1. The FA condition: Moving further away from the target when starting from an off-target location

2. The SO condition: Stepping directly off the target location

Further to this, we investigated data from the Error Awareness Dot Task (EADT). In this task, users had to perform a mouse click in response to each stimulus presented, with the exception of two conditions. Our study showed that it is possible to use single trial EEG to distinguish between the brain's responses to these two error conditions:

1. The colour condition: Failing to withhold the mouse click if the current stimulus is a blue dot

2. The repeat condition: Failing to withhold the mouse click if the current stimulus is the same colour as the previous stimulus

The differences between error types within each task were subtle, varying only according to the context in which they occurred, and the cognitive processes required to recognise them. Nevertheless, classification accuracy was greater than chance level for most participants of both tasks. Furthermore, group p-values for both tasks highly significant.

This project has therefore successfully shown, in various previously unexplored scenarios, that it is possible to decode EEG responses to different errors.

7.3 Decoding EEG Responses to Different Non-Erroneous Actions

The second objective of this research project was to investigate the possibility of decoding EEG responses to different types of non-erroneous actions. As discussed in chapter 4, this project has successfully shown that it is possible to decode these signals, classifying them against each other on a single-trial basis.

This objective was explored using the Cursor Task — another navigational task in which a virtual robot, denoted by a cursor, aimed to move towards a target location and correctly identify when it had reached the target. Existing state-of-the-art systems using reactive EEG signals had not previously explored the possibility of using a reactive EEG signal specifically to identify when the target had been reached. In our study, we investigated the brain signals produced in response to the following types of correct actions:

1. The TT condition: The virtual robot moves towards the target, but does not reach it

2. The TR condition: The virtual robot reaches the target

For the first time, the findings of this project have successfully shown that it is possible to distinguish between these two conditions, using single-trial EEG responses to these actions.

In addition to our own practical experiment, a further publicly available data set from a related virtual robot navigation task [29] was used to further verify our approach. The classification accuracy levels that we achieved were greater than chance level for all participants included in the testing phase from both tasks. Group p-values for both data sets were also highly significant.

This project has therefore successfully shown, for the first time, that it is possible to decode EEG responses to different non-erroneous actions.

7.4 A Real-Time Navigation Application Driven by Implicit Human-Robot Interaction and Machine Learning

The third objective of this research project was to implement a real-time system of implicit human-robot interaction, and the fourth and final objective was to improve this interaction via machine learning strategies.

A real-time paradigm was implemented and tested via simulated experiments. After each of the virtual robot's actions, the system retrieved a real, previously-recorded EEG trial to use as feedback. These trials were classified, and the classifier outputs were used to inform the future actions of the virtual robot. While state-of-the-art reactive EEG systems have focused on binary, error-vs-correct feedback, this thesis has presented a novel, detailed system of feedback: 4-way classification of movements — the TT, TR, FA, and SO conditions as detailed above — and additional binary classification of target identification actions.

A machine learning strategy was implemented to utilise these detailed classifications for semi-autonomous navigation. The majority of approaches to similar challenges have used reinforcement learning to learn the route from A to B. In this thesis, the challenge was reframed, with the assumption that the route between any two locations is already known. This allowed for the implementation of a novel approach, in which the information that was to be learned was the user's intended target. The system used Bayesian inference to build a probabilistic model of the likelihood of each location being the target. This model was used to inform the virtual robot's future movements, and determine when an appropriate level of confidence had been achieved to identify a location as the target. The use of Bayesian inference allowed not only the classifier outputs, but also the level of confidence in classification accuracy, to be factored into the probabilistic updates.

As discussed in chapter 5, our novel application of this machine learning strategy was compared to a system that used EEG feedback without the aid of any machine learning.

Comparisons were also carried out between a system using detailed EEG feedback, and a system using the existing state-of-the-art error-vs-correct feedback.

The findings of this thesis have shown that a system of detailed implicit brain-machine communication is possible, and that this novel system facilitates more efficient robot navigation than systems using state-of-the-art, binary error-vs-correct feedback. Furthermore, our findings also showed that our machine learning system provided more accurate target identification than a purely reactive system.

Real-time experiments with in-person participants have not been carried out due to current guidelines. However, chapter 6 of this thesis has discussed strategies for carrying out such experiments. In chapter 6, we have also discussed a number of future directions, extensions and expansions upon this research project, which could build upon the advances shown in this thesis and continue to take this avenue of research further. These possibilities include utilising transfer learning to further improve the accuracy and calibration time of the system, and the expansion of the system to implement long-term, adaptive learning.

7.5 Summary

In summary, the novel findings of this research project have been combined to create a novel framework of detailed implicit brain-machine communication. This allows precise information to be gathered while users merely need to observe the actions of a machine. Thus we can postulate that the mental burden upon the user will be reduced, compared to conventional BCI systems. When combined with a new application of Bayesian inference, the resulting system has been shown to facilitate more efficient machine navigation, and more accurate target identification, than existing state-of-the-art systems. Therefore, the research presented in this thesis opens new doors for a more efficient and user friendly BCI.

Bibliography

[1] R. Abiri, S. Borhani, E. W. Sellers, Y. Jiang, and X. Zhao. A comprehensive review of eeg-based brain–computer interface paradigms. *J. Neural Eng.*, 16:011001, 2019.

[2] I. Akinola, Z. Wang, J. Shi, X. He, P. Lapborisuth, J. Xu, D. Watkins-Valls, P. Sajda, and P. Allen. Accelerated robot learning via human brain signals, 2019.

[3] S. Amiri, R. Fazel-Rezai, and V. Asadpour. A review of hybrid brain-computer interface systems. *Adv. Human-Comput. Interact*, 2013:1–8, 2013.

[4] K. K. Ang and C. Guan. Brain-computer interface in stroke rehabilitation. *J Comput Sci Eng*, 7:139–146, 2013.

[5] Y. Arbel and E. Donchin. Parsing the componential structure of post-error erps: A principal component analysis of erps following errors. *Psychophysiology*, 46:1179–1189, 2009.

[6] X. Artusi, I. K. Niazi, M.-F. Lucas, and D. Farina. Performance of a simulated adaptive bci based on experimental classification of movement-related and error potentials. *IEEE Trans. Emerg. Sel. Topics Circuits Syst.*, 1:480–488, 2011.

[7] M. Arvaneh, C. Guan, K. K. Ang, and C. Quek. Eeg data space adaptation to reduce intersession nonstationarity in brain-computer interface. *Neural Computation*, 25:2146–2171, 2013.

[8] M. Arvaneh, T. E. Ward, and I. H. Robertson. Effects of feedback latency on p300-based brain-computer interface. In *Proc. 37th Annual International Conference of the IEEE Engineering in Medicine and Biology Society (EMBC'15)*, pages 2315–2318, Aug. 2015.

[9] A. Barbero and M. Grosse-Wentrup. Biased feedback in brain-computer interfaces. *J Neuroeng Rehabil*, 7:34, 2010.

[10] A. Bashashati, M. Fatourechi, R. K. Ward, and G. E. Birch. A survey of signal processing algorithms in brain-computer interfaces based on electrical brain signals. *Journal of Neural Engineering*, 4, Mar. 2007.

[11] J. Bayliss. Use of the evoked potential p3 component for control in a virtual apartment. *IEEE Trans. Neural Syst. Rehabil. Eng.*, 11:113–116, 2003.

[12] C. J. Bell, P. Shenoy, R. Chalodhorn, and R. P. N. Rao. Control of a humanoid robot by a noninvasive brain–computer interface in humans. *J. Neural Eng.*, 5:214–220, 2008.

[13] P. S. Bernstein, M. K. Scheffers, and M. G. H. Coles. Where did i go wrong? a psychophysiological analysis of error detection. *Journal of Experimental Psychology: Human Perception and Performance*, 21(6):1312–1322, 1995.

[14] R. Beveridge, S. Wilson, M. Callaghan, and D. Coyle. Neurogaming with motion-onset visual evoked potentials (mveps): Adults versus teenagers. *IEEE Trans. Neural Syst. Rehabil. Eng.*, 27:572–581, 2019.

[15] S. Bhattacharyya, A. Konar, and D. N. Tibarewala. Motor imagery, p300 and error-related eeg-based robot arm movement control for rehabilitation purpose. *Med. Biol. Eng. Comput.*, 52:1007–1017, 2014.

[16] N. Birbaumer, N. Ghanayim, T. Hinterberger, I. Iversen, B. Kotchoubey, A. Kübler, J. Perelmouter, E. Taub, and H. Flor. A spelling device for the disabled. *Nature*, 398, Mar. 1999.

[17] N. Birbaumer, A. Kubler, N. Ghanayim, T. Hinterberger, J. Perelmouter, J. Kaiser, I. Iversen, B. Kotchoubey, N. Neumann, and H. Flor. The thought translation device (ttd) for completely paralyzed patients. *IEEE Transactions on Rehabilitation Engineering*, 8(2):190–193, June 2000.

[18] B. Blankertz, L. Acqualagna, S. Dähne, S. Haufe, M. Schultze-Kraft, I. Sturm, M. Ušćumlic, M. A. Wenzel, G. Curio, and K.-R. Müller. The berlin brain-computer interface: Progress beyond communication and control. *Frontiers in Neuroscience*, 10, Nov. 2016.

[19] B. Blankertz, G. Dornhege, C. Schafer, R. Krepki, J. Kohlmorgen, K. . Muller, V. Kunzmann, F. Losch, and G. Curio. Boosting bit rates and error detection for the classification of fast-paced motor commands based on single-trial eeg analysis. *IEEE Transactions on Neural Systems and Rehabilitation Engineering*, 11(2):127–131, June 2003.

[20] B. Blankertz, C. Sannelli, S. Halder, E. M. Hammer, A. Kübler, K.-R. Müller, G. Curio, and T. Dickhaus. Neurophysiological predictor of smr-based bci performance. *NeuroImage*, 51, July 2010.

[21] B. Blankertz, M. Tangermann, C. Vidaurre, S. Fazli1, C. Sannelli1, S. Haufe, C. Maeder, L. Ramsey, I. Sturm, G. Curio, and K.-R. Müller. The berlin brain–computer interface: non-medical uses of bci technology. *Frontiers in Neuroscience*, 4, Dec. 2010.

[22] B. Blankertz, R. Tomioka, S. Lemm, M. Kawanabe, and K.-R. Müller. Optimizing spatial filters for robust eeg single-trial analysis. *IEEE Signal Processing Magazine*, 41:41–56, Jan. 2008.

[23] F. Bonin-Font, A. Ortiz, and G. Oliver. Visual navigation for mobile robots: A survey. *J. Intell. Robot. Syst*, 53:263–296, 2008.

[24] F. Breton, W. Ritter, R. Simson, and H. G. Vaughan. The n2 component elicited by stimulus matches and multiple targets. *Biol Psychol*, 27:23–44, 1988.

[25] A. Buttfield, P. W. Ferrez, and J. del R. Millán. Towards a robust bci: Error potentials and online learning. *IEEE Transactions on Neural Systems and Rehabilitation Engineering*, 2:164–168, 2006.

[26] M. E. Cano, Q. A. Class, and J. Polich. Affective valence, stimulus attributes, and p300: Color vs. black/white and normal vs. scrambled images. *Int J Psychophysiol*, 71:17–24, 2009.

[27] L. Carretié, J. Iglesias, T.García, and M.Ballesteros. N300, p300 and the emotional processing of visual stimuli. *Electroencephalogr. Clin. Neurophysiol.*, 103:298–303, 1997.

[28] V. Chamola, A. Vineet, A. Nayyar, and E. Hossain. Brain-computer interface-based humanoid control: A review. *Sensors*, 20:3620, 2020.

[29] R. Chavarriaga and J. d. R. Millán. Learning from eeg error-related potentials in noninvasive brain-computer interfaces. *IEEE Transactions on Neural Systems and Rehabilitation Engineering*, 18(4):381–388, Aug. 2010.

[30] R. Chavarriaga, A. Sobolewski, and J. del R. Millán. Errare machinale est: the use of error-related potentials in brain-machine interfaces. *Frontiers in Neuroscience*, 8:208, 2014.

[31] J. Cohen and J. Polich. On the number of trials needed for p300. *Int. J. Psychol.*, 25:249–255, 1997.

[32] M. A. Conroy and J. Polich. Affective valence and p300 when stimulus arousal level is controlled. *Cogn Emot*, 21:891–901, 2007.

[33] S. W. Davis, N. A. Dennis, S. M. Daselaar, M. S. Fleck, and R. Cabeza. Què pasa? the posterior–anterior shift in aging. *Cerebral Cortex*, 18:1201–1209, 2008.

[34] A. Delorme and S. Makeig. Eeglab: an open source toolbox for analysis of single-trial eeg dynamics including independent component analysis. *Journal of Neuroscience Methods*, 134:9–21, 2004.

[35] B. Derrick, D. Toher, and P. White. Why welch's test is type i error robust. *Quant Methods Psychol*, 12:30–38, 2016.

[36] G. Desouza and A. Kak. Vision for mobile robot navigation: A survey. *IEEE T Pattern Anal*, 24:237–267, 2002.

[37] G. Deutsch, W. T. Bourbon, A. C. Papanicolaou, and H. M. Eisenberg. Visuospatial tasks compared via activation of regional cerebral blood flow. *Neuropsychologia*, 26:445–452, 1988.

[38] E. Donchin, K. M. Spencer, and R. Wijesinghe. The mental prosthesis: assessing the speed of a p300-based brain-computer interface. *IEEE Trans. Rehabil. Eng.*, 8:174–179, 2000.

[39] T. Endrass, C. Franke, and N. Kathmann. Error awareness in a saccade countermanding task. *Journal of Psychophysiology*, 19:275–280, 2005.

[40] T. Endrass, B. Reuter, and N. Kathmann. Erp correlates of conscious error recognition: aware and unaware errors in an antisaccade task. *Eur J Neurosci*, 26:1714–1720, 2007.

[41] M. Falkenstein, J. Hohnsbein, J. Hoormann, and L. Blanke. Effects of crossmodal divided attention on late erp components. ii. error processing in choice reaction tasks. *Electroencephalogr Clin Neurophysiol*, 78:447–455, 1991.

[42] M. Falkenstein, J. Hoormann, S. Christ, and J. Hohnsbein. Erp components on reaction errors and their functional significance: a tutorial. *Biological Psychology*, 51:87–107, 2000.

[43] L. Farwell and E. Donchin. Talking off the top of your head: toward a mental prosthesis utilizing event-related brain potentials. *Electroencephalogr. Clin. Neurophysiol.*, 70:510–523, 1988.

[44] M. Fatourechi, A. Bashashati, R. K. Ward, and G. E. Birch. Emg and eog artifacts in brain computer interface systems: A survey. *Clinical Neurophysiology*, 118, Mar. 2007.

[45] R. Fazel-Rezai, B. Z. Allison, C. Guger, E. W. S. S. C. Kleih, and A. Kübler. P300 brain computer interface: current challenges and emerging trends. *Front Neuroeng.*, 5:14, 2012.

[46] P. W. Ferrez and J. del R. Millán. Error-related eeg potentials generated during simulated brain–computer interaction. *IEEE Transactions on Biomedical Engineering*, 55(3):923–929, Mar. 2008.

[47] P. W. Ferrez and J. del R. Millán. Simultaneous real-time detection of motor imagery and error-related potentials for improved bci accuracy. In *Proc. 4th International Brain-Computer Interface Workshop and Training Course*, pages 197–202, Graz, Austria, 2008.

[48] P. W. Ferrez and J. D. R. Millán. You are wrong! - automatic detection of interaction errors from brain waves. In *Proc. Nineteenth International Joint Conference on Artificial Intelligence*, pages 1413–1418, Edinburgh, Scotland, Aug. 2005.

[49] A. Finke, A. Lenhardt, and H. Ritter. The mindgame: A p300-based brain–computer interface game. *Neural Netw*, 22:1329–1333, 2009.

[50] F. Galán, M. Nuttin, E. Lew, P. Ferrez, G. Vanacker, J.Philips, and J. del R.Millán. A brain-actuated wheelchair: Asynchronous and non-invasive brain–computer interfaces for continuous control of robots. *Clin. Neurophysiol.*, 119:2159–2169, 2008.

[51] W. J. Gehring, B. Goss, M. G. Coles, D. E. Meyer, and E. Donchin. A neural system for error detection and compensation. *Psychological Science*, 4, Nov. 1993.

[52] C. J. Gonsalvez and J. Polich. P300 amplitude is determined by target-to-target interval. *Psychophysiology*, 39:388–396, 2002.

[53] C. Grady, J. Maisog, B. Horwitz, L. Ungerleider, M. Mentis, J. Salerno, P. Pietrini, E. Wagner, and J. Haxby. Age-related changes in cortical blood flow activation during visual processing of faces and location. *Journal of Neuroscience*, 14:1450–1462, 1994.

[54] J. Grizou, I. Iturrate, L. Montesano, P. Oudeyer, and M. Lopes. Calibration-free bci based control. In *Proc. AAAI Conference on Artificial Intelligence*, Québec City, Québec, Canada, July 2014.

[55] C. Guger, S. Dabana, C. H. Eric Sellers, G. Krausza, R. Carabalonac, F. Gramaticac, and G. Edlinger. How many people are able to control a p300-based brain–computer interface (bci)? *Neurosci. Lett.*, 462:94–98, 2009.

[56] C. Guger, W. Harkam, C. Hertnaes, and G. Pfurtscheller. Prosthetic control by an eeg-based brain-computer interface (bci). In *Proc. AAATE 5th European Conference for the Advancement of Assistive Technology*, pages 590–595, Düsseldorf, Germany, Nov. 1999.

[57] F. Guo, B. Hong, X. Gao, and S. Gao. A brain–computer interface using motion-onset visual evoked potential. *J Neural Eng*, 5:477–485, 2008.

[58] G. Hajcak, C. B. Holroyd, J. S. Moser, and R. F. Simons. Brain potentials associated with expected and unexpected good and bad outcomes. *Psychophysiology*, 42:161–170, 2005.

[59] S. Harty, P. R. Murphy, I. H. Robertson, and R. G. O'Connell. Parsing the neural signatures of reduced error detection in older age. *NeuroImage*, 161:43–55, 2017.

[60] N. A. Heard and P. Rubin-Delanchy. Choosing between methods of combining p-values. *Biometrika*, 105:239–246, 2018.

[61] R. Hester, J. J. Foxe, S. Molholm, M. Shpaner, and H. Garavan. Neural mechanisms involved in error processing: A comparison of errors made with and without awareness. *NeuroImage*, 27:602–608, 2005.

[62] I. Iturrate, J. M. Antelis, A. Kübler, and J. Minguez. A noninvasive brain-actuated wheelchair based on a p300 neurophysiological protocol and automated navigation. *IEEE Trans. Robot.*, 25:614–627, 2009.

[63] I. Iturrate, R. Chavarriaga, L. Montesano, J. Minguez, and J. del R Millán. Teaching brain-machine interfaces as an alternative paradigm to neuroprosthetics control. *Scientific Reports*, 5, Sept. 2015.

[64] I. Iturrate, L. Montesano, and J. Minguez. Robot reinforcement learning using eeg-based reward signals. In *Proc. IEEE International Conference on Robotics and Automation (ICRA'10)*, pages 4822–4829, Anchorage, AK, USA, May 2010.

[65] I. Iturrate, L. Montesano, and J. Minguez. Single trial recognition of error-related potentials during observation of robot operation. In *Proc. International Conference of the IEEE Engineering in Medicine and Biology (EMBC'10)*, pages 4181–4184, Buenos Aires, Argentina, 2010.

[66] I. Iturrate, L. Montesano, and J. Minguez. Task-dependent signal variations in eeg error-related potentials for brain–computer interfaces. *J Neural Eng*, 10:026024, 2013.

[67] A. K. Jain and B. Chandrasekaran. Dimensionality and sample size considerations in pattern recognition practice. In P. Krishnaiah and L. Kanal, editors, *Handbook of Statistics*, volume 2, pages 835–855. North Holland, Amsterdam, Netherlands, 1982.

[68] B. H. Jansen, A. Allam, P. Kota, K. Lachance, A. Osho, and K. Sundaresan. An exploratory study of factors affecting single trial p300 detection. *IEEE Trans. Biomed. Eng.*, 51:975–978, 2004.

[69] G. D. Johnson, N. R. Waytowich, D. J. Cox, and D. J. Krusienski. Extending the discrete selection capabilities of the p300 speller to goal-oriented robotic arm control. In *3rd IEEE RAS and EMBS International Conference on Biomedical Robotics and Biomechatronics*, pages 572–575, Tokyo, Japan, 2010.

[70] S. Kanoh, K. Miyamoto, and T. Yoshinobu. A p300-based bci system for controlling computer cursor movement. In *Proc. 33th Annual International Conference of the IEEE Engineering in Medicine and Biology Society (EMBC)*, pages 6405–6408, Boston, MA, USA, 2011.

[71] A. Kaplan, S. Shishkin, T. Ganin, I. Basyul, and A. Zhigalov. Adapting the p300-based brain-computer interface for gaming: A review. *IEEE Trans. Comput. Intell. AI in Games*, 5:141–149, 2013.

[72] E. Keogh and A. Mueen. Curse of dimensionality. In C. Sammut and G. I. Webb, editors, *Encyclopedia of Machine Learning*, pages 257–258. Springer, Boston, MA, USA, 2010.

[73] H. Kim, J. Biggs, W. Schloerb, M. Carmena, M. Lebedev, M. Nicolelis, and M. Srinivasan. Continuous shared control for stabilizing reaching and grasping with brain-machine interfaces. *IEEE Trans. Biomed. Eng.*, 53:1164–1173, 2006.

[74] I.-H. Kim, J.-W. Kim, S. Haufe, and S.-W. Lee. Detection of braking intention in diverse situations during simulated driving based on eeg feature combination. *J Neural Eng*, 12:016001, 2015.

[75] S. K. Kim, E. A. Kirchner, A. Stefes, and F. Kirchner. Intrinsic interactive reinforcement learning - using error-related potentials for real world human- robot interaction. *Scientific Reports*, 7:17562, 2017.

[76] S. C. Kleih, F. Nijboer, S. Halder, and A. Kubler. Motivation modulates the p300 amplitude during brain-computer interface use. *Clin. Neurophysiol.*, page 102331, 2010.

[77] G. H. Klem, H. O. L. Èders, H. Jasper, and C. Elger. The ten-twenty electrode system of the international federation. In G. Deuschl and A. Eisen, editors, *Recommendations for the Practice of Clinical Neurophysiology*, pages 3–6. Elsevier Science B.V., 1999.

[78] J. Kohlmorgen, G. Dornhege, M. L. Braun, B. Blankertz, K.-R. Müller, G. Curio, K. Hagemann, A. Bruns, M. Schrauf, and W. E. Kincses. Improving human performance in a real operating environment through real-time mental workload detection. In J. d. R. M. Guido Dornhege, T. Hinterberger, D. McFarland, and K.-R. Müller, editors, *Toward Brain-Computer Interfacing*, pages 409–422. MIT Press, Cambridge, MA, USA, 2007.

[79] L. Korczowski, M. Congedo, and C. Jutten. Single-trial classification of multi-user p300-based brain-computer interface using riemannian geometry. In *Proc. 37th Annual International Conference of the IEEE Engineering in Medicine and Biology Society (EMBC)*, pages 1769–1772, Milan, Italy, 2015.

[80] L. R. Krol, L. M. Andreessen, and T. O. Zander. Passive brain-computer interfaces: A perspective on increased interactivity. In C. S. Nam, A. Nijholt, and F. Lotte, editors, *Brain-Computer Interfaces Handbook*, pages 69–86. CRC Press, Boca Raton, FL, USA, 2018.

[81] L. R. Krol, P. Haselager, and T. O. Zander. Cognitive and affective probing: A tutorial and review of active learning for neuroadaptive technology. *J. Neural Eng.*, 2019.

[82] J. K. Kruschke and T. M. Liddell. Bayesian data analysis for newcomers. *Psychon Bull Rev*, 25:155–177, 2018.

[83] D. J. Krusienski, E. W. Sellers, F. Cabestaing, S. Bayoudh, D. J. McFarland, T. M. Vaughan, and J. R. Wolpaw. A comparison of classification techniques for the p300 speller. *Journal of Neural Engineering*, 3:299, 2006.

[84] D. J. Krusienski, E. W. Sellers, D. J. McFarland, T. M. Vaughan, and J. R. Wolpaw. Toward enhanced p300 speller performance. *Journal of Neuroscience Methods*, 167:15–21, 2008.

[85] M. Kuba, Z. Kubová, J. Kremláček, and J. Langrová. Motion-onset veps: Characteristics, methods, and diagnostic use. *Vision Res.*, 47:189–202, 2007.

[86] E. A. Lacey. *Behavioural and Electrophysiological Aspects of Error Processing in Alzheimer's Disease and Healthy Ageing*. PhD thesis, Trinity College Dublin, Dublin, Ireland, 2020.

[87] T. Lampe, L. D. Fiederer, M. Voelker, A. Knorr, M. Riedmiller, and T. Ball. A brain-computer interface for high-level remote control of an autonomous, reinforcement-learning-based robotic system for reaching and grasping. In *Proc. 19th International Conference on Intelligent User Interfaces*, IUI '14, pages 83–88, New York, NY, USA, 2014. ACM.

[88] M. J. Larson, S. A. Baldwin, D. A. Good, and J. E. Fair. Temporal stability of the error-related negativity (ern) and post-error positivity (pe): The role of number of trials. *Psychophysiology*, 47:1167–1171, 2010.

[89] A. Lenhardt, M. Kaper, and H. Ritter. An adaptive p300-based online brain-computer interface. *IEEE Trans. Neural Syst. Rehabil. Eng.*, 16:121–130, 2008.

[90] J. Lever, M. Krzywinski, and N. Altman. Points of significance: Model selection and overfitting. *Nat. Methods*, 13:703, 2016.

[91] Y. Li, J. Long, T. Yu, Z. Yu, C. Wang, H. Zhang, and C. Guan. An eeg-based bci system for 2-d cursor control by combining mu/beta rhythm and p300 potential. *IEEE Trans. Biomed. Eng.*, 57:2495–2505, 2010.

[92] M. Lidierth. filtfilthd. Accessed: November 2017.

[93] Y.-P. Lin, Y. Wang, C.-S. Wei, and T.-P. Jung. Assessing the quality of steady-state visual-evoked potentials for moving humans using a mobile electroencephalogram headset. *Frontiers in human neuroscience*, 8:182, 2014.

[94] Z. Lin, Y. Zeng, L. Tong, H. Zhang, C. Zhang, and B. Yan. Method for enhancing single-trial p300 detection by introducing the complexity degree of image information in rapid serial visual presentation tasks. *PLoS One*, 12:e0184713, 2017.

[95] F. Lotte. On the need for alternative feedback training approaches for bci. In *Proc. Berlin BCI workshop on Advances in Neurology 2012*, Sept. 2012.

[96] F. Lotte, L. Bougrain, A. Cichocki, M. Clerc, M. Congedo, A. Rakotomamonjy, and F. Yger. A review of classification algorithms for eeg-based brain–computer interfaces: a 10 year update. *J. Neural Eng.*, 15:031005, 2018.

[97] F. Lotte, M. Congedo, A. Lécuyer, F. Lamarche, and B. Arnaldi. A review of classification algorithms for eeg-based brain–computer interfaces. *Journal of Neural Engineering*, 4, Jan. 2007.

[98] F. Lotte, A. van Langhenhove, F. Lamarche, T. Ernest, Y. Renard, B. Arnaldi, and A. Lécuyer. Exploring large virtual environments by thoughts using a brain–computer interface based on motor imagery and high-level commands. *Presence: Teleoperators and Virtual Environments*, 19:54–70, Feb. 2010.

[99] T. M. Loughin. A systematic comparison of methods for combining p-values from independent tests. *Comput. Stat. Data Anal.*, 47:467–485, 2004.

[100] T. Lüth, D. Ojdanič, O. P. Ola Friman, and A. Gräser. Low level control in a semi-autonomous rehabilitation robotic system via a brain-computer interface. In *IEEE 10th International Conference on Rehabilitation Robotics*, pages 721–728, Noordwijk, Canada, 2007.

[101] T. T. Mac, C. Copot, D. T. Tran, and R. D. Keyser. Heuristic approaches in robot path planning: A survey. *Robot Auton Syst*, 86:13–28, 2016.

[102] D. Marshall, D. Coyle, and S. Wilson. Motion-onset visual evoked potentials for gaming: A pilot study. In *24th IET Irish Signals and Systems Conference*, page 56, Letterkenny, Ireland, 2013.

[103] S. G. Mason and G. E. Birch. A general framework for brain-computer interface design. *IEEE Transactions on Neural Systems and Rehabilitation Engineering*, 11:70–85, Mar. 2003.

[104] MATLAB, the Statistics and Machine Learning Toolbox, and the Signal Processing Toolbox. *Release 2018b*. The MathWorks Inc., Natick, Massachusetts, USA, 2018.

[105] S. M. McClure, M. K. York, and P. R. Montague. The neural substrates of reward processing in humans: The modern role of fmri. *The Neuroscientist*, 10(3):260–268, 2004.

[106] J. Meng, S. Zhang, A. Bekyo, J. Olsoe, B. Baxter, and B. He. Noninvasive electroencephalogram based control of a robotic arm for reach and grasp tasks. *Scientific Reports*, 6, Dec. 2016.

[107] J.-A. Meyer and D. Filliat. Map-based navigation in mobile robots:: Ii. a review of map-learning and path-planning strategies. *Cogn. Syst. Res*, 4:283–317, 2003.

[108] J. Mladenovic, J. Frey, M. Joffily, E. Maby, F. Lotte, and J. Mattout. Active inference as a unifying, generic and adaptive framework for a p300-based bci. *J Neural Eng*, 17:016054, 2020.

[109] G. R. Müller-Putz, C. Breitwieser, F. Cincotti, R. Leeb, M. Schreuder, F. Leotta, M. Tavella, L. Bianchi, A. Kreilinger, A. Ramsay, M. Rohm, M. Sagebaum, L. Tonin, C. Neuper, and J. d. R. Millán. Tools for brain-computer interaction: a general concept for a hybrid bci. *Front. Neuroinform.*, 5, 2011.

[110] P. R. Murphy, I. H. Robertson, D. Allen, R. Hester, and R. G. O'Connell. An electrophysiological signal that precisely tracks the emergence of error awareness. *Frontiers in Human Neuroscience*, 6:65, 2012.

[111] P. R. Murphy, I. H. Robertson, S. Harty, and R. G. O'Connell. Neural evidence accumulation persists after choice to inform metacognitive judgments. *eLife*, 4:e11946, 2015.

[112] L. F. Nicolas-Alonso and J. Gomez-Gil. Brain computer interfaces, a review. *Sensors (Basel)*, 12:1211–1279, Feb. 2012.

[113] S. Nieuwenhuis, K. R. Ridderinkhof, J. Blom, G. P. Band, and A. Kok. Error-related brain potentials are differentially related to awareness of response errors: Evidence from an antisaccade task. *Psychophysiology*, 38:752–760, 2001.

[114] J. Omedes, I. Iturrate, J. Minguez, and L. Montesano. Analysis and asynchronous detection of gradually unfolding errors during monitoring tasks. *Journal of Neural Engineering*, 12, July 2015.

[115] J. Omedes, A. Schwarz, G. R. Müller-Putz, and L. Montesano. Factors that affect error potentials during a grasping task: toward a hybrid natural movement decoding bci. *Journal of Neural Engineering*, 15, June 2018.

[116] R. Ortner, B. Z. Allison, G. Korisek, H. Gaggl, and G. Pfurtscheller. An ssvep bci to control a hand orthosis for persons with tetraplegia. *IEEE Transactions on Neural Systems and Rehabilitation Engineering*, 19(1):1–5, Feb. 2011.

[117] T. J. M. Overbeek, S. Nieuwenhuis, and K. R. Ridderinkhof. Dissociable components of error processing: On the functional significance of the pe vis-a-vis the ern/ne. *J Psychophysiol*, 19:319–329, 2005.

[118] R. G. O'Connell, P. M. Dockree, M. A. Bellgrove, S. P. Kelly, R. Hester, H. Garavan, I. H. Robertson, and J. J. Foxe. The role of cingulate cortex in the detection of errors with and without awareness: a high-density electrical mapping study. *Eur J Neurosci*, 25:2571–2579, 2007.

[119] M. Palankar, K. J. D. Laurentis, R. Alqasemi, E. Veras, R. Dubey, Y. Arbel, and E. Donchin. Control of a 9-dof wheelchair-mounted robotic arm system using a p300 brain computer interface: Initial experiments. In *2008 IEEE International Conference on Robotics and Biomimetics*, pages 348–353, Feb. 2009.

[120] L. Parra, C. Alvino, A. Tang, B. Pearlmutter, N. Yeung, A. Osman, and P. Sajda. Linear spatial integration for single-trial detection in encephalography. *NeuroImage*, 17:223–230, 2002.

[121] L. C. Parra, C. D. Spence, A. D. Gerson, and P. Sajda. Response error correction - a demonstration of improved human-machine performance using real-time eeg monitoring. *IEEE Transactions on Neural Systems and Rehabilitation Engineering*, 11, June 2003.

[122] X. Perrin, R. Chavarriaga, F. Colas, R. Siegwart, and J. del R.Millán. Brain-coupled interaction for semi-autonomous navigation of an assistive robot. *Robotics and Autonomous Systems*, 58:1246–1255, 2010.

[123] R. Pezzetta, V. Nicolardi, E. Tidoni, and S. M. Aglioti. Error, rather than its probability, elicits specific electrocortical signatures: a combined eeg-immersive virtual reality study of action observation. *J Neurophysiol.*, 120:1107–1118, 2018.

[124] G. Pfurtscheller, B. Z. Allison, C. Brunner, G. Bauernfeind, T. Solis-Escalante, R. Scherer, T. O. Zander, G. Mueller-Putz, C. Neuper, and N. Birbaumer. The hybrid bci. *Frontiers in Neuroscience*, 4, Apr. 2010.

[125] T. Picton. The p300 wave of the human event-related potential. *Journal of clinical neurophysiology*, 9:456–479, 1992.

[126] G. Pires, M. Castelo-Branco, and U. Nunes. Visual p300-based bci to steer a wheelchair: A bayesian approach. In *2008 30th Annual International Conference of the IEEE Engineering in Medicine and Biology Society*, pages 658–661, Aug. 2008.

[127] J. Polich, J. E. Alexander, L. O. Baue, S. Kuperman, S. Morzorati, S. J. O'Connor, B. Porjesz, J. Rohrbaugh, and H. Begleiter. P300 topography of amplitude/latency correlations. *Brain Topogr*, 9:275–282, 1997.

[128] J. Polich, T. Brock, and M. W.Geisler. P300 from auditory and somatosensory stimuli: probability and inter-stimulus interval. *Int J Psychophysiol*, 11:219–222, 1991.

[129] J. Polich, P. C. Ellerson, and J. Cohen. P300, stimulus intensity, modality, and probability. *Int J Psychophysiol*, 23:55–62, 1996.

[130] J. B. Polikoff, H. T. Bunnell, and W. J. Borkowski. Toward a p300-based computer interface. In *RESNA'95 Annual Conf.*, pages 178–180, Vancouver, Canada, 1995.

[131] S. Raudys and A. Jain. Small sample size effects in statistical pattern recognition - recommendations for practitioners. *IEEE Trans. Pattern Anal. Mach. Intell.*, 13:252–264, 1991.

[132] B. Rebsamen, E. Burdet, C. Guan, H. Zhang, C. L. Teo, Q. Zeng, M. Ang, and C. Laugier. A brain-controlled wheelchair based on p300 and path guidance. In *1st IEEE/RAS-EMBS International Conference on Biomedical Robotics and Biomechatronics*, pages 1101–1106, Pisa, Italy, 2006.

[133] B. Rebsamen, C. Guan, H. Zhang, C. Wang, C. Teo, M. Ang, and E. Burdet. A brain controlled wheelchair to navigate in familiar environments. *IEEE Trans. Neural Syst. Rehabil. Eng.*, 18:590–598, Dec. 2010.

[134] B. Reuderink, C. Mühl, and M. Poel. Valence, arousal and dominance in the eeg during game play. *Int J Auton Adapt Commun Syst*, 6:45–62, 2013.

[135] A. Roc, L. Pillette, J. Mladenović, C. Benaroch, B. N'Kaoua, C. Jeunet, and F. Lotte. A review of user training methods in brain computer interfaces based on mental tasks. *J Neural Eng*, 2020.

[136] K. J. Rothman. No adjustments are needed for multiple comparisons. *Epidemiology*, 1:43–46, 1990.

[137] A. S. Royer, A. J. Doud, M. L. Rose, and B. He. Eeg control of a virtual helicopter in 3-dimensional space using intelligent control strategies. *IEEE Trans. Neural Syst. Rehabilitation Eng.*, 18:581–589, 2010.

[138] G. D. Ruxton. The unequal variance t-test is an underused alternative to student's t-test and the mann–whitney u test. *Behav Ecol*, 17:688–690, 2006.

[139] S. W. S, B. Krieg-Brückner, H. Mallot, K. Schweizer, and C. Freksa. Spatial cognition: The role of landmark, route, and survey knowledge in human and robot navigation. In M. Jarke, K. Pasedach, and K. Pohl, editors, *Informatik '97 Informatik als Innovationsmotor. Informatik aktuell*, pages 41–50. Springer, Berlin, Heidelberg, 1997.

[140] A. Sato, A. Yasuda, H. Ohira, K. Miyawaki, M. Nishikawa, H. Kumano, and T. Kuboki. Effects of value and reward magnitude on feedback negativity and p300. *Neuroreport*, 16:407–411, 2005.

[141] G. Schalk and E. C. Leuthardt. Brain-computer interfaces using electrocorticographic signals. *IEEE Reviews in Biomedical Engineering*, 4:140–154, 2011.

[142] G. Schalk, J. R. Wolpaw, D. J. McFarland, and G. Pfurtscheller. Eeg-based communication: presence of an error potential. *Clinical Neurophysiology*, 111, Dec. 2000.

[143] L. Schiatti, J. Tessadori, N. Deshpande, G. Barresi, L. King, and L. Mattos. Human in the loop of robot learning: Eeg-based reward signal for target identification and reaching task. In *Proc. ICRA 2018 - IEEE International Conference on Robotics and Automation*, pages 4473–4480, Brisbane, Australia, Sept. 2018.

[144] N. M. Schmidt, B. Blankertz, and M. S. Treder. Online detection of error-related potentials boosts the performance of mental typewriters. *BMC Neuroscience*, 13(1):19, Feb. 2012.

[145] D. Schneider, C. Beste, and E. Wascher. On the time course of bottom-up and top-down processes in selective visual attention: An eeg study. *Psychophysiology*, 49:1660–1671, 2012.

[146] W. Schultz. Book review: Reward signaling by dopamine neurons. *The Neuroscientist*, 7(4):293–302, 2001.

[147] W. Schultz, P. Dayan, and P. R. Montague. A neural substrate of prediction and reward. *Science*, 275(5306):1593–1599, 1997.

[148] E. W. Sellers and E. Donchin. A p300-based brain–computer interface: Initial tests by als patients. *Clin Neurophysiol*, 117:538–548, 2006.

[149] D. Smith, E. Donchin, L. Cohen, and A. Starr. Auditory averaged evoked potentials in man during selective binaural listening. *Electroencephalogr. Clin. Neurophysiol.*, 28:146–152, 1970.

[150] G. Spinelli, G. Tieri, E. Pavone, and S. Aglioti. Wronger than wrong: Graded mapping of the errors of an avatar in the performance monitoring system of the onlooker. *NeuroImage*, 167:1–10, 2018.

[151] M. Spüler and C. Niethammer. Error-related potentials during continuous feedback: using eeg to detect errors of different type and severity. *Frontiers in Human Neuroscience*, 9:155, Mar. 2015.

[152] M. Spüler, M. Bensch, S. Kleih, W. Rosenstiel, M. Bogdan, and A. Kübler. Online use of error-related potentials in healthy users and people with severe motor impairment increases performance of a p300-bci. *Clinical Neurophysiology*, 123:1328–1337, 2012.

[153] S. M. Stigler. Thomas bayes's bayesian inference. *Journal of the Royal Statistical Society: Series A (General)*, 145:250–258, mar 1982.

[154] Y. Su, Y. Qi, J. xun Luo, B. Wu, F. Yang, Y. Li, Y. ting Zhuang, X. xiang Zheng, and W. dong Chen. A hybrid brain-computer interface control strategy in a virtual environment. *Journal of Zhejiang University SCIENCE C*, 12:351–361, 2011.

[155] M. Ullsperger, A. G. Fischer, R. Nigbur, and T. Endrass. Neural mechanisms and temporal dynamics of performance monitoring. *Trends in Cognitive Sciences*, 18:259–267, 2014.

[156] G. Vanacker, J. Del R. Millán, E. Lew, P. W. Ferrez, F. G. Moles, J. Philips, H. Van Brussel, and M. Nuttin. Context-based filtering for assisted brain-actuated wheelchair driving. *Comput. Intell. Neurosci.*, 2007:025130, 2007.

[157] M. Velliste, S. Perel, M. C. Spalding, A. S. Whitford, and A. B. Schwartz. Cortical control of a prosthetic arm for self-feeding. *Nature*, 453:1098, 2008.

[158] G. Visconti, B. D. Seno, M. Matteucci, and L. Mainardi. Automatic recognition of error potentials in a p300-based brain-computer interface. In *Proc. 4th International Brain-Computer Interface Workshop and Training Course*, pages 283–243, Graz, Austria, 2008.

[159] M. Völker, R. T. Schirrmeister, L. D. J. Fiedere, W. Burgard, and T. Ball. Deep transfer learning for error decoding from non-invasive eeg. In *Proc. 2018 6th International Conf. on Brain-Computer Interface (BCI)*, pages 1–6, GangWon, South Korea, 2018.

[160] S. Wang, C. Lin, C. Wu, and W. A. Chaovalitwongse. Early detection of numerical typing errors using data mining techniques. *IEEE Transactions on Systems, Man, and Cybernetics - Part A: Systems and Humans*, 41(6):1199–1212, Nov. 2011.

[161] C. Wirth, P. M. Dockree, S. Harty, E. Lacey, and M. Arvaneh. Towards error categorisation in bci: single-trial eeg classification between different errors. *J Neural Eng*, 2019.

[162] C. Wirth, E. Lacey, P. Dockree, and M. Arvaneh. Single-trial eeg classification of similar errors. In *Proc. 40th Engineering in Medicine and Biology Conference*, Honolulu, HI, USA, July 2018.

[163] C. Wirth, J. Toth, and M. Arvaneh. Four-way classification of eeg responses to virtual robot navigation. In *Proc. 42nd Annual International Conference of the IEEE Engineering in Medicine and Biology Society (EMBC'20)*, July 2020.

[164] C. Wirth, J. Toth, and M. Arvaneh. You have reached your destination: A single trial eeg classification study. *Front. Neurosci.*, 2020.

[165] M. Wolber and E. E. Wascher. The posterior contralateral negativity as a temporal indicator of visuo-spatial processing. *J Psychophysiol*, 19:182–194, 2005.

[166] J. R. Wolpaw, N. Birbaumer, W. J. Heetderks, D. J. McFarland, P. H. Peckham, G. Schalk, E. Donchin, L. A. Quatrano, C. J. Robinson, and T. M. Vaughan. Brain-computer interface technology: A review of the first international meeting. *IEEE Transactions on Rehabilitation Engineering*, 8, June 2000.

[167] J. R. Wolpaw, N. Birbaumer, D. J. McFarland, G. Pfurtscheller, and T. M. Vaughan. Brain-computer interfaces for communication and control. *Clinical Neurophysiology*, 113, June 2002.

[168] J. R. Wolpaw, D. J. McFarland, G. W. Neat, and C. A. Forneris. An eeg-based brain-computer interface for cursor control. *Electroencephalogr. Clin. Neurophysiol.*, 78:252–259, 1991.

[169] Y. Wu and X. Zhou. The p300 and reward valence, magnitude, and expectancy in outcome evaluation. *Brain res.*, 1286:144–122, 2009.

[170] B. Yazmir and M. Reiner. I act, therefore i err: Eeg correlates of success and failure in a virtual throwing game. *International Journal of Psychophysiology*, 122:32–41, 2017.

[171] N. Yeung and A. G. Sanfey. Independent coding ofreward magnitude and valence in the human brain. *J Neurosci*, 24:6258–6264, 2004.

[172] E. Yin, Z. Zhou, J. Jiang, F. Chen, Y. Liu, and D. Hu. A novel hybrid bci speller based on the incorporation of ssvep into the p300 paradigm. *J. Neural Eng.*, 10:026012, 2013.

[173] R. Yousefi, A. R. Sereshkeh, and T. Chau. Exploiting error-related potentials in cognitive task based bci. *Biomed Phys Eng Express*, 5:015023, 2019.

[174] H. Yuan and B. He. Brain-computer interfaces using sensorimotor rhythms: Current state and future perspectives. *IEEE Transactions on Biomedical Engineering*, 61, May 2014.

[175] T. O. Zander, J. Brönstrup, R. Lorenz, and L. R. Krol. Towards bci-based implicit control in human–computer interaction. In S. H. Fairclough and K. Gilleade, editors, *Advances in Physiological Computing*, pages 67–90. Springer London, London, 2014.

[176] T. O. Zander and C. Kothe. Towards passive brain-computer interfaces: applying brain-computer interface technology to human-machine systems in general. *Journal of Neural Engineering*, 8, Mar. 2011.

[177] T. O. Zander, C. Kothe, S. Jatzev, and M. Gaertner. Enhancing human-computer interaction with input from active and passive brain-computer interfaces. In D. S. Tan and A. Nijholt, editors, *Brain-Computer Interfaces: Applying our Minds to Human-Computer Interaction*, pages 181–199. Springer London, London, 2010.

[178] T. O. Zander, C. A. Kothe, S. Welke, and M. Rötting. Enhancing human-machine systems with secondary input from passive brain-computer interfaces. In *Proc. 4th International Brain-Computer Interface Workshop and Training Course*, pages 197–202, Graz, Austria, 2008.

[179] T. O. Zander, L. R. Krol, N. P. Birbaumer, and K. Gramann. Neuroadaptive technology enables implicit cursor control based on medial prefrontal cortex activity. *Proc Natl Acad Sci U S A*, 113:14898–14903, 2016.

[180] H. Zhang, R. Chavarriaga, Z. Khaliliardali, L. Gheorghe, I. Iturrate, and J. d R Millán. Eeg-based decoding of error-related brain activity in a real-world driving task. *Journal of Neural Engineering*, 12, Nov. 2012.